The influence of group effects on micropile behaviour

Plaxis 3D modelling

J.A.W. Molendijk

Cover image
A cross section of the phase deviatoric strain 3D contours at the final loading stage
at the center line of a nine pile Plaxis 3D model with 10D pile group spacing

z

x
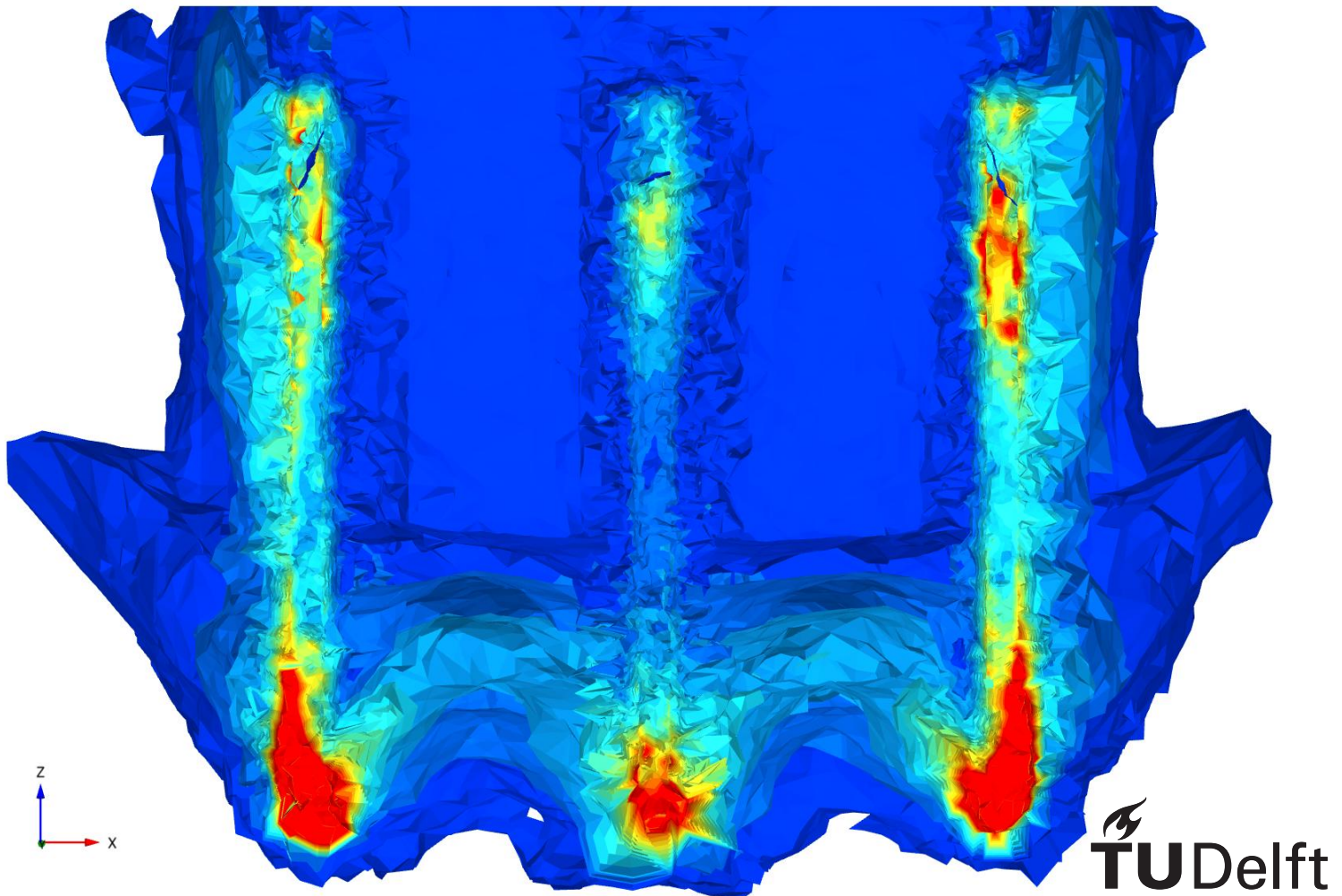
TUDelft

The influence of group effects on micropile behaviour

Plaxis 3D modelling

by

J.A.W. Molendijk

to obtain the degree of Master of Science
at the Delft University of Technology,
to be defended publicly on Tuesday March 6, 2018 at 16:00 AM.

Student number: 4152522
Project duration: February 6, 2017 – October 16, 2017
Thesis committee: dr. ir. W. Broere TU Delft, supervisor
Prof. dr. K. G. Gavin TU Delft
dr. ir. C. van der Veen TU Delft
ir. drs. R. E. P. de Nijs Witteveen+Bos
ir. A. S. Greeuw Witteveen+Bos

An electronic version of this thesis is available at `http://repository.tudelft.nl/`.

TUDelft

Preface

This Master's thesis is the final assignment to obtain the degree of Master of Science for the master programme Civil engineering, track Geo-engineering at the faculty of Civil Engineering and Geosciences, Delft University of Technology. The research was conducted at both Witteveen+Bos Consulting Engineers and Delft University of Technology and supervised by the thesis committee.

I would like to thank Wout Broere, Richard de Nijs and Alex Greeuw for the discussions, support and guidance throughout the project. Furthermore, I would like to express my gratitude towards Professor Gavin and dr. Van der Veen for their input during the committee meetings.

During the first four months of this research I worked at the Amsterdam office of Witteveen+Bos for several days a week. I am grateful for the pleasant working environment provided to be me by my colleagues at Witteveen+Bos. I enjoyed my time there and learned a lot about geo-engineering in practice. Lastly I would like to thank my fellow graduating students from Geo-engineering for the support and discussions during the summer period at the university.

J.A.W. Molendijk
Delft, October 2017

Summary

Micropiles are in-situ made piles with a relatively small diameter of at most 0.30 meters. In the current Dutch guideline a group effect factor is introduced to account for the interaction between micropiles in groups. This factor originates from research with driven prefab piles. However, there is only a limited amount of research focussed on group effects for tensile axially loaded micropiles. In this thesis a numerical approach to investigate group effects for tensile axially loaded micropiles is presented.

First, a single micropile model is developed in 2D and 3D with the geotechnical finite element method software Plaxis. In this model, only the pressure grouting phase is assumed to influence the in-situ soil conditions significantly. Model parameters such as size, pile and soil behaviour are obtained from a case in Amsterdam. In the Amsterdam case six pile failure load tests were performed. In the plane strain 2D modelling approach the single pile model consists of embedded beam rows. The load-displacement behaviour of this model shows satisfying correlation with load-displacement behaviour measured in the pile load tests.

After the development of a 2D single pile model the final 3D single pile model with volume elements is presented. In the 3D single pile model, a simulation of the pressure grouting phase of the piles is introduced. This is done because soil property dependent capacity and stiffness behaviour of the modelled piles is crucial for the group effect investigation. By modelling the pressure grouting phase both the micropile capacity and stiffness behaviour are modelled more accurately. The 3D single pile modelling approach is validated by comparing the load-displacement behaviour of the model with field test results. Results produced from the 3D single pile model closely match the field data. A sufficiently accurate mesh for the 3D models is selected by comparing the 3D modelling results with a more precise 2D axisymmetric model.

In 3D, six different group models are developed. These group models are made to represent a practical situation in a building pit were multiple piles are mobilised. Three models with a different internal pile group spacing are developed for both a standard soil stiffness case and a high soil stiffness case. The three different spacings used are 5D, 10D and 15D. From these models the influence of the soil stiffness and pile group spacing on the capacity per micropile and secant stiffness at 70% of the failure level, $k_{sec;0.7}$, is determined. Next to the previously mentioned relations the dominant failure mechanism is determined for each spacing case. The capacity reductions of the individual micropile capacity for the 5D and 10D spacing cases compared to the 15D cases are 50% and 23%, respectively. For the $k_{sec;0.7}$ value, reductions are again observed when comparing the 5D and 15D spacings, with a 8% reduction for the standard stiffness case and a 4% reduction for the high stiffness case. Comparing the $k_{sec;0.7}$ for the 10D and 15D spacings shows no significant reduction in stiffness for both the standard and stiff case. The 5D and 10D models show that soil plug pull-out failure develops, for the 15D spacing case single pile slip is the dominant failure mechanism.

The modelling approach includes some assumptions and simplifications. The soil is modelled with three homogeneous layers which behave according to the Hardening Soil model. The input parameters of the models are determined by correlating the conditions at the test site to a nearby site where more site investigation was performed. Only linear elastic volume elements are used to model the micropile, the stiffness of the groutbody is used as fitting parameter and directly after the installation the full groutbody stiffness is reached. Installation effects are assumed positive and the micropiles are loaded at the top of the pressurized groutbody. The group model is not validated with field data. In the models all piles are installed simultaneously and the applied tensile load is equal for every pile in the group.

It can be concluded that the 3D modelling approach is appropriate for single micropiles and has practical limitations for pile groups. The internal spacing of the pile groups is negatively correlated to the group effect and the soil stiffness has no significant influence on the group effect. The current modelling approach is different from the Dutch standards, after validation of the pile group model the dominant failure mechanism for 10D pile groups could be adjusted in the standards but additional safety is required for this calculation.

For future research it is recommended to validate the pile group modelling approach with geo-centrifuge or full-scale tests. The numerical pile group model can be further improved by researching the boundary and mesh sensitivity of the results more extensively. For the interface behaviour and installation effect simulation more modelling approaches are possible and thus should be researched for comparison. Finally the efficiency of the model can be improved by reducing the amount of plastic points or using a Mohr-Coulomb soil model for limit state calculations.

Contents

List of Figures

List of Tables

List of Symbols

Symbol	Unit	Definition
A	m^2	Pile group lay-out specific surface
A_r	–	Area ratio
c	kN/m^2	Cohesion
c'	kN/m^2	Effective cohesion
D	m	Diameter
h	m	Layer thickness
E	kN/m^2	Young's modulus
F	kN	Force
$F_{r;t;d}$	kN	Ultimate tensile capacity
f_1	–	Installation factor
f_2	–	Tension pile group factor
G	kN/m^2	Shear stiffness
K	–	Lateral earth pressure coefficient
k	kN/m	Spring stiffness
$k_{sec;0.7}$	kN/m	Micropile secant stiffness at 70% of the ultimate tensile capacity
L	m	Length
M	kN/m^2	Stress redistribution factor
O	m	Perimeter
P	%	Percentage change
p_a	kN/m^2	Atmospheric pressure
p'	kN/m^2	Mean effective stress
q_c	MPa	Cone resistance
R_f	–	Failure ratio
T_s	kN	Side resistance or shaft friction
u	m	Displacement
z	m	Depth
α	–	Pile specific factor
β	–	$K \cdot \tan\delta$
γ'	kN/m^3	Effective soil weight
$\gamma_{0.7}$	–	Shear strain at 72.2 percent of the initial small strain shear stiffness
δ	deg	Interface friction angle
η	–	Group efficiency factor
ν	–	Poisson's ratio
τ	kN/m^2	Shear stress
σ	kN/m^2	Total stress
σ'	kN/m^2	Effective stress
ϕ	deg	Internal friction angle
ϕ'	deg	Effective internal friction angle
ψ	deg	Dilatancy angle

List of Abbreviations

Term	Definition
AASHTO	American Association of State Highway and Transportation
API	American Petroleum Institute
CPT	Cone Penetration Test
CTC	Center-to-center
DIN	Deutches Institut für Normung [German standards institute]
DTU	Documents Techniques Unifiés [Uniform technical documents]
EBE	Embedded beam element
EBR	Embedded beam row
EC7	Eurocode 7
FEM	Finite Element Method
FHWA	Federal Highway Administration
FOREVER	Fondations Renforcées Verticalement [Vertically reinforced foundations]
HS model	Hardening soil model
HSs model	Hardening soil small strain stiffness model
IBZ	Ingenieursbureau Zuidasdok [Engineering firm]
ICP	Imperial College Press
ISF	Interface Shear Factor
MC model	Mohr-Coulomb model
N2N	Node-to-node anchor
NAP	Normaal Amsterdams Peil [Dutch height reference level]
NF	Norme Française [French standards]
NGI	Norwegian Geotechnical Institute
POP	Pre-overburden pressure
OCR	Over consolidation ratio
SPT	Standard Penetration test
UWA	University of Western Australia

1

Introduction

Micropiles were introduced by professor F. Lizzi in the 1950's, who introduced them in Italy [30]. Originally micropiles were developed for rehabilitation projects: after the second world war many foundations had to be restored. Micropiles are defined as piles with a relatively small diameter of approximately 200 mm to 300 mm, resulting in a large length to diameter ratio. Generally micropiles consist of steel rebar and a groutbody that is is pressurized during or after installation. Micropiles are divided into several classes based on the installation method. The micropile classification system differs per country or region due to varying installation procedures and the use of micropiles for various applications. This research is related to Dutch practice and therefore reference is made to the Dutch micropile classification system, which has five different classes:

Type A: A double casing is used for the boring process. The groutbody can be pressurized for this type of micropiles. See figure 1.1 for a visualisation of the installation process.

Type B: A single casing is used for the boring process. The groutbody can be pressurized for this type of micropiles.

Type C: Micropiles that are installed without a casing, the grout is injected through the steel rebar.

Type D: A continuous flight auger is used for installation, mixing the soil and grout.

Type E: The casing is vibrated during installation to reach the right depth.
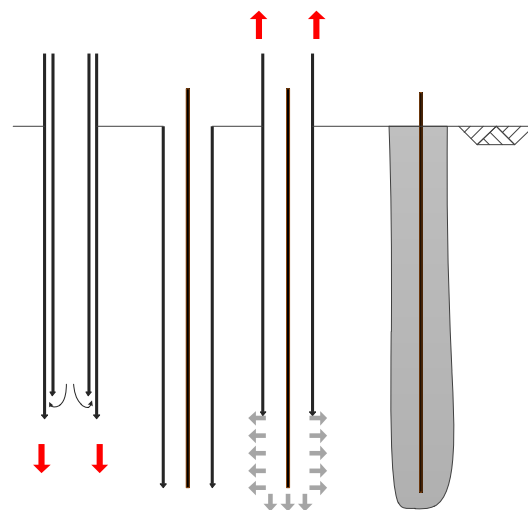
Figure 1.1: An illustration of the installation process of type A micropiles.

The use of micropiles as vertical foundation has strongly increased in The Netherlands during the past fifteen years. Compared to other systems where no vibrations are induced, micropiles are cheaper and easier to install. Often micropiles are used as tension piles, to resist the uplift forces on the floor of a building pit caused by high groundwater levels. For larger construction projects many closely spaced micropiles are needed to resist these uplift forces. The quality of micropiles is strongly dependent on the execution, one of the disadvantages of micropiles. Therefore a minimum of three percent of the installed micropiles must be tested for every project. The uncertainty in the performance of micropiles affects the safety factors used in design practice. Since micropiles are always tested individually a safety factor is included that accounts for the group effect. This safety factor originates from research done for driven, prefab tension piles. How appropriate this factor is for micropiles is investigated in this research.

1

1.1. Research objective

The main research objective is to investigate the influence of group effects on micropile behaviour. Therefore the main research question is formulated as follows:

> ***"How do group effects influence the strength and stiffness of micropiles in axial, tensile loading?"***

The geotechnical FEM software Plaxis is used for the numerical modelling in this research. Since group effects are a 3D phenomenon and the time frame of the research is limited to about 9 months, the study is limited to the development and evaluation of a 3D numerical model to investigate the behaviour of micropile groups. No laboratory or full-scale experiments are performed. To answer the main question several subquestions are answered first. The following subquestions are formulated:

I. What is an appropriate model for a single micropile under axial, tensile loading?

II. How does pile spacing influence the size of the group effect?

III. How can installation effects be included?

IV. What is an appropriate 3D model?

V. How can the findings of the research be validated and included in the design code?

1.2. Reading guide

The research consists of several parts which are described and introduced below.

Literature study

In the literature study relevant background on tension piles, shaft friction, pile group behaviour and numerical modelling of piles in general and with Plaxis is presented. The literature study provides the theoretical basis of the research and shows what specifics are know and unknown for tension pile group modelling.

Finite element modelling

In the second part of the research the finite element modelling is introduced first. The study starts with the development and validation of a 2D model in Chapter 3. This 2D model is made to see what the limitations of pile modelling are in a fast and convenient way. After the 2D model, Chapter 4 introduces and explains the 3D single pile model. Following the validation of the 3D single pile model is the section on the pile group model. The results of the 3D pile group model are discussed in the third section of Chapter 4.

Discussion, conclusion and recommendations

In Chapters 5 and 6 the results that were found in the research are discussed and several conclusions are derived from the research. In the discussion the limitations of the research and the influence of these limitations on the results of the research are explained. In the conclusion the main research question and subquestions are answered. Next to answers on these questions more general conclusions are presented. The report ends with recommendations for further research and improvements of the current research in Chapter 7.

I

Theoretical background

2

Literature study

In this chapter the theoretical foundation of pile design is discussed, combined with design methods that are applied in international practice. First the basic relation between theory and design practice is discussed, afterwards more fundamental processes in shaft friction development are described.

Furthermore, the effect of tensile loading on the shaft capacity and the behaviour of piles in groups are investigated. Several numerical, physical and analytical researches related to tensile loading and group effects are presented. The last main topic discussed in this literature study is state-of-the-art procedures for pile modelling in finite element method (FEM) software.

2.1. Theory and practice in pile design

The determination of the capacity of a pile foundation is based on two concepts: shaft friction and pile base resistance. Since this research is focussed on tension piles, no pile base resistance is developed. Therefore only theories related to the shaft friction development in pile foundations are treated in this literature study.

The basis of geotechnical pile design is formed by empirical formula's, but Kulhawy for example presented a theoretical formulation for the tensile capacity of bored piles [25]. The following equation is used to determine the side resistance T_s of a pile.

$$T_s = \int_0^L K(z) z \gamma' \tan \delta \pi D \, \mathrm{d}z \tag{2.1}$$

In literature the product of depth z and effective soil weight γ' is often denoted as the vertical effective stress level $\sigma'_v(z)$. In equation (2.1) it can be seen that three groups of parameters directly influence the capacity:

1. The geometry of the pile (length L and diameter D)
2. The soil properties (effective soil-weight γ' and lateral earth pressure coefficient K)
3. Pile-soil interaction (interface friction angle δ)

The theoretical formulation of shaft friction presented in (2.1) cannot easily be applied in practice, the exact determination of δ and $K(z)$ prove to be difficult. Finding appropriate values for these parameters is done in varying ways. Through the last years several methods have been developed and applied in design codes all over the world. The theoretical formulation is mostly simplified, for example by relating capacity to in-situ tests such as cone penetration test (CPT) & the standard penetrations test (SPT) and/or pile load tests. Several of the first formulations were made by Fleming [17] and Reese [41]. The method of Fleming uses a $K(z)$ of 0.90 for all sands and a value for δ between the peak friction angle ϕ_{peak} and the constant volume friction angle ϕ_{cv}. Reese provides a formula based on 41 pile tests, where the unit side friction is determined through multiplying a factor β with the vertical effective stress. The formula for β is depth dependent and values for β are limited between 0.25 and 1.20. In the formula of Reese [41], the β value incorporates both the K-value and the interface friction angle δ.

Other well-known methods used for pile foundation design are the API-00, UWA-05, Fugro-05, NGI-05 and ICP-05. All these methods use correlations between CPT-values and the shaft resistance. Important to take into account is the fact that these relations were established by testing driven steel piles (open and closed ended). These guidelines originate from offshore practice, the applicability to tension loaded micropiles is therefore limited. Below a general equation and parameters for three of these methods are shown in equation (2.2) and table 2.1 from Randolph [40], completed with values for v found in El-Reedy [11].

$$\tau_s = a q_c \left(\frac{\sigma'_{v0}}{p_a}\right)^p A_r^b \left(max\left\{\frac{L-z}{D}, v\right\}\right)^{-c} (\tan\delta_{cv})^d \left(min\left\{\frac{L-z}{D}\frac{1}{v}, 1\right\}\right)^e \tag{2.2}$$

The first factors are related to the cone resistance q_c and the normalised in-situ vertical effective stress σ'_{v0}, multiplied with the area ratio A_r. The second part of the equation is related to the friction interface with $(\tan\delta_{cv})$. The equation is scaled for both parts, with factors related to the pile dimension (length and diameter L, D) and results from field tests (a-v).

Table 2.1: The input parameters for the different methods corresponding to equation 2.2 [11, 40].

Method		*a*	*b*	*c*	*d*	*e*	*p*	*v*
		Parameters						
Fugro-05	compression	0.043	0.45	0.90	0	1	0.05	$2\sqrt{A_r}$
	tension	0.025	0.42	0.85	0	0	0.15	$2\sqrt{A_r}$
Simplified ICP-05	compression	0.023	0.2	0.4	1	0	0.1	$4\sqrt{A_r}$
	tension	0.016	0.2	0.4	1	0	0.1	$4\sqrt{A_r}$
Offshore UWA-05	compression	0.030	0.3	0.5	1	0	0	2
	tension	0.022	0.3	0.5	1	0	0	2

In the German code DIN4014 (Bored piles) the SPT blowcount is related to the unit side friction [24]. A factor a is multiplied with the 'N' value from the SPT test, where a is 4.14 for coarse sands and 2.73 for fine sands. Complementary to the EC7, the German DIN1054 provides specific design rules for earthworks and foundations, including micropiles. This national annex provides both an empirical approach and a pile test related approach for the determination of the shaft friction. In France the national annex is NF P94-262, which replaced the DTU 13.2 and Fascicule 62.

In the United States the Federal Highway Administration (FHWA) and the American Association of State Highway and Transportation Officials (AASHTO) formulated empirical design rules on micropile design. These design rules followed from a comprehensive desk study sponsored by the FHWA in 1993 [1]. In the FHWA guideline the shaft friction is assumed equal for compressive and tensile loading. When referring to the group effect the FHWA standard states that it can be beneficial due to the increase in stress by the pressure grouting process. An important note must be placed at the fact that this presumes compressive loading when the micropiles are in use. Although the developed shaft friction for single piles is assumed the same for tension and compression, no consideration is presented for a possibly different influence of the loading direction on the interaction within groups of piles.

2.1.1. Dutch national annex

In this subsection the design rules relevant for the group effect for micropile design applied in Dutch practice are elaborated [7]. The theoretical basis for the Dutch design rules is formed by literature review, a geo centrifuge test and numerical studies which can be found in CUR 2001-4 [8]. This research dates from the mid 90's.

Old Dutch tension pile guideline

Before the current Dutch guideline on tension pile capacity, two methods were applied: a CPT-related method and a 'slip-method'. The formulation of both methods is shown below.

$$\tau_{max} = \alpha \cdot q_c \tag{2.3}$$

$$\tau_{max} = K \cdot \sigma'_v \cdot \tan\delta \tag{2.4}$$

In equation (2.3) the CPT-method is shown, the factor α is pile-type dependent and is determined through full scale field tests. This α-value is multiplied with the cone resistance q_c.

The second method is shown in equation (2.4), which is related to the theoretical formulation of shaft friction in equation (2.1). In equation (2.4) interface friction angle δ is dependent on the pile type and the lateral earth pressure coefficient K is dependent on the relative density and the pile type. For application of this method in practice, an additional table with values for δ and β is provided. Both methods have their own advantages and disadvantages in terms of applicability, accuracy and theoretical foundation.

The first method was used as the basis for the current design rule because of its practical correlation with the much applied CPT. The current design rule incorporates new factors, taking the pile installation and the group effect into account.

Group effect in strength calculations

For quantifying the group effect in micropile design the dimensionless reduction factor f_2 is used. This factor is based on the assumption that the cone resistance is reduced after tensile loading (and therefore the developed shaft friction of adjacent piles is reduced). This results in the following formula [8]:

$$f_2 = \frac{q_{c;z;2}}{q_{c;z;1}} \tag{2.5}$$

Where $q_{c;z;2}$ is the design value of the cone resistance after tensile loading and $q_{c;z;1}$ is the design value of the cone resistance before tensile loading. Since $q_{c;z;2}$ cannot be determined through a CPT, it is estimated with the following formula [8]:

$$q_{c;z;2} = -M_i + \sqrt{M_i^2 + (2\sigma'_{v;d;j;0} + \gamma'_{h;i} \cdot h_i)\left(2\sigma'_{v;d;j;0} + \gamma'_{h;i} \cdot h_i - 2\sum_{n=0}^{i-1} T_{d;n}\right)} \tag{2.6}$$

With the vertical effective stress $\sigma'_{v;d}$, effective soil weight γ'_d, layer thickness h and the design value of the shaft resistance T_d. Factor M_i is defined as:

$$M_i = \frac{f_{1;i} \cdot O_{p;i} \cdot \alpha_t \cdot q_{c;d;i} \cdot 1000 \cdot h_i}{A} \tag{2.7}$$

This includes the pile perimeter $O_{p;i}$, pile specific factor α_t, the design cone resistance $q_{c;d}$, pile group lay-out specific surface A and layer thickness h. Dimensionless factor f_1, representing installation effects, is set to 1.0 in the guideline [7]. For driven piles f_1 is larger than 1.0, if installation has a proven, positive effect on the cone resistance. The factor M can be seen as a stress redistribution factor, where the mobilised shaft friction is redistributed over the available surface area in the pile group. In the formula presented in equation (2.6) the calculated design-value of the shaft friction $T_{d;n}$ lowers the vertical effective stress. The equilibrium of forces used for the determination of this reduction is shown in figure 2.1.
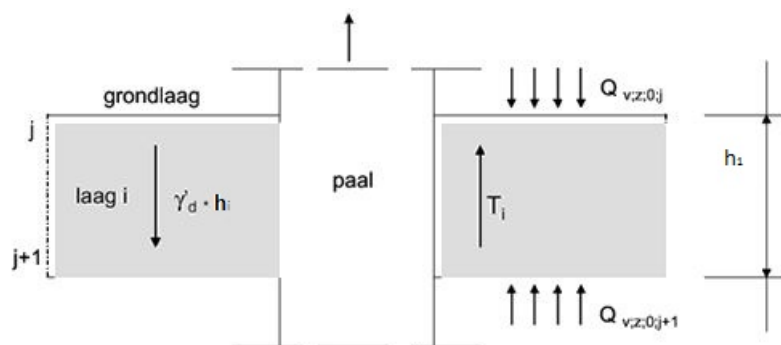
Figure 2.1: Force equilibrium on a section of a tension pile.

Since the mobilized shaft friction of the previous layer (i-1) must be known in (2.6), one starts with calculating the shaft friction reduction at the top of the grout body of the pile and works towards the tip of the pile. The shaft friction reduction due to the decreased vertical effective stress σ'_v along the pile surface increases strongly with depth.

The group-reduced tensile slip capacity for m soil layers is determined with equations (2.8) and (2.9).

$$T_{d;i} = M_i \cdot f_{2;i} \tag{2.8}$$

$$F_{r;tens;d} = A \cdot \sum_{i=1}^{m} T_{d;i} \tag{2.9}$$

Pull-out capacity of the soil plug

The calculation method mentioned in the former paragraph checks the slip capacity of a single pile in a group. The Dutch code defines a second failure mechanism for piles in a group: pull-out of the soil plug. In (2.10) the calculation of the maximum pull-out capacity of the micropile, $F_{r;tens;max;d}$, considering the soil plug is shown. The volume of the soil plug that contributes to the resistance of the tension force is schematically represented by a cone V_{cone} and a cylinder $V_{cylinder}$. The volumes are multiplied with the design value of the effective soil weight γ'_d to determine the maximum resisting force.

$$F_{r;tens;max;d} = \left(V_{cone} + V_{cylinder} \right) \cdot \gamma'_d \tag{2.10}$$

The diameter of the mobilised soil cylinder and cone is determined by the pile group spacing, an example lay-out is shown in figure 2.2. The angle of the cone at the pile tip is dependent on the pile type (installation effects) and position of the pile in the pile group (center pile or corner pile). The angle varies between $0.5\phi'$ for the least favourable case and 45 degrees for the most favourable case.
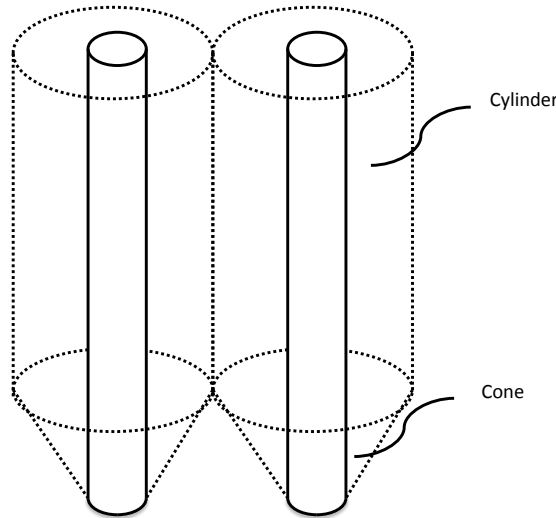
Figure 2.2: The soil volumes taken into account in the calculation for the soil plug failure mechanism.

The normative capacity of the pile group is equal to $min\{F_{r;tens;d}, F_{r;tens;max;d}\}$ from (2.9) and (2.10).

Group effect in stiffness calculations

The calculation of the group reduction factor f_2 for stiffness is very similar to the calculation in the strength analysis. The procedure is described in the addendum to CUR 236 [6]. For the determination of the f_2 in this particular case the characteristic values are taken and the mobilised shaft friction is used instead of the maximum shaft friction. The formula's for the determination of the characteristic value of the axial spring stiffness $k_{axial;char}$, relevant to the factor f_2, are listed below.

$$k_{axial;char} = \frac{F_{char}}{u_{char}} \tag{2.11}$$

The characteristic value of the force, F_{char}, is determined for all pile segments. This is shown in equation (2.12). In this equation the mobilized shear stress, $\tau_{mob;i}$, is used instead of τ_{max}. The mobilized shear stress is multiplied with the pile perimeter O, segment height h_i and group effect factor $f_{2;i}$. For the determination of $f_{2;i}$ equation (2.6) and (2.7) are used, where characteristic values are taken for σ'_v and γ'. The $\alpha_t \cdot q_{c;d;i}$ in equation (2.7) is replaced by $\tau_{mob;i}$.

$$dF_i = \tau_{mob;i} \, O \, h_i \, f_{2;i} \qquad\qquad (2.12)$$

The maximum effect of the axial spring stiffness group reduction is limited at 15% according to the current Dutch guideline. Therefore the impact of the group effect on the stiffness calculations is less significant compared to the impact on the strength calculations.

2.2. Tensile loading versus compressive loading

As mentioned in the introduction of this literature study, only shaft friction is taken into account in the research review. The development of shaft friction along a pile in compressive loading is difficult to formulate based on fundamental principles, as mentioned before. Nevertheless the major findings in compressive shaft capacity are presented in this section first. Afterwards fundamental explanations for possible deviations in compressive and tensile shaft capacity are shown.

It is known that shaft friction development shows a relatively stiff response compared to base resistance [17]. For a long period a so-called 'critical depth' was used in design: after a certain depth the unit shaft friction seems to have reached a constant value. Relatively recent discoveries show that the shaft friction most likely reaches a limit due to friction degradation: gradual densification of soil around the pile during installation [39]. For micropiles under compressive loading this theory must be treated with care, installation effects are different and difficult to determine for the varying micropile types. As shown in research by De Nicola [9], the compressive unit shaft friction generally increases with depth reaching a maximum and declines towards the pile tip (roughly a hyperbolic shape). In compressive loading the soil surrounding the pile is often assumed to be densified due to the loading. The effective vertical stress level is assumed to increase, increasing the shaft friction during compressive loading.

An important factor in shaft friction capacity, which influences capacity both in tension and compression, is the effect of installation. Including this effect in capacity calculations is very difficult and multiple researches have been performed to find the key parameters [2, 10, 12]. Despite the effort of several researchers no general accepted method of including installation effects in pile design has yet been developed. Due to this uncertainty additional safety is included in most design methods: to prevent severe overestimation of the shaft capacity. Installation affects the soil stress and critical state and the final pile diameter in case of in-situ constructed piles. In a simplified approach applied in numerical modelling these effects are taken into account by pile volumetric strains (either increase or decrease of the initial diameter) and increased or decreased horizontal effective stress and interface friction.

There is no general agreement within the field of geotechnical engineering whether the shaft friction capacity of piles developed during compression or tension is the same. Several studies have been performed, resulting in opposite results or explanations, see for example a discussion by Fellenius and O'Neill [15]. From research on tension piles three effect's are mentioned which might cause changes in the vertical effective stress and therefore in the tension pile capacity. The three other effects are highlighted in the following subsections.

2.2.1. Principal stress rotation

In research done by Lehane the effect of principal stress rotation is explained [28]. When no force is applied to the pile the orientation of the principal stresses are such that there is no shear stress, see the left-side of figure 2.3. When a tension force is applied to the pile, the principal stresses will rotate towards to surface. This rotation is due to the redistribution of stresses caused by the shear friction between the pile and the soil, developing shear stresses. The right-side of figure 2.3 shows the new orientation.
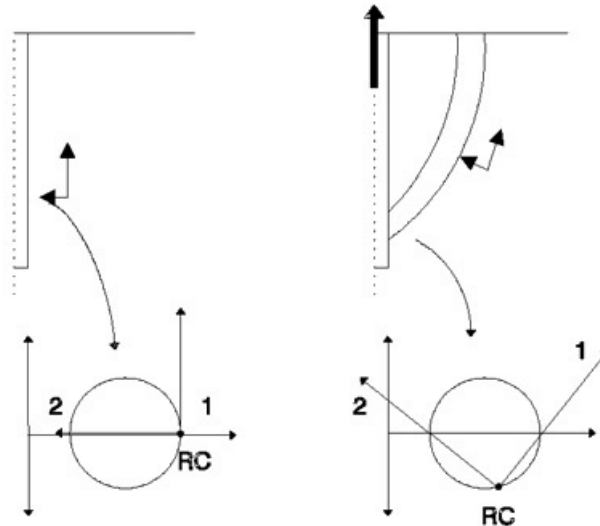
Figure 2.3: The rotation of principal stresses [7].

An important note is placed at the observations of Lehane, where the rotation was observed in instrumented pile tests on driven piles in sand [28]. Although the equalization of stress after installation is mentioned, some residual stresses remain. The installation effects of a micropile are different: the stress state will differ for every micropile type and installation procedure used. Therefore the starting point of the analysis will be different compared to driven piles. For the principal stress rotation shown in figure 2.3, no residual stresses were assumed. The difficulty of quantifying the principal stress rotation is explained by de Nicola [9], especially when a difference between compressive or tensile loading must be explained. The residual stresses after installation largely influence the effect of principal stress rotation.

2.2.2. Dilation

In research by Lehane and Houlsby the effect of dilation on the shaft friction is described [21, 28, 29]. Dilation means that a densely packed, drained, granular soil increases in volume due to shearing, see figure 2.4.

Whether dilation causes a difference in compressive or tensile capacity of a pile in identical soil conditions depends on the magnitude of the displacements along the pile surface. Due to volume changes related to shearing the shaft friction increases, but for larger displacements a residual level is reached.
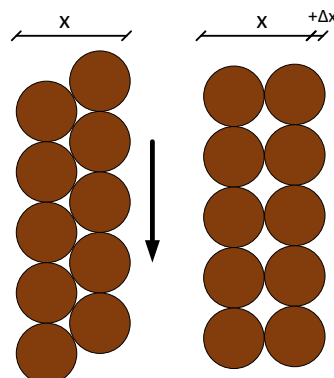
Figure 2.4: Dilation simplified.

The effect of dilation Δx on the radial effective stress σ'_{rd} is quantified in research by Lehane and Houlsby [21, 28], where the mass shear stiffness G and radius R are included:

$$\Delta\sigma'_{rd} = 2\Delta x \frac{G}{R} \tag{2.13}$$

From the 1993 research of Lehane it is concluded that the effect is less significant for large diameter piles and even reduces to zero [28]. Another remark made in this paper is the decreasing contribution of dilation to the shaft capacity at increasing stress levels. It is advised that the extrapolation of results (obtained from small-scale tests) to full-scale cases is done with care.

2.2.3. The Poisson effect
Poisson's effect, elaborated in the 1994 paper of de Nicola, can simply be described by the contraction or widening of the pile shaft [9]. The effect of a tensile force is shown on the left of figure 2.5, the effect of a compressive force is shown in the right. From these effects it follows that tensile loading might cause a reduction in shaft friction and compressive loading might cause an increase. The relevance of this effect strongly depends on the dimension of the pile, the magnitude of the load and the Poisson's ratio of the micropile.
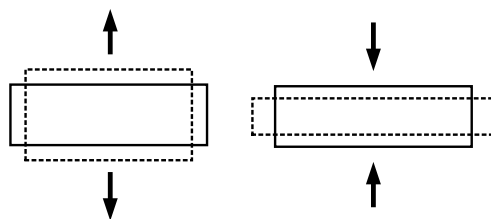
Figure 2.5: Poission's effect illustrated: a tension force [l] and a compressive force [r] applied to an element.

Below in figure 2.6 the result from the numerical research of De Nicola is presented, showing the impact of the Poisson effect on the ratio between the tensile and compressive shaft capacity. On the horizontal axis the multiplied, dimensionless ratios L/D and G/E_p are shown. The first ratio is related to the pile geometry, with length L and diameter D. The second ratio is related to the system stiffness, with soil shear stiffness G and pile stiffness E_p. As expected a decrease in comparative shaft capacity is shown for increasing length and soil shear stiffness.
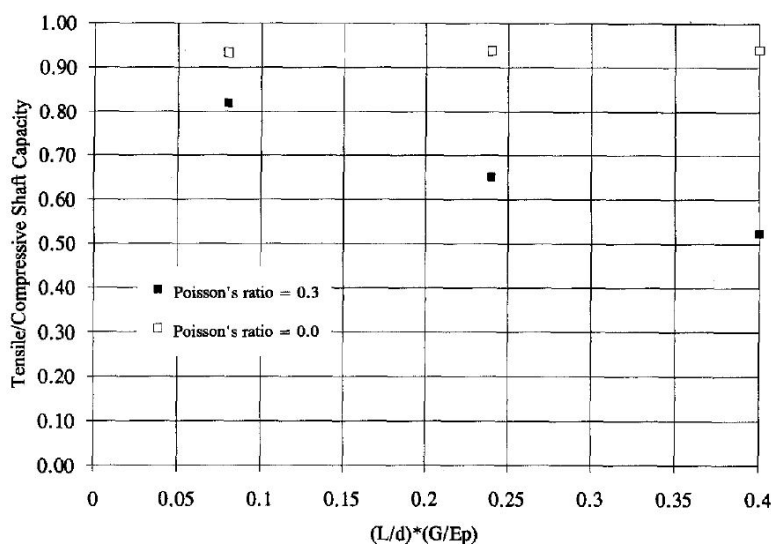
Figure 2.6: The impact of Poisson's effect [9]. The black squares are results for a Poisson's ratio of 0.3, the open squares are the results for a Poisson's ratio of 0.

The question remains what the physical boundaries of these three effects on the soil state are and therefore how other piles are influenced. The effects do indicate the relevance of the in-situ stress conditions (principal stress rotation), sand state and soil stiffness (dilation) and pile geometry and system stiffness (Poisson's effect).

2.3. Research on pile group behaviour

Since piles are mostly used as foundation element loaded in compression, most research is related to downward axially loading. Pile group behaviour and pile interaction is discussed briefly for compression cases before the elaboration of tension pile group research.

The major difference with compression pile group behaviour when compared to tension pile group behaviour, is the development of pile base resistance and additional capacity from the actual structure interacting with the soil. In the paper by Randolph several researches on the analysis of pile groups are discussed [39]. Pile groups generally behave less stiff than single piles due to interaction effects, where the settlement of a pile influences the settelement of a neighbouring pile. Similar results are presented in Juran [23] and Fleming [17]. Furthermore Juran and Fleming present research showing slightly increased capacity of micropiles in group configuration when installed in granular soils. This increase in strength is attributed to positive installation effects, as mentioned in the previous section, which might occur with high pressure grouting. But this higher capacity generally does not lead to a more economic design. The settlement of a pile group loaded in compression is often normative for the design and the capacity of the group is less relevant for the final pile group dimensions.

2.3.1. Tension pile group behaviour

Research on the tensile capacity of micropile or bored pile groups is scarce. In this section the small-scale experiments, numerical models and analytical solutions related to tension pile group behaviour are presented.

First the results from a small scale experiment performed by Gaaver [18] are presented. Gaaver researched the tensile capacity of a group of non-displacement steel model piles in sand. This small-scale experiment was performed at 1g, with L/D ratio's of 14, 20 and 26. Between the different piles of the group a spacing of 2.5D was applied. The results show a dramatic decrease of the pile efficiency when placed in larger groups, see figure 2.7. For each group, an increase in efficiency can be seen with an increase in relative density of the surrounding soil. The efficiency parameter η is calculated by comparing the capacity of a single pile and the average capacity of one pile in a group.
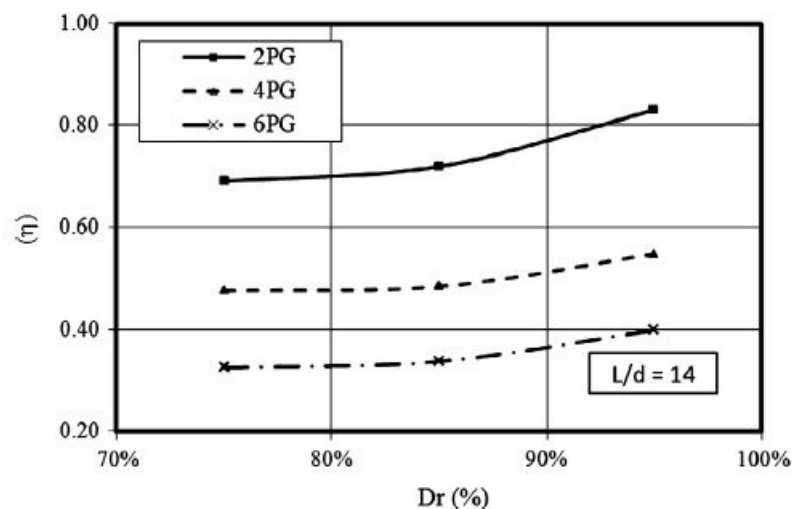
Figure 2.7: Group efficiency for different pile groups versus relative density.

The results cannot be directly scaled to the prototype, both the stress state and soil particle dimensions are not realistic when doing so. Scale-effects might influence for example the failure mechanism and the effect of dilation on the shaft friction. Furthermore, the author used a fixed spacing of 2.5D, therefore the results can not be extrapolated to different pile group spacings in practice.

Small-scale experiments on in-situ casted micropiles were performed by Sharma [45]. These tests show results for square groups of four micropiles with different L/D ratio's and varying spacing. The micropiles were installed by driving an aluminium tube vertically and pouring a water-cement mixture afterwards. Looking at the efficiency of the pile groups, it is concluded that all pile groups have a lower capacity per pile than single piles. The authors conclude the efficiency of the pile group is higher for larger L/D ratio's and more

closely spaced piles. In the paper the latter is explained by 'a stronger grout to ground bond'. A research similar to [45] is presented by Shanker [44], resulting in different conclusions. According to the experiments done by Shanker group efficiency, in this case steel model piles, increases with spacing. Moreover, efficiency decreases with an increase in the L/D ratio. A third small-scale experiment about pile group efficiency under pull-out loads can be found in research by Vanitha [50]. The research is focussed on pile anchor capacity but includes tests on piles without an additional anchor at the base. The author concludes that the isolation spacing, e.g. internal spacing in a pile group where the efficiency is 100%, is 4 to 6D. The efficiency increases with larger L/D ratio's according to the author. From these small-scale experiments no satisfying general conclusion can be drawn.

For the French national research project on micropiles (FOREVER) a full scale axial tension load test was performed on a micropile group consisting of three micropiles [32]. Important parameters in the full-scale load tests were the triangular pattern, the small bond length of 5 meters in chalk and pressuremeter determined soil stiffness and friction parameters. Unfortunately, this full scale load test did not contribute to a clear conclusion on micropile group influence, as stated by Juran [23]. The conclusion was drawn that a positive group effect could develop, limiting the displacements of a micropile group compared to individual piles. From the research it was recommended to use the pile group modelling program GOUPEG and pressuremeter data to derive a 'group effect factor' for the design of pile groups. It was also concluded that including a realistic group effect in design is no easy task.

At the International Workshop on Micropiles in 1999 Herbst [20] presented a German case study where 6500 micropiles were installed to retain uplift forces with a maximum of 17 meters head. The soil consists of glacial deposits: medium coarse sands and clay layers. The piles varied in length from 17.50 to 26.50 meters and were spaced at 2.72 meters. In the pile testing program groups of five piles were tested simultaneously. According to the author, no significant differences between the corner and center piles were observed during the pile tests.

An analytical solution for the capacity of pile groups is presented in research by Shelke [46]. This analysis is based on the development of arches in the soil, according to the author this analysis is only relevant for driven piles. It is assumed that the arching action is insignificant for prebored piles and the analysis is therefore not applicable. Despite this limitation mentioned by the author, the analytical solution is still presented here. Due to the uncertainty about the installation effects in micropile installation, soil arching might still occur during tensile loading when for example high pressure grouting is applied during the installation.

In the analysis the failure surface is determined to be represented by a log spiral. The net capacity consists of the weight of the soil mass and the friction along the failure surface minus the weight of the pile and a possible cap.
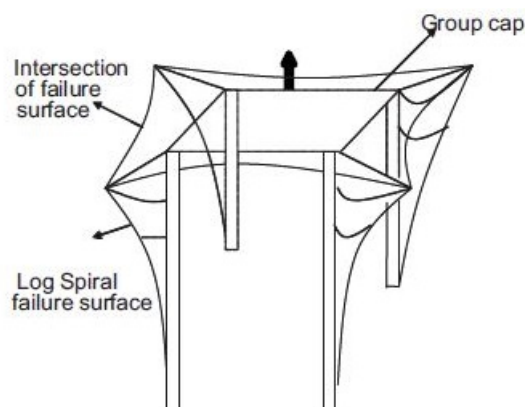
Figure 2.8: The assumed failure surface in [46].

The start of the failure surface is assumed to be at the base of the pile for L/D ratio's lower than 15, for larger ratio's the start of failure surface is assumed at a fixed depth/length ratio. Along the remaining length the failure is assumed at the pile-soil interface.

The results of researches on tension pile group behaviour found in this section of the literature motivate the need for additional research on the topic.

2.4. Numerical modelling of pile behaviour

In this section numerical research on pile behaviour is presented, highlighting the important parameters and the applicability of the numerical research. Moreover, Plaxis specific modelling limitations and opportunities are shown for the 2D and 3D software.

2.4.1. Shaft friction modelling research

Where in practice values of the unit shaft friction are mostly obtained from empirical methods, research focusses on more complex analytical or numerical procedures which capture unattended factors.

For example Loukidis [31] uses an advanced constitutive model with two-surface plasticity for a parametric study. The model incorporates both small and large strains soil response and takes intermediate effective stress and anisotropy into account. In this model failure is predefined in a zone just next to the pile-soil interface, creating a shear band parallel to the pile. The pile itself is not modelled in the research and assumed perfectly rigid. Loukidis concludes with relations between the K-value for lateral earth pressure and model parameters such as relative density, initial overburden pressure and pile diameter. The K-value is positively correlated to the relative density and negatively correlated to the initial overburden pressure and pile diameter. Similar results are found in research by Masarucci, where the pile was modelled with linear elastic volume elements [33].

In research by Rotta Loria the sensitivity of the determination of the shaft friction capacity was investigated through a variation of pile-soil interface parameters [42]. It is concluded that the angle of interface shear strength and dilatancy are the main factors, where cohesion is the third most influential factor. The Young's modulus and Poisson's ratio are concluded to be less influential. Lastly it is observed that great care must be taken with the selection of the interface parameters, variations in predicted versus measured shaft friction up to 220 % are observed when the results are compared to a centrifuge test.

The mentioned researches stress the importance of a realistic K parameter, dependent on in-situ stress conditions, pile installation, relative density and pile loading. The δ value is another important parameter related to the mean particle size D_{50} and pile roughness. The same conclusion is drawn in laboratory research from Fiovarante [16] and found in an analytical approach presented in a paper by Lashkari [27].

2.4.2. Plaxis

Mostly three types of model geometries are used in numerical pile or tension anchor research: axisymmetric, plane strain and 3D models. The first model geometry is not suitable for modelling pile group behaviour due to the limitations of the axisymmetry, where as plane strain models are difficult due to variable plane strain conditions in pile groups as can be seen in figure 2.9. Due to the efficiency of 2D modelling and the capability of 2D models to capture for example single pile behaviour, 2D models are often used in foundation design.
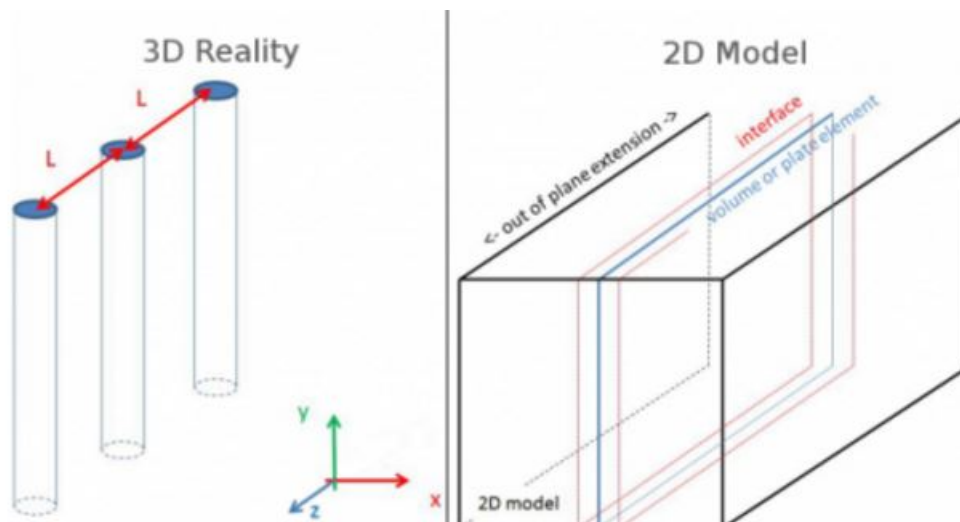
Figure 2.9: The difficulty with modelling a pile row in a 2D model [37].

The options for pile modelling in Plaxis 2D and 3D are described in the following paragraphs.

Plaxis 3D

In the Plaxis 3D program piles can be modelled using volume elements, beam elements or embedded beam elements. A volume element is the most obvious choice since this gives the user the option to choose a pile diameter, stiffness, position in the mesh and interface parameters. The major disadvantage of volume elements is the relatively heavy calculation procedure that is needed. An alternative is regular beam elements, but these have no pile volume or soil interaction behaviour which results in unrealistic pile behaviour.

The embedded beam element is a relatively new development, which has been recently validated for 3D cases [13]. The embedded beam can arbitrarily cross the generated 3D mesh and is connected to surrounding elements with special interface elements. These interface elements are a crucial feature of the embedded beam element. Due to these interfaces the embedded beam element interacts with the soil. Moreover, with the definition of a pile diameter, a zone is created where the soil is forced to behave elastically. This elastic behaviour is according to a set of predefined pile parameters.

The embedded beam element has been validated for both compressive and tensile loading cases: field tests with both driven and bored piles were used. It is noted that bored piles can be modelled more realistically than driven piles. This is mainly due to the relatively limited installation effects during bored pile installation. Currently installation procedures can not be completely modelled with FEM.

In research by Tschuchnigg embedded beam elements are verified and applied in a practical case with Plaxis 3D, some improvements are suggested but the results show to be reasonably good compared to alternative modelling approaches [48, 49].

Some improvements on the modelling of driven pile behaviour are shown by Broere, these can be applied with volume elements [5]. Implementation of these improvements are considered in the numerical part of this research.

Plaxis 2D

According to literature two types of elements are commonly used in Plaxis 2D for the modelling of a pile: solid volume elements and the embedded beam row. With a solid volume element the pile diameter can be chosen and is part of the mesh. Stiffness and strength parameters can be assigned to the element. Compromises have to be made on the out-of-plane strength and stiffness, which do not represent the actual situation accurately. By adjusting the $R_{interface}$ in Plaxis the model can be adjusted to show acceptable results for specific cases [37], in return this adjustment can result in unrealistic shear planes.

The embedded beam element can also be used in 2D modelling where a 2D embedded pile row is implemented in Plaxis. This 2D embedded pile row has been validated through comparison with the 3D embedded beam elements and 3D volume piles [47]. An important feature and input parameter of the embedded beam row is the interface stiffness factor (ISF), which determines the out of plane stiffness of the embedded beam row. In the research performed by Sluis a relation between the out of plane pile spacing and equivalent diameter to the ISF was determined for the case of stiff piles. These values are used as default values in Plaxis, it is recommended to determine realistic ISF's for less stiff piles. This is due to the influence of lower pile-soil stiffness ratio's on the ISF.

Two other options for pile modelling are regular beam elements (plates in 2D) with interfaces and node-to-node anchors. The first option has drawbacks similar to volume elements, being continuous in the out-of-plane direction. Node-to-node anchors are not continuous and therefore soil can 'flow around', but pile-soil interaction is completely absent in this element. Both limitations are quite significant and therefore these elements are not considered in this research for pile sections where pile-soil interaction is relevant.

II

Finite element modelling

Finite element modelling

In this part of the report the numerical research is presented. To investigate the load-displacement behaviour of axially tensile loaded pile groups finite element modelling is used. With finite element modelling the physical problem domain is discretized in small elements. When a force is introduced in the system the elements deform and transfer stresses and strains to neighbouring elements until a new equilibrium is reached. The response of the elements is determined through user-determined stress-strain relationships, that must be appropriate for the material that is modelled. In this research the geotechnical finite element method (FEM) software Plaxis is used. First some background about the available soil models in Plaxis is given. Afterwards the finite elements models for the 2D and 3D modelling approaches are presented in separate chapters.

Plaxis finite element software

The modelling is done with Plaxis 2D and 3D, in this section the relevant constitutive modelling options in these programs are described. Three constitutive models for soil behaviour are described: Mohr-Coulomb, Hardening soil and Hardening soil small strain stiffness. These three models are selected because they are the three recommended and most used models for granular soils in Plaxis [38].

Constitutive models

Modelling the behaviour of soils includes complex non-linear, inhomogeneous and anisotropic behaviour. There are different levels of models, from basic to expert and newly developed scientific models. This research does not aim to develop a new constitutive model, therefore relevant models available from literature will be elaborated here. The models are described concisely, mainly focussed on differences between the models and the applicability of the models in this research.

Mohr-Coulomb

Most likely one of the most used soil models in numerical modelling is the basic Mohr-Coulomb model. The model approximates soil behaviour via a linear elastic, perfectly plastic stress-strain relationship. This behaviour is shown on the left of figure 2.10. As shown in the figure, the model response to virgin loading, unloading and reloading is purely elastic. The Mohr-Coulomb model is known to be a crude approximation of real soil behaviour, but is often used to get a first and fast estimation of the relevant parameters and dimensions in geotechnical designs [38]. The formulation of the linear elastic behaviour is known as Hooke's Law. The perfectly plastic failure is defined according to the criterion shown in equation (2.14).

$$\tau_f = c' + \sigma'_n \cdot tan(\phi') \tag{2.14}$$

The shear stress at failure of the soil τ_f is related to the effective cohesion c', the effective internal friction angle ϕ' and the normal effective stress σ'_n.
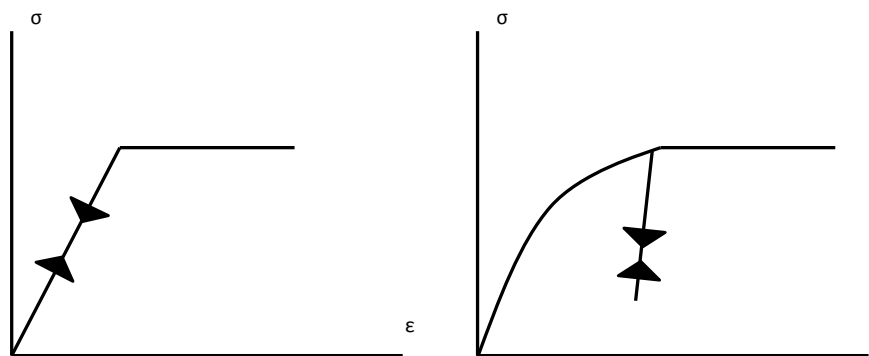
Figure 2.10: The stress-strain behaviour of the Mohr-Coulomb model [l] and the Hardening soil model [r].

Hardening soil

The hardening soil model, often referred to as the 'HS model', uses a non-linear stress-strain relationship which is shown on the right of figure 2.10. Additionally to this non-linear stress-strain behaviour, the different response of soils in unloading-reloading is incorporated. The graph shows that the stiffness is stress dependent in the HS model. The user provides three stiffness parameters at reference pressures: E_{50}, E_{oed} and E_{ur}. The E_{50} stiffness is the secant stiffness at 50% of the failure load, the E_{oed} is the tangent stiffness in a oedometer test and the E_{ur} is the unloading reloading stiffness determined in a triaxial test. Failure of the soil is defined according to the perfectly-plastic Mohr-Coulomb criterion, see equation (2.14). The failure level is defined as a percentage of the asymptote of the hyperbolic formulation of the hardening soil model [38].

Hardening soil, small strain stiffness

The extended HSs model includes the small strain response of the soil. Soil behaves significantly stiffer at very small strains. By including the small strain stiffness response the model is more accurate in cases where small strains are relevant, such as settlements further away from an excavation or during cyclic loading. In this model the small strain response is included via the shear modulus reduction curve: the shear modulus is higher for smaller strains and gradually decreases with increasing strain levels. The $\gamma_{0.7}$ parameter can be used by the user to determine at what strain level the stiffness reduces, the reference small strain stiffness parameter G_0^{ref} determines the starting level of the curve [38], see figure 2.11.
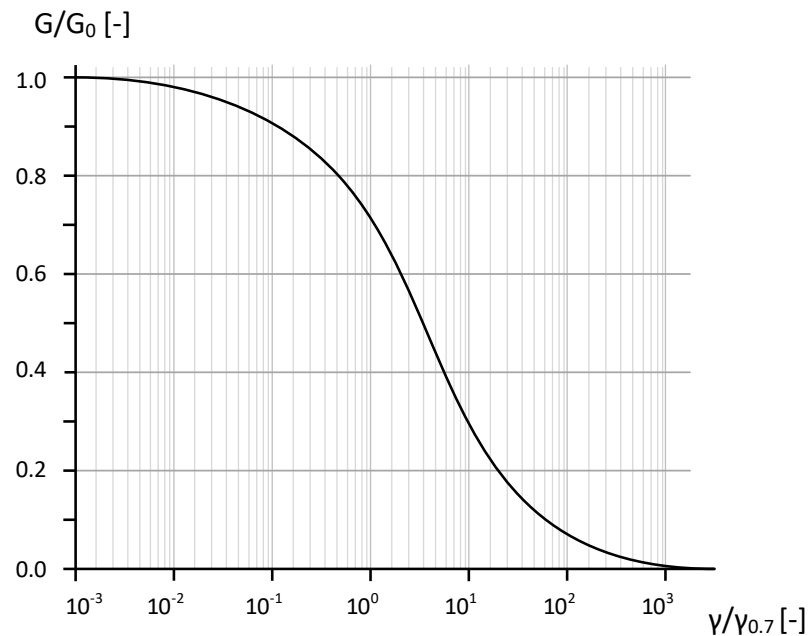
Figure 2.11: The shear modulus reduction curve: soil behaves stiffer at smaller strain levels.

3

Finite element modelling in 2D

The modelling of piles in 2D poses challenges considering the real 3D situation and the 2D modelling options that are available. For a more detailed description of these challenges see the section on 2D FEM modelling in the literature study. The goal of the 2D pile modelling is finding an appropriate single micropile model that can be validated through comparison with full-scale load tests performed on single micropiles. The final goal of this thesis is gaining insight in the group effect for micropiles under tensile loading. Assumptions and decisions made during the 2D modelling phase are related to this final goal.

The selected pile type for the validation of the 2D FEM results is micropile type 'A', see the chapter Introduction. The installation of pile type A follows the hereafter described procedure [7]:

1. The pile tip depth is reached with the double casing rig by boring and flushing the soil between the inner and outer casing with either water or a grout mixture with a high water cement (w/c) ratio (>1.0).
2. After reaching the right depth, the inner casing is removed and a GEWI bar is placed.
3. The water/grout mixture used for the flushing is replaced by a grout mixture with a lower water cement ratio (0.45 - 0.50).
4. Finally the outer casing is pulled up, in steps of 0.5 meter at the time.
5. After each step of 0.5 meter an overpressure is applied to the groutbody. This overpressure is generally 10 to 20 bar. This phase is referred to as the high pressure post grouting phase.

This pile type A is chosen because of its wide usage in The Netherlands and the relatively controllable installation process. In this chapter general background on the different structural elements available in Plaxis 2D is explained first. Afterwards the field data is described, this data includes the geotechnical parameters of the site and the load-displacement data from six micropile load tests in two different geological layers. Following the field data description is the section on the validation of the final 2D FEM models. Lastly the field data and 2D FEM model results are discussed.

For a more detailed understanding of the finite element models made in 2D the reader is redirected to the Appendix. In Appendix A.3 the development process of the 2D FEM models is examined. The choices for the soil model and structural elements are described first and the input parameters and mesh are presented afterwards. Following the description of the model mesh is the section on the FEM 2D intermediate model results and a comparison of these results to the field data. After this section the final 2D FEM model is described in more detail.

3.1. Pile model options in 2D

Micropile type A consists of a GEWI bar and a grout body, both elements are modelled in the 2D FEM program Plaxis. Several structural elements are available to model these parts of the micropile. In this section the different available options are described.

3.1.1. Structural options

In Plaxis the following structural options are considered relevant for pile modelling:

◇ Node-to-node anchor
◇ Plate
◇ Volume element
◇ Embedded beam row

All structural options are visualised in figure 3.1, stretched in the out-of-plane direction. The node-to-node anchor connects two nodes in Plaxis and gives the user the possibility to define the axial stiffness EA and an out-of-plane spacing of the anchor. There is no interaction with the soil between the nodes of a node-to-node anchor. A plate requires the input of several additional parameters. Next to the axial stiffness EA, a plate has a flexural rigidity EI and therefore a thickness d. Moreover the weight γ and the Poisson's ratio ν are defined. Plate elements can have interfaces where the soil-structure interaction is modelled with adjusted parameters. Structural volume elements are generally defined as linear-elastic, non-porous 'soil materials'. This requires the input of a self-weight γ, stiffness E and Poisson's ratio ν. Just like plate elements, volume elements can have user defined interfaces that govern the soil-structure interaction behaviour.

The embedded beam row (EBR) is a more advanced feature which has been recently developed and validated, for a more detailed description the reader is referred to the literature study. The EBR requires the input of a self-weight γ, stiffness E and diameter D. Additionally to these common input parameters, the user can define the skin resistance (both axially and laterally) and base resistance of the embedded beam row. To simulate 3D behaviour the interface stiffness factor is introduced (ISF) which corrects the interface stiffness and is related to the shear stiffness of the soil G_{soil}. The behaviour around the skin is linear-elastic perfectly plastic, the behaviour at the base is non-linear [49].

For reliable pile displacements the ISF is difficult but crucial to determine. The interface stiffness factor is dependent on the pile spacing, pile diameter, pile stiffness and soil stiffness. Default values in Plaxis are based on validation of the EBR for stiff piles [47]. These default values for very stiff piles proved to be independent of the pile-soil stiffness ratio. According to the research by Sluis reliable values for less stiff piles, like micropiles, can be obtained through comparison with a 3D model.
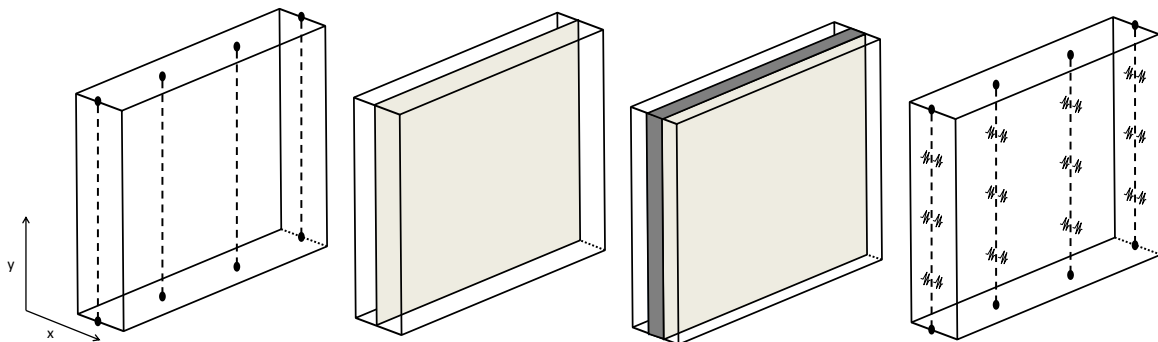
Figure 3.1: Structural options relevant for 2D pile modelling in Plaxis, from left to right: node-to-node anchor, plate, volume element and the embedded beam row.

3.2. Field data

The single pile models are validated through comparison with field data. This field data is obtained from six pile load tests and the geotechnical parameter determination for a construction project in the region of Amsterdam, The Netherlands. In this section the geotechnical data is presented first and the pile load test data is presented afterwards.

3.2.1. Geotechnical parameters

For a large tunnelling project in the center of Amsterdam (North/South metro line) a reliable data set for the soil parameters in this area is available. This data set is based on numerous in-situ and laboratory tests. From CPT data at the site of the test piles, the depth and thickness of the different known geological layers in Amsterdam is derived. For an estimate of the soil parameters, the data from the North/South metro line project is applied to the same geological layers that were identified at the pile load test site. Soil behaviour is known to be highly variable due to heterogeneity, to obtain more reliable parameters a more extensive site investigation should be performed. Because of time constraints and a relatively low sensitivity of the proposed 2D model for the soil input parameters, the currently used correlation is reviewed as sufficient.

The CPT data is presented in Appendix A.1. The height reference of the CPT data is NAP, which is the Dutch national reference height. The ground and water level at the CPT locations are at +0.83 m NAP, -0.37 m NAP respectively for CPT 1 and +0.62 m NAP, -0.58 m NAP respectively for CPT 2. The first 3.50 meter of soil has been pre bored and the bored material is classified according to standard NEN 5104. The pre boring was done because of the presence of cables and ducts in these top layers. In table 3.1 below the general layering at the pile load test site is described.

Table 3.1: An overview of the geological layers, determined from the CPT profiles.

Geological formation	Material	Top level layer [m+NAP]
Fill, man-made	Sand, silty	$+0.83/+0.62$
Dutch peat	Peat	$-2.67/-2.88$
Mudflat deposits	Clay, sandy	-4.50
Base peat	Peat	-10.0
First sand layer	Sand	-12.5
Allerød	Clayey/silty sand	-15.0
Second sand layer	Sand	$-17.0/-17.5$

Both CPT's show the presence of the first and second sand layer at -12.5m NAP to -17.5m NAP and -17.5m NAP to -27.5 NAP, respectively. The second sand layer is thicker than the first sand layer and the cone resistance of the second sand layer is higher. The capacity of the micropiles is based on the shaft resistance developed in the first or second sand layer in Amsterdam, therefore these layers are the most crucial in the model. In figure 3.2 the general depth profile from table 3.1 is visualised, the first and second sand layer are marked.
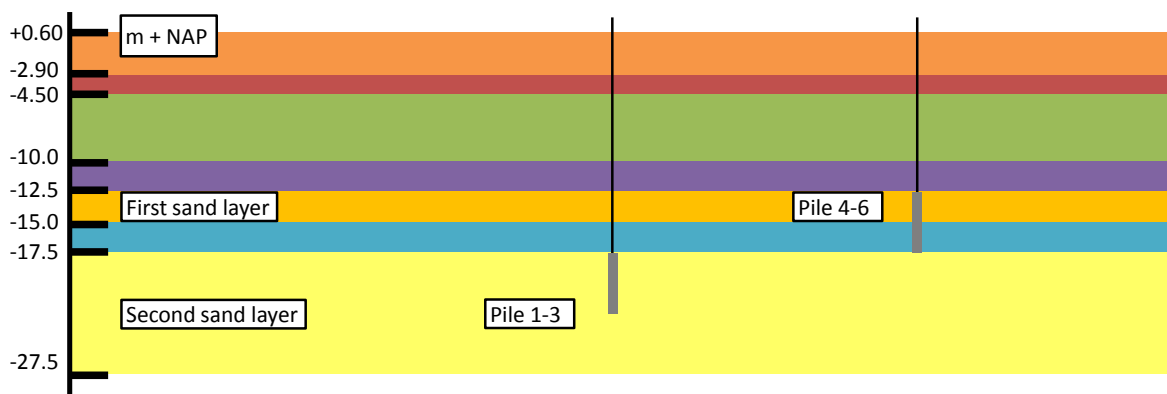
Figure 3.2: General subsurface profile at the pile test site.

3.2.2. Pile load tests

To determine the capacity of type A piles in the first and second sand layer separately, a total of six pile load tests to failure were performed. These tests were performed according to the Dutch guideline CUR236. After the pre loading step of 100 kN six stages of loading and unloading were applied in all tests, for two piles additional loading stages were added. The forces applied at each stage are a percentage of the pre determined maximum failure load: 40%, 55%, 70%, 80%, 90% and 100%. The pre load is applied to calibrate the displacement and load measurement devices. After each loading step there is a short unloading phase where the load level is returned to 100 kN. From these unloading stages the plastic deformation after each loading stage can be determined. Normally piles are loaded upto 115% of their capacity during failure tests, but during the failure tests presented here the predefined failure criterion was already reached at the 100% loading stage. This predefined failure criterion is called 'creep measure'. The maximum allowable value for the creep measure during a pile load test is 2.0 mm according to the CUR 236 [7]. Below in equation (3.1) the formula for the creep measure k_s is given. The difference in displacement u at time t_1 and t_2 divided by the logarithm of the time ratio determines the creep measure.

$$k_s = \frac{u_1 - u_2}{\log\left(\frac{t_2}{t_1}\right)} \tag{3.1}$$

In figure 3.2 the lay-out of the test piles in both sand layers is shown. The data from the pile load failure tests is presented in figure 3.3 to 3.6. All test piles consist of a GEWI 63.5 bar and a groutbody of 5 meters. The first graph shows the time-displacement data from piles 1 to 3 which were installed in the second sand layer and have a total length of 23.5 meters. The pre-calculated capacity of these piles is 1414 kN. The first two loading stages have a duration of 15 minutes, the following three loading stages last 30 minutes. The final loading stage at 100% of the failure load has a duration of 60 minutes.
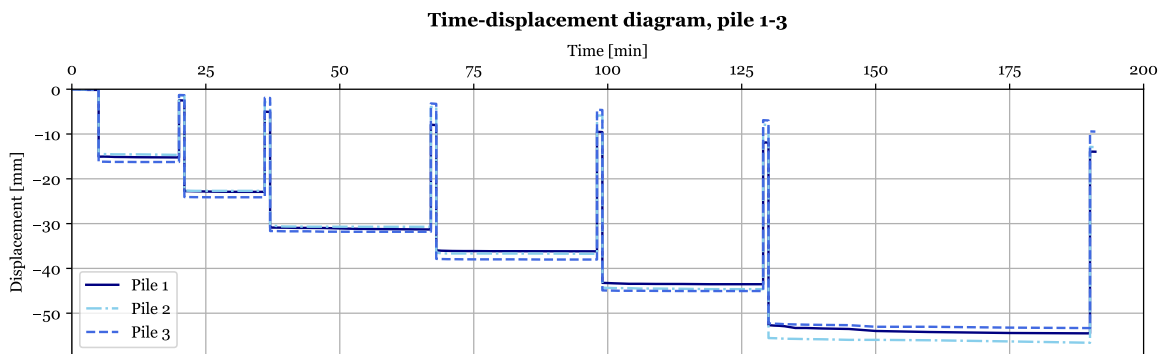
Figure 3.3: Time-displacement behaviour of the pile heads of three micropiles installed in the second sand layer of Amsterdam.

Figure 3.4 shows the time-displacement data from piles 4 to 6 which were installed in the first sand layer and have a total length of 18.5 meters. The determined capacity for these piles is 377 kN. For piles 5 and 6 an additional stable loading stage of 120% of the theoretical maximum capacity was reached. Both piles were tested until failure with loads of respectively 139% (pile 6) and 143% (pile 5).
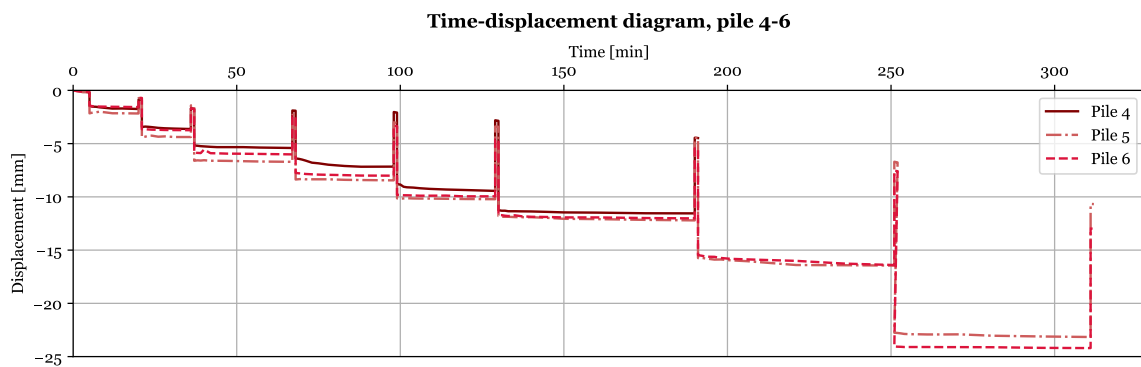
Figure 3.4: Time-displacement behaviour of the pile heads of three micropiles installed in the first sand layer of Amsterdam.

The time-displacement diagrams show the clear distinction between the plastic and elastic deformations during the different loading stages. Moreover, in the data of the load tests performed on pile 4 to 6 the progressive failure mechanism of a tension pile is clearly visible. In engineering a load-displacement diagram is often used for the determination of limiting loads.

The third graph shows the load-displacement behaviour of the first three micropiles. The slight curve in the diagram shows the increasing displacement and decreasing stiffness of the pile-soil response at higher loads. The plastic displacements after each loading stage, visible on the left at a load of 100 kN, gradually increase. This data was processed to make the elastic unloading-reloading stages visible and show the plastic deformation during virgin loading. It must be noted that the processed data is derived from point measurements, no continuous measurements were performed.
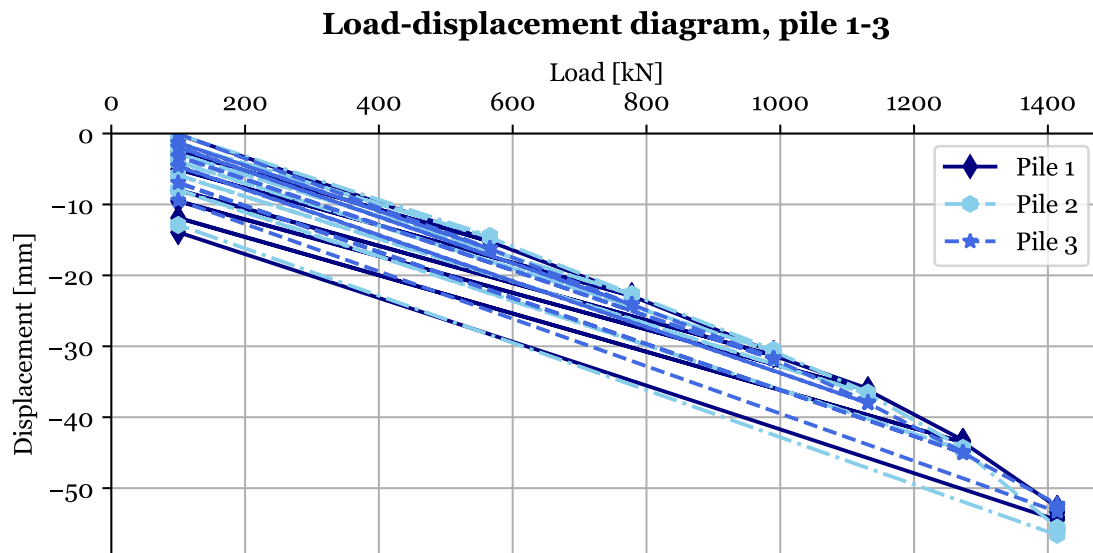
Figure 3.5: Load-displacement behaviour of the three micropile heads installed in the second sand layer of Amsterdam.

In figure 3.6 below the load-displacement behaviour of piles 4 to 6 is presented. Again the data is processed to show linear elastic unloading-reloading curves. The additional loading stages of pile 5 and 6 show the trend towards complete failure of the tension piles. The load-displacement data of each pile is presented separately in Appendix A.2.
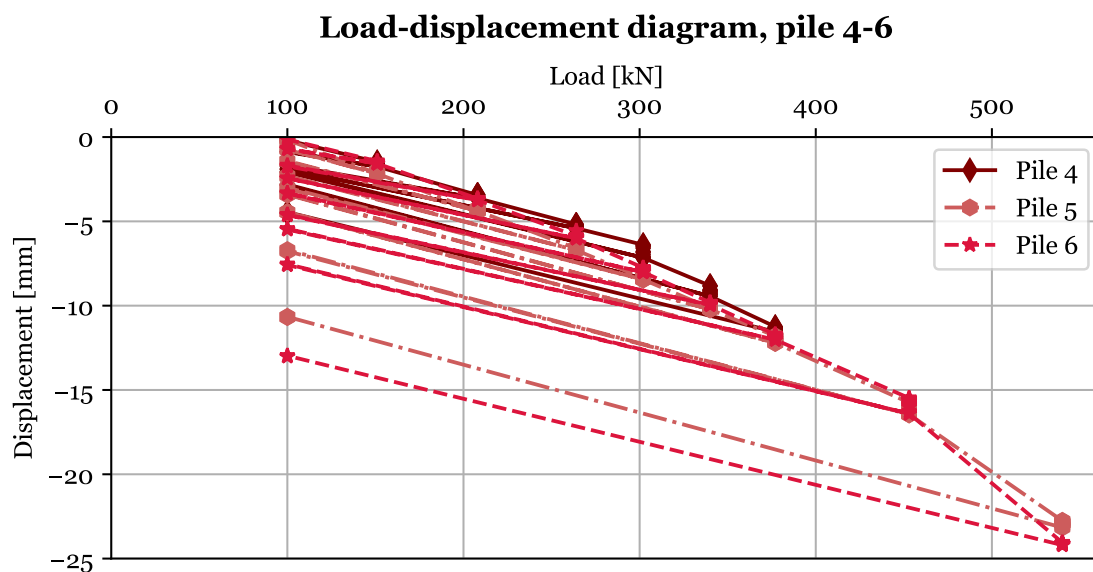
Figure 3.6: Load-displacement behaviour of the pile heads of three micropiles installed in the first sand layer of Amsterdam.

3.3. Validation

In this section the model data from the final Plaxis 2D models and the field tests point data are compared. The final fits with the field data are shown below in figure 3.7 and 3.8. These fits were made with the 2D plane strain EBR model with a linear capacity referred to as 'Plaxis 2D model 3'. The EBR was selected after considering the different 2D pile modelling options described in section 3.1. The soil was modelled with the HSs constitutive model. The development process of the 2D model 3 is explained in more detail in Appendix A.3, where the input parameters and model mesh are presented. The intermediate output results are presented in Appendix A.4. With the intermediate output results that are compared to the field data in Appendix A.5, small improvements could be made that lead to the final 2D models.
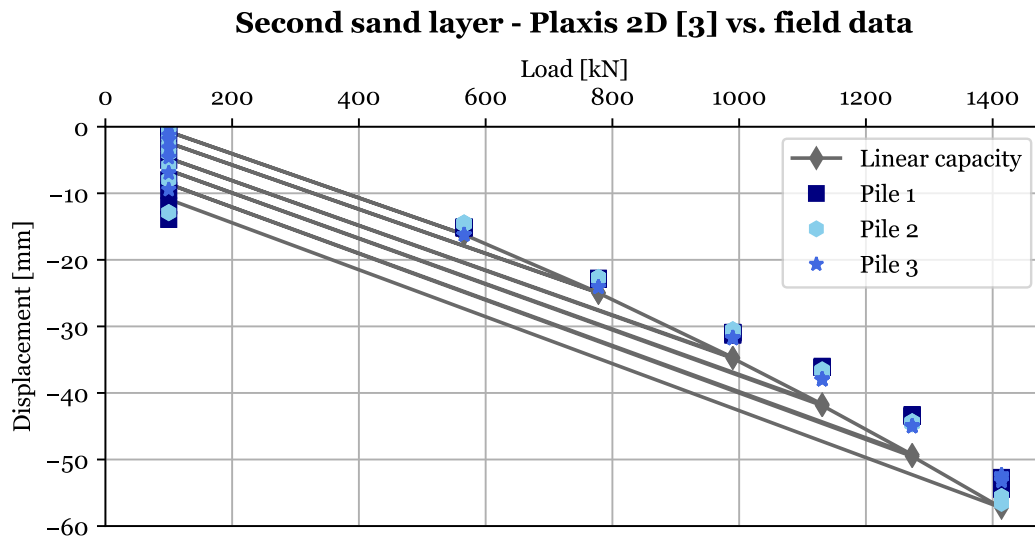
Figure 3.7: The newly fitted 2D model data versus the field data for the second sand layer.

The fit with the pile load tests from the first sand layer is accurate, see figure 3.8. Both the displacements in the loading and unloading stages match with the average of the field data.
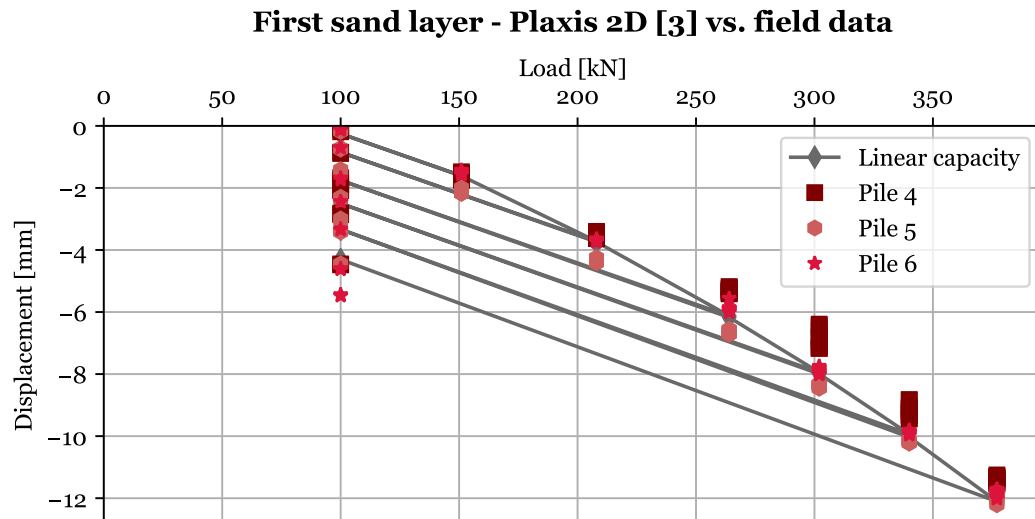
Figure 3.8: The newly fitted 2D model data versus the field data for the first sand layer.

The remaining deviation between the Plaxis model results and the field data could be the result of a non-linear stiffness of the groutbody or/and softening of the grout-soil interface. Furthermore, installation effects cause differences in pile performance of each single pile, this is further elaborated in the Chapter 5.

The deviation is especially visible in the comparison of the field data and Plaxis results of the second sand layer in figure 3.7. For the loading stages a higher initial stiffness that slowly decreases is observed, next to non-linearly increasing plastic strains. This could be the result of softening behaviour in the interface, where the peak strength is reached and the residual strength is lower. A second possible explanation is gradual cracking of the groutbody, leading to a lower stiffness in later stages of the load test and therefore a softer response. This second explanation might explain the difference between the fits for the first and the second sand layer. Since the loads are lower in the pile load tests of the first sand layer, cracking might not be an issue. From the current analysis no conclusive answer can be presented since no specific prove for the explanations is provided.

3.3.1. Discussion 2D model
The presented results and comparison between the 2D model and field data are discussed in this subsection.

Plaxis 2D

With the current two modelling techniques of the interface strength (linear capacity and layer dependent) the strength is either fully user defined or dependent on the subsoil. An important part of this research is investigating the effect of tensile loading of a micropile on the effective stress distribution in the subsurface. Since the capacity of a micropile is based on the development of shear resistance along the shaft, effective stress redistributions caused by neighbouring piles affects the capacity. In the results of all models the effect of the tensile loading on the vertical and horizontal stress levels is relatively limited. In figure 3.9 below it is concluded that both the affected area as the magnitude of the effective horizontal stress changes is small. Whether this is a good match with reality can not be validated with the current data. This is further investigated in the 3D modelling phase.
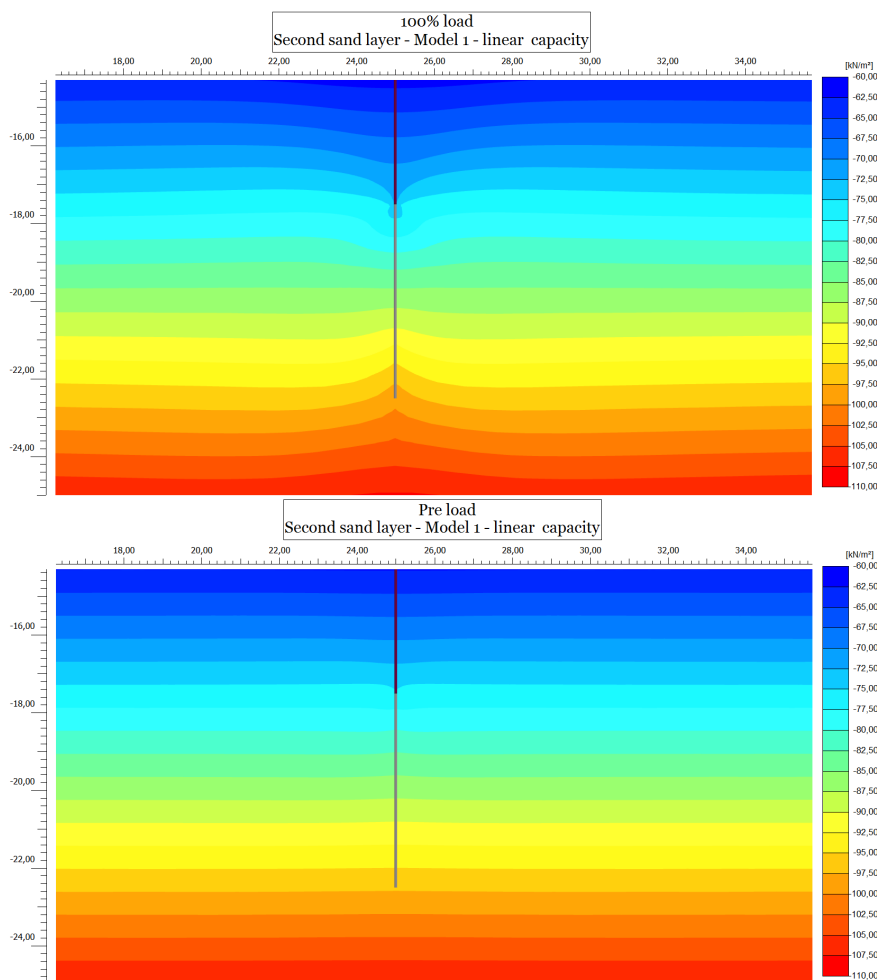
Figure 3.9: The effect of the tension load on the horizontal effective stress distribution in the second sand layer, model 1.

Furthermore, by adjustment of the K_0-value for the layer dependent model the initial effective stress distribution in the layer surrounding the groutbody might not be realistic. A more detailed analysis of the CPT results is needed to determine a realistic limit of the K_0-value for the different geological layers. The effects of installation on the K_0-value are unknown as well, the inclusion of installation effects is further investigated in the 3D modelling part of this research.

The models with EBR's that were made in the axisymmetric environment do not work due to numerical issues. Most likely workarounds are available to solve the current errors. One can think of small adjustments in the geometry to avoid the symmetry axis. As mentioned before this is not done in this stage of the research because of the ambition to model pile groups, for which axisymmetric models are not suited.

Modelling in plane strain has is limitations for piles since properties are averaged in out-of-plane direction. The embedded beam row, which is used in the current 2D model, has a special parameter that governs the interface behaviour: the ISF. A fundamental formulation of this factor does not exist while the model results are very sensitive to this value. In the final model results the ISF was set to 1.0 to create a relatively stiff interface. A better formulation of the ISF, dependent on more than the pile spacing and equivalent diameter, improves the validity of modelling single piles with the embedded beam row.

Field data

The current data set for the soil model is not site specific. This is expected to have a minor influence, since the pile head displacement results are not very sensitive to the soil parameters. But a slightly better fit might be obtained after adjustment of the soil stiffness parameters, since these values partially govern the elastic interface behaviour.

For the current validation only six pile load tests are used. For the 3D modelling phase a broader data set must be used to improve the reliability of the validation. Furthermore, details of the execution of the pile load test and a continuous measurement are not present. With a continuous measurement the behaviour during the load and unloading trajectories could be analysed more detailed as well. Details relating to the load application procedure and calibration of measurement devices can increase the precision of the modelled loading procedure.

3.3.2. Conclusion 2D model

In section 3.3 it is shown that the Plaxis 2D model is very well capable of capturing the load-displacement behaviour of micropiles. The different steps that were needed to fit the model results with the field data are taken into account for the 3D modelling phase. In the 3D modelling phase group effects are investigated after the validation of a 3D single pile model. From the 2D modelling phase it is concluded that both the embedded beam element with a linear pre determined capacity and a layer dependent capacity are suited to fit pile load tests. The soil response in the models, both on stress and strain levels, is significantly different. The influence on the group effect of this difference response is investigated in the 3D modelling phase. Furthermore the validity of the adjusted soil parameters for the layer dependent model is researched.

<div style="text-align: right; font-size: 3em;">4</div>

Finite element modelling in 3D

In this chapter the 3D finite element model is described and validated. After the validation of the single pile model, the group model is described and the results of the group model are presented.

4.1. 3D single pile model validation

For the 3D single pile validation the same field data is used as in the 2D FEM modelling phase. The field data description can be found in Section 3.2. The 3D FEM single pile models are discussed in the next subsection. The presentation of the 3D single pile model results follows after the description of the 3D single pile models. The stress and strain levels in the soil and at the interface of the pile during the pile load test are analysed and discussed. Next to the validation with the field data, the results of the 3D model and a 2D axisymmetric model are compared. The comparison with the 2D model is made to determine the accuracy of the 3D FEM model. The axisymmetric 2D model has a finer mesh and makes use of 15-noded 2D triangular elements instead of 10-noded 3D tetrahedral elements. With more nodes per area and a fourth order instead of second order integration procedure, the stress and strain distribution in the 2D models is more precise than in the 3D models. To prove the general concept of the modelling procedure, field data used for validation is extended for the 2D axisymmetric models. This extended validation is presented in Appendix B.4.

4.1.1. Single pile models

In this subsection the validated 3D models are described. The development process of the lay-out of these models was non-linear and included several modelling options that were reviewed and in the end discarded. The model development process is described in Appendix B.1.

The final 3D single pile model consists fully of volume and interface elements, the meshes are shown in figure 4.1. The size of the 3D mesh is limited at 8.0 x 8.0 x 20.0/25.0 meters. The 3D model size was based on the boundary influences seen in the 2D models and first 3D models. The current size is selected because of the good balance between mesh size and limited boundary influences. The 3D view is filtered in such a way that the residual grout elements and the groutbody elements are visible in the mesh. The three different soil layers are (from top to bottom): mudflat deposits in soft red from 0.0 m to -12.5 m, the first sand layer in light blue from -12.5 m to -17.5 m and the second sand layer in soft green from -17.5 m to -20.0 m/-25.0 m. The residual groutbody is shown as bright green elements and the groutbody is shown in yellow. The visible contour lines are the element deformation contours, the element contours are not explicitly visible.
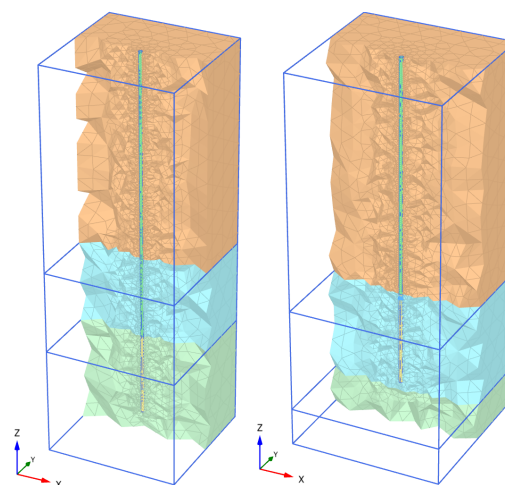
Figure 4.1: 3D meshes for the final model: on the left side the model for the second sand layer pile load tests, on the right side the model for the first sand layer pile load tests.

Mesh refinement and quality

The mesh is made of the standard 10-noded triangles, the mesh size was set at medium coarseness. For a sufficient mesh quality the mesh was refined with a coarseness factor of 0.3536 in a volume around the pile elements. This coarseness factor reduces the element size in the specified area/volume. For a 3D mesh set at medium coarseness the target size of the elements is 0.7089 meter, a coarseness factor of 0.5 changes this target size to 0.3545 meter. With a finer mesh there are more nodes per volume, therefore the stress and strain levels are calculated in more detail. For the second sand layer model the mesh quality, which is defined as the ratio between the inner and outer sphere of an element, was insufficient (< 0.20). Therefore, another larger soil volume around the pile was assigned a coarseness factor of 0.5. The coarseness of the pile elements is set to the maximum value of 8.0. This coarseness factor was chosen because of the small pile diameter and the linear elastic behaviour of the pile: smaller pile elements do not significantly improve the results of the calculation. Smaller pile elements would lead to a more difficult meshing procedure and a slower calculation procedure. All around the volume elements interface elements are active during the calculation. First the volume elements and interface elements representing the upper 12.5/17.5 meters of the pile are reviewed, afterwards the details of the bounded micropile length (groutbody) are explained.

Unbounded micropile length

The behaviour of the upper part of the pile is dictated by the 63.5 mm in diameter GEWI bar. The GEWI bar is not modelled explicitly in these models, the residual grout/betonite/soil mixture around the GEWI bar in the top layers is modelled as one zone of volume elements. This part of the pile is modelled as a stiff element with a weak interface. The modelling approach is chosen because of the almost frictionless behaviour of the GEWI bar in the mixed soil/grout around it, which was measured in the field tests. In these field tests a special coating was applied around the GEWI bar to ensure this nearly frictionless behaviour. With the stiff element and weak interface there is almost no load transfer from the top part of the pile to the soft top layers in the numerical model. Therefore, this modelling approach is deemed sufficiently close to reality. A disadvantage of this approach is that the load-displacement behaviour of the GEWI bar is not included in the model. The EA of the volume elements would have to be equal to the EA of the GEWI bar to include the load-displacement behaviour of the GEWI. As a consequence the upper volume elements would then have to be modelled with a relatively low stiffness, lowering the actual load transferred to the groutbody. In reality almost the full load is transferred by the GEWI bar to the groutbody, due to additional frictionless sleeve around the GEWI bar and the high stiffness of the bar. This frictionless behaviour inside a set of small en stiff volume elements cannot be modelled in a realistic and straightforward manner in the current version of Plaxis 3D. A surface load is introduced in the model at the top of groutbody, to spread the load over the nodes that represent the top of the groutbody. The displacements due to the elongation of the GEWI bar are manually added to the displacements at the center of the top of the groutbody. The elastic elongation of the GEWI bar is calculated according to basic elastic theory, see equation (4.1). The GEWI bar is assumed to be behave linearly elastic, which is an accurate assumption for these steel bars [35].

$$\Delta l = \frac{F}{EA} \cdot l \tag{4.1}$$

Bounded micropile length

The groutbody is modelled as an element with a relatively low stiffness when compared to the stiffness of reinforced concrete, the behaviour of the interface of the groutbody is set to be dependent on the properties of the surrounding soil (Plaxis default option). At the start of the calculation the installation process is simulated in three different phases. The concept of the installation simulation procedure is presented in figure 4.2. Firstly, surface loads perpendicular to the entire surface of the 3D groutbody are activated and the groutbody volume is deactivated (to avoid tension failure detected by Plaxis). This means that there are surface loads active radially at the side of the groutbody and perpendicular to the surface at the top and bottom of the groutbody. The magnitude of these surface loads is set to the grout pressures used in pile installation for the field tests. In the calculation phase after the application of the surface loads, the groutbody element is activated, while the surface loads remain active. With the activation of the groutbody a new equilibrium can be determined with the displaced soil surrounding the groutbody. In the third phase of the installation simulation the surface loads are deactivated and a new equilibrium with the soil response is determined. At the end of the third phase displacements are reset. The installation process is simulated to create a zone with higher horizontal effective stresses around the pile interface, while maintaining the theoretical dimensions of the pile. The red arrows in figure 4.2 represent the increased horizontal effective stress levels at the pile-soil interface.

Most of the horizontal reaction force due to installation process remains in the soil, see the subsection on the 3D FEM results. Without this installation simulation process the capacity and stiffness of the 3D pile model is much lower than the observed capacity and stiffness in the field load tests.
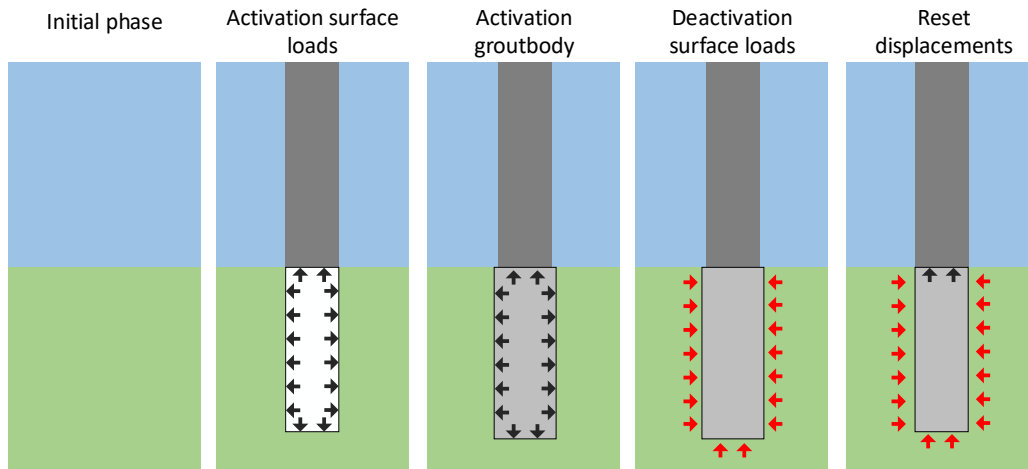
Figure 4.2: A conceptual figure of the five first calculation stages, from left to right: the initial phase, the three steps of the installation simulation procedure and the first loading step where the groutbody displacements are reset and the tensile load is applied.

Since the final 3D single pile model consists only out of volume and interface elements, a 2D axisymmetric model is developed as well. The 2D axisymmetric option was not used in the 2D FEM modelling phase because of stability issues with line elements in the symmetry axis. This is no longer an issue with volume elements as pile model. The 2D axisymmetric model is a fast and accurate model, used as comparison for the accuracy of the 3D model results. The 2D axisymmetric model mesh and input parameters are described in Appendix B.3. The input parameters of the final 3D single pile models are presented in Appendix B.2.

4.1.2. Single pile model results

In this subsection the results of the final 3D FEM model are presented. The results are presented for the two validation cases. For each case the following results are presented: the load-displacement diagram, the development of the relative shear stress on the interface, the development of the horizontal effective stress in the soil and the vertical displacements in the soil. First the results of the three pile load tests installed in the second sand layer of Amsterdam are presented, afterwards the results of the pile load tests performed in the first sand layer of Amsterdam are elaborated.

Results second sand layer model

Below in figure 4.3 the load-displacement diagram of the 3D model is shown. The different loading and unloading stages are the same as applied in the pile load tests, see subsection 3.2.2.
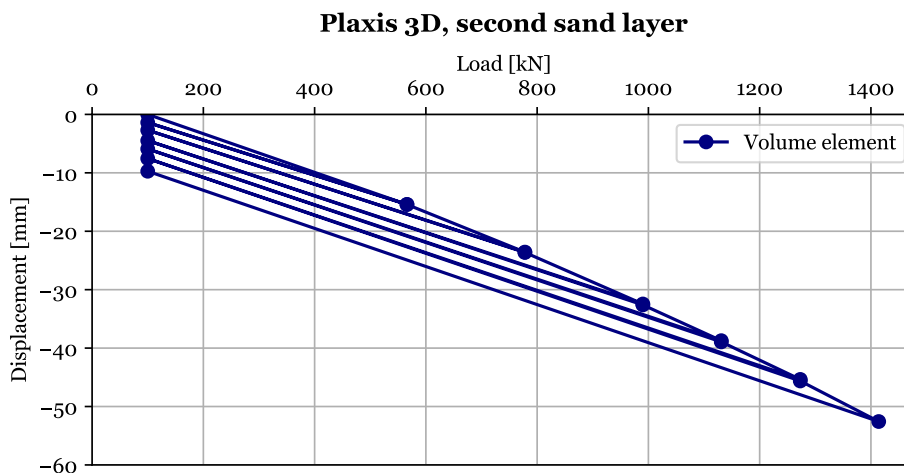
Figure 4.3: The load-displacement diagram of the Plaxis 3D model for the second sand layer.

The increasing amount of plastic displacements after each loading phase is due to partial failure in the interface of the groutbody. Since the groutbody is modelled as relatively soft, the upper part of the groutbody displaces more and the maximum shear stress at the interface is reached sooner than in the lower parts of the groutbody. In figure 4.4 the development of the relative shear stress on the interface is shown. The relative shear stress, τ_{rel}, is a dimensionless parameter and determined according to equation (4.2). In the equation τ_{rel} is calculated by dividing τ_{mob}, the actual developed shear stress at the interface, with τ_{max}, which is the maximum shear stress possible at the interface.

$$\tau_{rel} = \frac{\tau_{mob}}{\tau_{max}} \tag{4.2}$$

In figure 4.4 a frontview is given of the interface of the groutbody. The relative shear stress is shown on a scale from zero to one, zero being the circumference of the groutbody. In the results some local fluctuations can be seen. This is most likely due to the coarser mesh and lower element quality in the 3D model. Since the maximum shear stress on the interface is increased by the simulated installation phases it is not constant around the interface. Despite the fluctuations, the increasing mobilisation of the shear stress over the depth of the groutbody during the different loading stages is clearly visible.
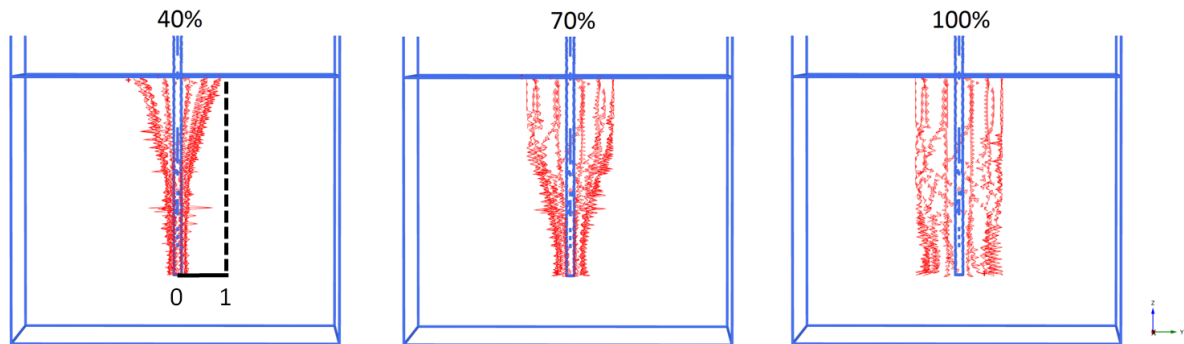
Figure 4.4: The relative shear stress development on the interface of the Plaxis 3D model for the second sand layer.

Next, the development of the effective horizontal stress in the soil is shown. The horizontal effective stress is directly related to the maximum shear stress than can be mobilised at the interface. Since the horizontal effective stress state of the soil is affected by the pile load test these results are relevant for further stages of the research related to the pile-soil-pile interaction. The results of the 3D model are presented for a cross section from [3.9;4.0] to [8.0;4.0] over a depth of about 9 meters around the groutbody. This cross section is made for easy comparison with the 2D axisymmetric model results.
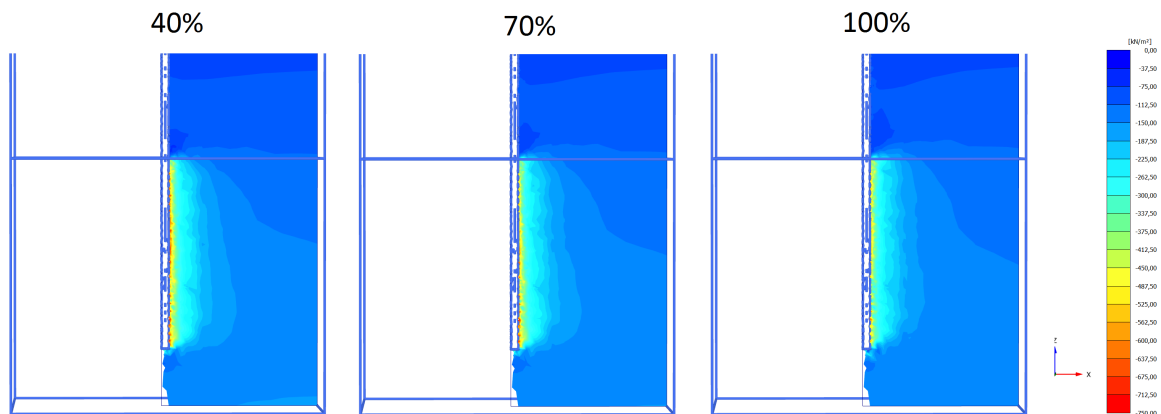
Figure 4.5: The horizontal effective stress development in the Plaxis 3D model for the second sand layer.

The high horizontal stresses around the groutbody gradually decay, there are two explanations for this trend. First of all, the finite element calculation procedure is, simply speaking, solving unbalanced equations to determine equilibrium. Due to the simulated installation process very high horizontal stresses are introduced in the soil. For each loading stage these stresses are spread over more elements to reach a new equilibrium and therefore a small portion of the installation effect is lost. How installation affects the stress levels around the groutbody during its lifespan in reality remains unknown, no conclusive data or research is available for comparison. Secondly, the tensile force introduced in the groutbody affects the principal stress direction in the interface. After the simulated installation process the principal stress direction at the interface is horizontal, after introducing the the tensile force the principal stress is rotated by approximately 45 degrees. This lowers the horizontal effective stress in the soil, the principal stress rotation is shown in figure 4.6, where output of the 2D axisymmetric model is shown.

After the installation phases

After the 100% load phase
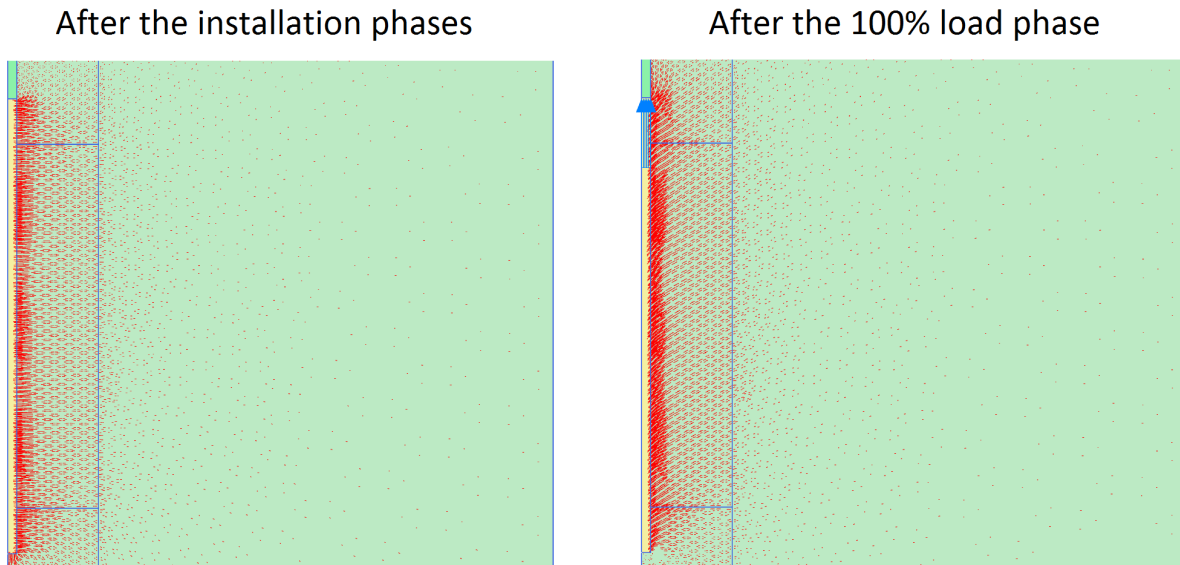
Figure 4.6: The principal stress direction compared: after the final installation stage [l] and final load stage [r].

Lastly the vertical displacements in the soil are presented as output. The vertical displacements are presented to show the displacements in the grout body and the interaction with the surrounding soil. The scale in the figure starts at 0.00 mm (dark blue) and goes up to 2.00 mm (dark red). This is scale is chosen to show a clear distinction between the model displacements in the 40% and 100% load phases. Moreover, peak friction at the interface is developed at pile displacements of 2.00 mm to 10.00 mm [19].
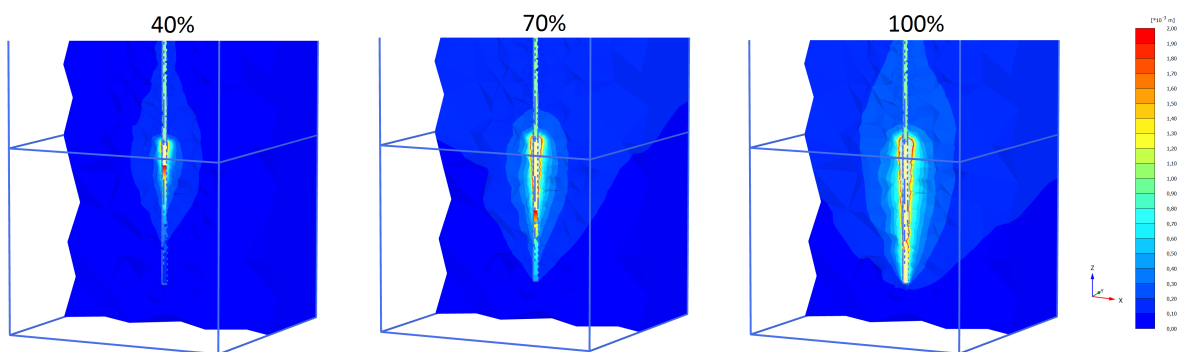
Figure 4.7: The development of the vertical displacements in the Plaxis 3D model for the second sand layer.

Results first sand layer model

After the model for the second sand layer a similar model was made to validate the modelling approach with the field data of the pile load tests conducted in the first sand layer. Below in figure 4.8 the load-displacement diagram of the first sand layer model is shown. Again the loading and unloading stages are the same as in the field data and the different stages are clearly visible in the results.
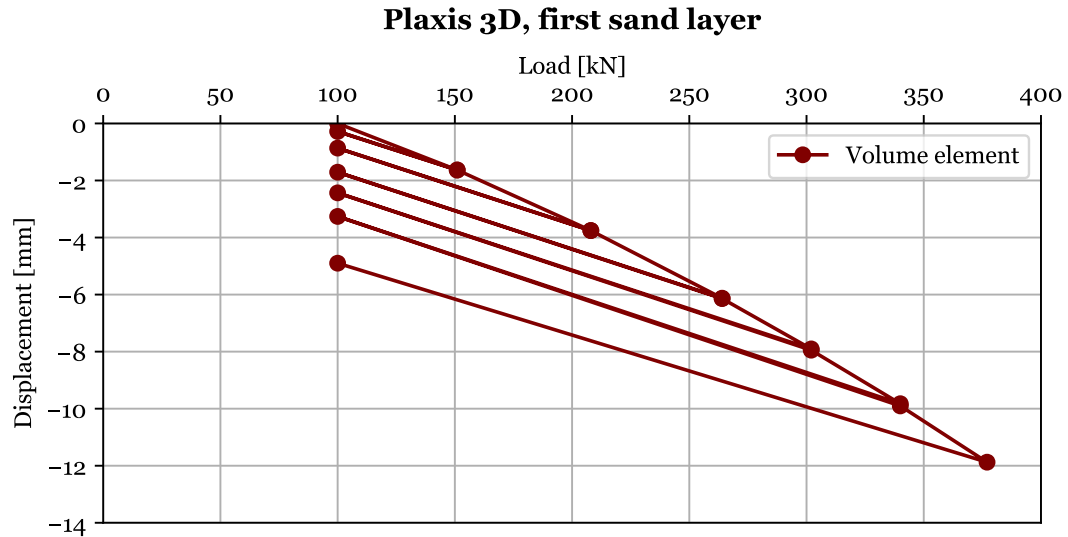
Figure 4.8: The load-displacement diagram of the Plaxis 3D model for the first sand layer.

The relative shear stress is presented in the same way as for the second sand layer, where 0 shear mobilisation is shown at the circumference of the pile and the maximum level is 1.0. Again the gradual mobilisation over the different loading stages is shown, although the shear stress mobilisation proceeds at a relatively larger surface for earlier loading stages compared to the second sand layer model.
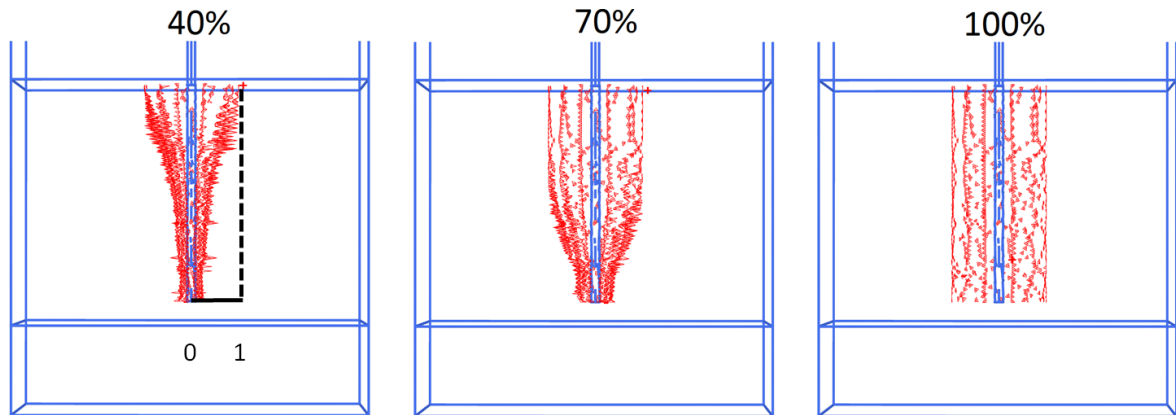
Figure 4.9: The relative shear stress development on the interface of the Plaxis 3D model for the first sand layer.

Due to varying grout pressures used during installation of the piles in the first sand layer, the horizontal effective stresses along the upper four meters of the groutbody are lower. Because of the large range in stresses the decrease in horizontal effective stress of the different loading stages is more difficult to distinguish in figure 4.10. Nevertheless, the decay in horizontal effective stress can be seen especially around the interface of the groutbody.
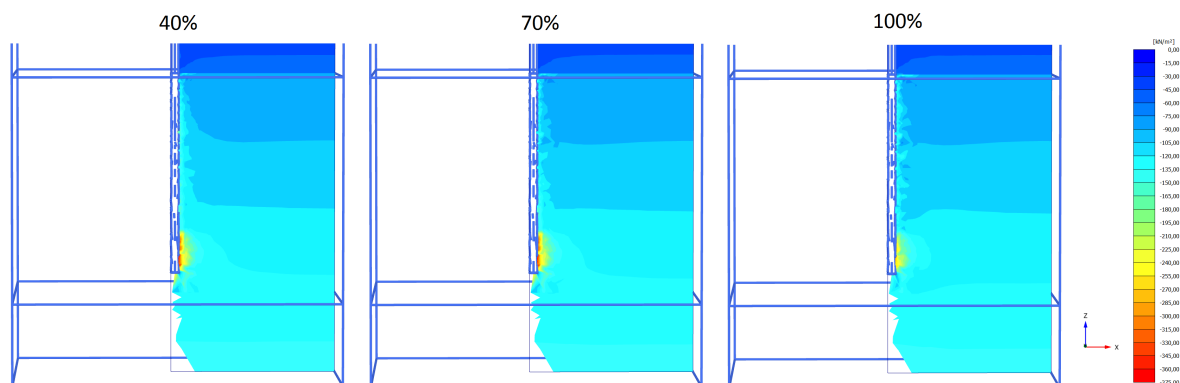
Figure 4.10: The horizontal effective stress development in the Plaxis 3D model for the first sand layer.

In figure 4.11 the vertical displacements during the different phases are presented. The scale is adjusted, compared to the results of the second sand layer model, it ranges from 0.00 mm to 1.00 mm. This lower range is chosen because of the lower loads and displacements in this model. Although the range of displayed vertical displacements is very small, the gradual development of the displacements in the groutbody and surrounding soil are clearly visible.
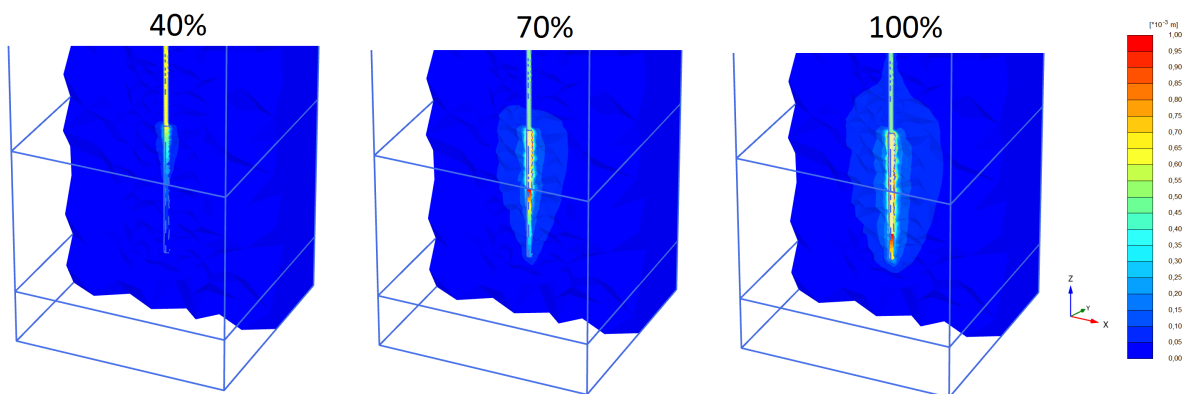
Figure 4.11: The development of the vertical displacements in the Plaxis 3D model for the first sand layer.

4.1.3. Validation
The load-displacement results of the 3D micropile models are validated through comparison with field data. The stress distribution in the soil of the 3D models is compared with the stress distribution in the 2D axisymmetric models to verify the accuracy of the 3D models.

3D and 2D model comparison

In the figures below the horizontal effective stress distribution of the 2D and 3D models are compared. Quite significant differences are seen, these differences are both due to the mesh accuracy and variation in the chosen input parameters. In figure 4.12 the comparison for the first sand layer is shown, the scale ranges from 0.0 kN/m^2 (dark blue) to -375 kN/m^2 (dark red). Both the 3D and 2D output are shown with the same scale range for the horizontal effective stress. The first significant difference that can be seen is the horizontal effective stress distribution at rest, at the right boundary of both the 2D and 3D models. Due to different K_0-parameters that are used in both models the initial horizontal effective stress level in the 3D model is significantly higher. A reliable K_0-parameter is difficult to estimate, see Appendix B.2 for a more elaborate explanation of the chosen K_0-parameters. The difference in decay of the horizontal stress of the different phases is due to a different mesh accuracy. The 3D model consist of 10-noded triangular elements where the 2D model consists of 15-noded elements. This accuracy is also the reason a higher K_0-parameter was used in the 3D calculations: this compensates for the more irrelugar horizontal effective stress distribution after the installation simulation. When a lower K_0-value is used for the 3D calculations the capacity and stiffness of the modelled micropile are significantly lower than those of the field micropiles. Another solution would be a more refined mesh, this option is not chosen due to time constraints for this research. This lower accuracy and the effects on the chosen input parameters must be taken into account for the modelling of the micropile group in the next section of the research. With the modelling of the micropile group the balance between accuracy and speed of the model will become more critical. Unfortunately the results of the group modelling can not be compared with a 2D axisymmetric model.
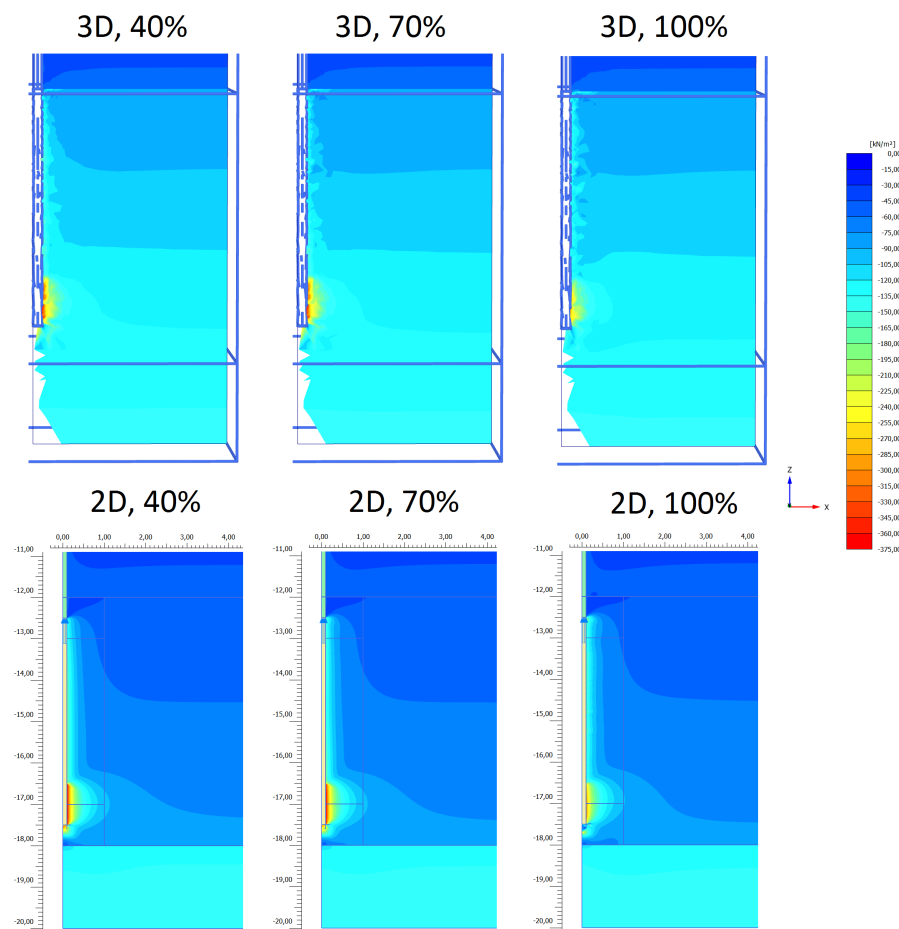
Figure 4.12: Comparison between the horizontal effective stress distribution in de the 2D and 3D model for the first sand layer.

The comparison for the second sand layer shows a greater match between the 3D and 2D model results. This mainly due to the fact that the same value was used for the K_0-parameter in the 3D and 2D model. Over the length of the groutbody in the second sand layer no variation in grouting pressures was applied. The horizontal effective stress levels close to the groutbody are equal over the depth of the pile shaft in this model, the degradation of the horizontal effective stress due to the tensile loading is more clearly visible in the comparison. A clear trend in the decay of the horizontal effective stress level from the top of the groutbody downwards is observed.
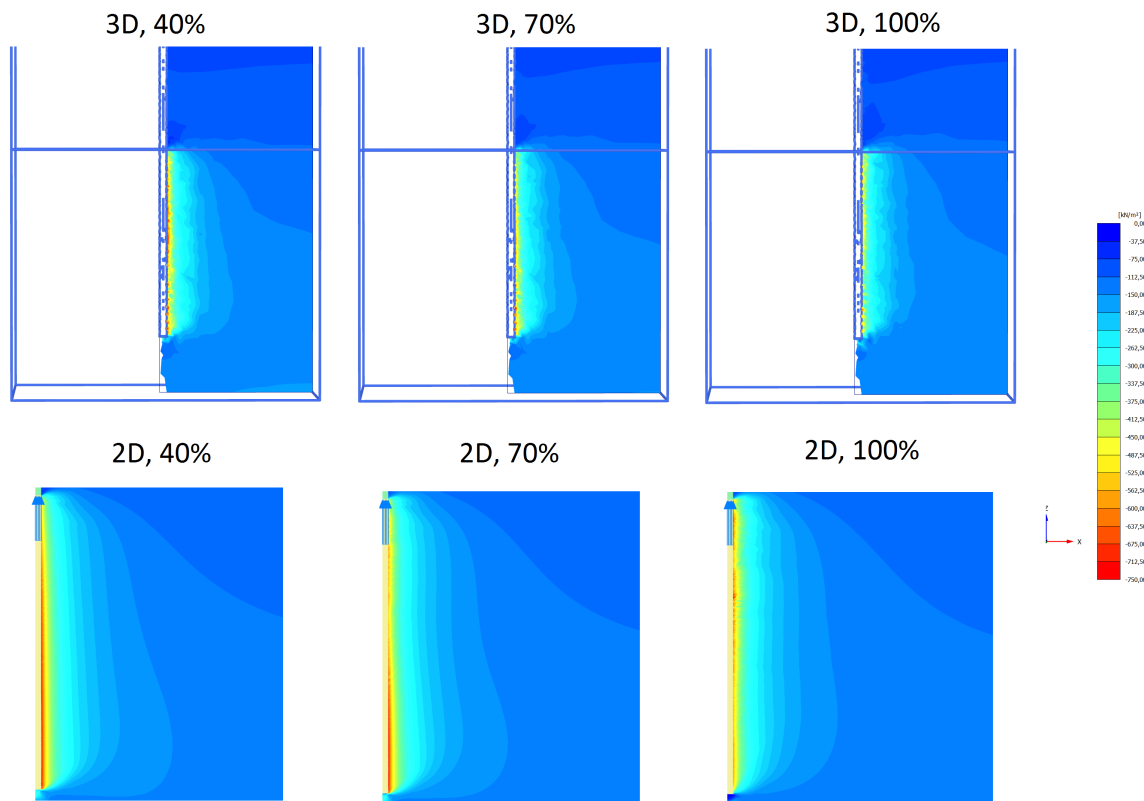
Figure 4.13: Comparison between the horizontal effective stress distribution in de the 2D and 3D model for the second sand layer.

It is concluded that the precision of the finer mesh of the 3D model for the second sand layer is sufficient to determine the degradation of the horizontal effective stress at the interface and in the far field. In further stages of this research at least the same refinement must be used for the 3D micropile group models. No further investigation into mesh refinements for the single pile model are performed at this stage since the 3D micropile single modelling concept is proven to accurately model the load-displacement behaviour with the current meshes, see the next paragraph.

Field data comparison

The load-displacement diagrams of both the 3D model for the first and second sand layer are plotted with the point data of the field tests. In the results comparison of the second layer it can be seen that the displacements towards failure are at the lower boundary of the field data variation. This behaviour is due to a constant groutbody stiffness in the 3D model, in reality the stiffness of the groutbody decreases with higher loads. This non-linear stiffness of the groutbody is mostly due to cracking of grout [35]. The overall fit is good: the deviations between the model and the average field data remains in the range of the variation seen within the field data.
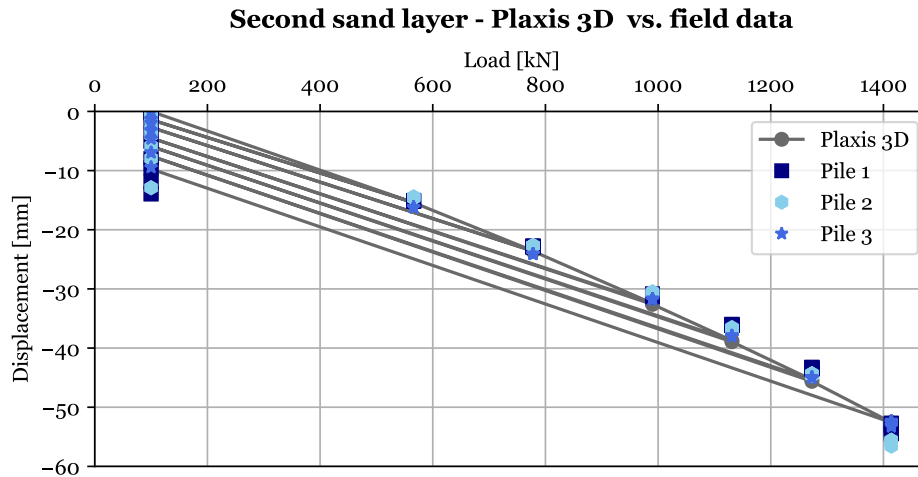
Figure 4.14: The load-displacement diagram of the Plaxis 3D model for the second sand layer.

The most significant fit parameters were the groutbody stiffness, the soil strength and horizontal effective stress levels. The reader is referred to Appendix B.2 for a more detailed explanation of the chosen input parameters. In the comparison with the data of the first sand layer it can be seen that the model fit is good as well. The models follows almost exactly the average field data trend, due to the lower loads it is likely that the non-linear behaviour of the stiffness of the micropile is of less significance.
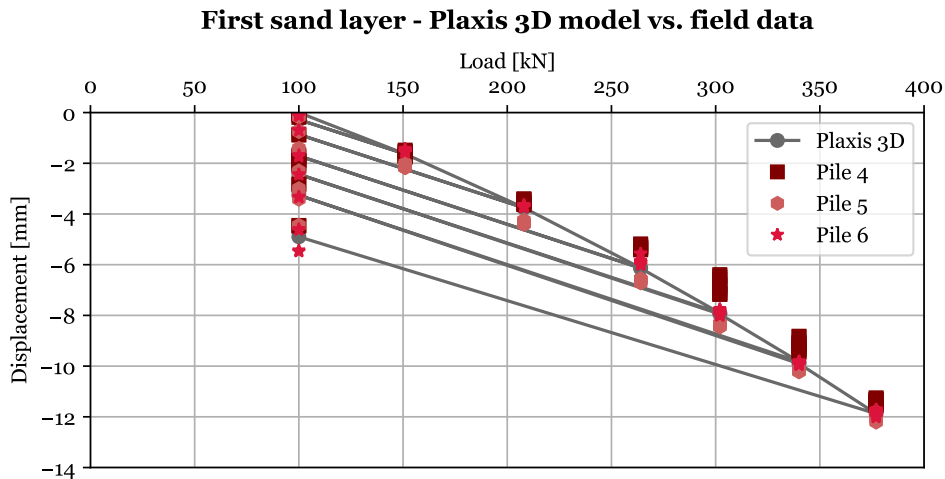
Figure 4.15: The load-displacement diagram of the Plaxis 3D model for the first sand layer.

For both Amsterdam sand layers the 3D FEM models show the same load-displacement behaviour as found in the micropile load tests. The validation is extended in Appendix B.4 with a micropile load test data set from The Hague. This validation extension is done to prove the modelling concept works for geologically differing soil conditions and piles installed by varying parties.

4.2. 3D pile group models

In this section the 3D pile group modelling research is described. The model geometry, pile group lay-out and parameter variations are explained. The final pile group models, their mesh and input parameters are elaborated in Appendix B.5.1.

4.2.1. Model dimensions

The group effect in axially loaded tension pile groups is relevant for construction projects where dozens of micropiles are closely spaced to prevent uplift. For this research a virtual pile group in soil conditions equal to the Amsterdam field data set is made, but with realistic dimensions for a construction project. The piles are assumed to be installed from -11.0 m NAP to -22.5 m NAP, where the length of the micropiles in the sand layers (10.0 m) is considered to be transferring load to the surrounding soil. In figure 4.16 a simplified cut of the 3D group model is shown. The different soil layers are shown according to section 3.2 of Chapter 3. The soft top layers are modelled as one layer and the Allerød and first sand layer are modelled as one, which is the same approach as for the single pile validation. The model includes the environment near the micropiles and stops at the boundaries of the building pit, the mesh starts at -11.0 meters. The stress history is included in the soil parameter sets as a pre-overburden pressure (POP). The additional soil weight at the boundary of the building pit is neglected. This simplification is expected to have a limited influence on the stress level in the models, the horizontal effective stress levels at the pile-soil interface are dominated by the installation procedure.

The pile spacing is varied in the research to investigate the the significance of this parameters in the group effect, see subsection 4.2.2. The geometry presented in figure 4.16 is adjusted in such a way that the minimally required boundaries, as found in the 3D single pile model validation, are maintained.
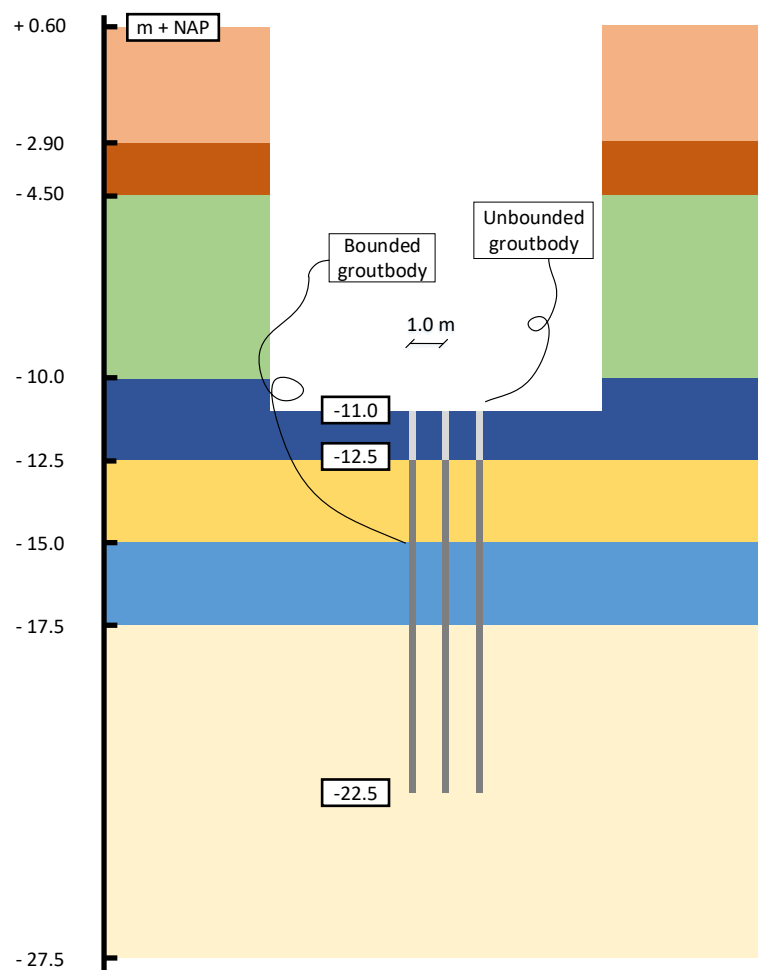
Figure 4.16: An exemplary simplified cross-section of the 3D group model.

Pile group lay-out

First different model lay-outs are investigated, in the final model lay-out a center group pile must be available to be compared with a single reference pile. This can be achieved with three basic lay-outs: a group of five piles, a group of nine piles and an 'infinite' pile group by using symmetry. The pile group lay-out investigation is presented in Appendix B.5. From this investigation it is concluded that the nine pile group is the most useful lay-out for this research. For the nine pile group three different center-to-center spacings are investigated: 1.0 meter, 2.0 meter and 3.0 meter. Since the pile diameter D is taken as constant (0.20 meter) in this research, the center-to-center distance is expressed in diameters: 5D spacing, 10D spacing and 15D spacing. These spacings are either realistic for micropile practice (10D and 15D cases) or interesting to research due to expected strong interaction effects (5D spacing). All piles are installed and loaded simultaneously in the model.

Pile group loading

Each pile in the pile groups is loaded according to the prescribed loading procedure for production piles [7]. The applied percentile loading stages are the same as for the pile load tests described in section 3.2.2. The 100% load in the group models is equal to the 100% load of 880 kN applied in the acceptance tests for the production piles of the Amsterdam case, see Appendix B.8.

4.2.2. Parameter variations

Next to the pile group spacing the soil stiffness is varied to determine the influence of the soil stiffness on the group effect. The current group effect factor f_2 in the Dutch national annex is one of the main reasons that led to this research, see subsection 2.1.1. The factor is based on the theory that the development of shear stress along the micropile shaft leads to a reduction in horizontal effective stress influencing the capacity of a neighbouring pile. The group effect factor for both strength and stiffness calculations therefore depends on the following parameters: pile length, diameter, horizontal effective stress level at the interface, internal friction angle, cohesion and pile group lay-out. To limit the scope of the research, only the soil stiffness is varied next to the pile group spacing. The soil stiffness influences the horizontal effective stress distribution in the soil, whether this has a positive or negative impact on the group effect is unknown. The stiffness of soil is often an uncertain parameter in projects and can vary by a factor of 3-8 based on CPT correlations [26]. Due to this great variation in practice and the uncertain impact of the soil stiffness its influence is included in this research.

As described in subsection 2.1.1, there are two failure mechanisms defined: either the slip capacity of each individual micropile is reached or the pull-out of a soil plug occurs. For the 5D meter and 15D spacings cases a clear difference in failure mechanism is expected. Where the 5D spacing case is more likely to show soil plug pull-out behaviour, the 15Ds spacing case is more likely to show failure on individual slip capacity. The following parameter sets are used:

Standard case:
- Group of nine, 10 meter long piles, internal spacing of 1.0 meter (5D)
- Group of nine, 10 meter long piles, internal spacing of 2.0 meter (10D)
- Group of nine, 10 meter long piles, internal spacing of 3.0 meter (15D)

Stiff case:
- Group of nine, 10 meter long piles, internal spacing of 1.0 meter, 200% soil stiffness
- Group of nine, 10 meter long piles, internal spacing of 2.0 meter, 200% soil stiffness
- Group of nine, 10 meter long piles, internal spacing of 3.0 meter, 200% soil stiffness

The detailed input parameters of the material models can be found in Appendix B.5.1.

4.3. 3D pile group model results

In this section the results of the final 3D pile group models are presented. In Appendix B.6 intermediate results are presented that were obtained during the development of the models. First the load-displacement diagrams of the different models for the standard case are presented and compared. Afterwards the failure mechanism and interaction levels developing in the pile groups are investigated by looking at the horizontal effective stress development, relative shear stress development and total vertical displacements plus phase deviatoric strain levels at the last loading stage.

4.3.1. Standard case

In this subsection the pile group model results for the standard cases are presented. In the next subsection the results from the standard cases are, where relevant, compared to the stiff cases.

Load-displacement behaviour

This research is focussed on the influence of the group effect on the load displacement behaviour of micropiles. Below in figure 4.17 the load-displacement behaviour of the center group piles for different pile group spacings are compared to each other and a reference single pile. All simulations were run until a loading stage where it was not deemed possible to increase the load any further. For almost all model the plastic displacements after the final successful loading stage are close to 8.0-10 mm. In Appendix B.6 the unfinished calculations of the failure stages are presented. The final loading stage for the 5D pile group model is the 60% load stage, for the 10D pile model it is the 95% load stage and for the 15D pile model is is the 120% load stage. The reference piles were run until the 130% load stage, where the plastic displacements after unloading reached approximately 10 mm. For the reference pile one would expected an ultimate limit state when the shear stress on the interface is fully mobilised, but with these high load levels the deformations in the interface of the upper pile section became so large that the horizontal effective stress levels are unreliable, see Appendix B.6 with the intermediate model results. These issue's led to the decision to define failure with the ultimate plastic displacement limit of 10 mm. This limit was chosen because it is the highest plastic displacement level reached in the 3D single pile validation models, test piles field data and the 3D group models.

Load-displacement diagram, pile group spacing comparison, standard case
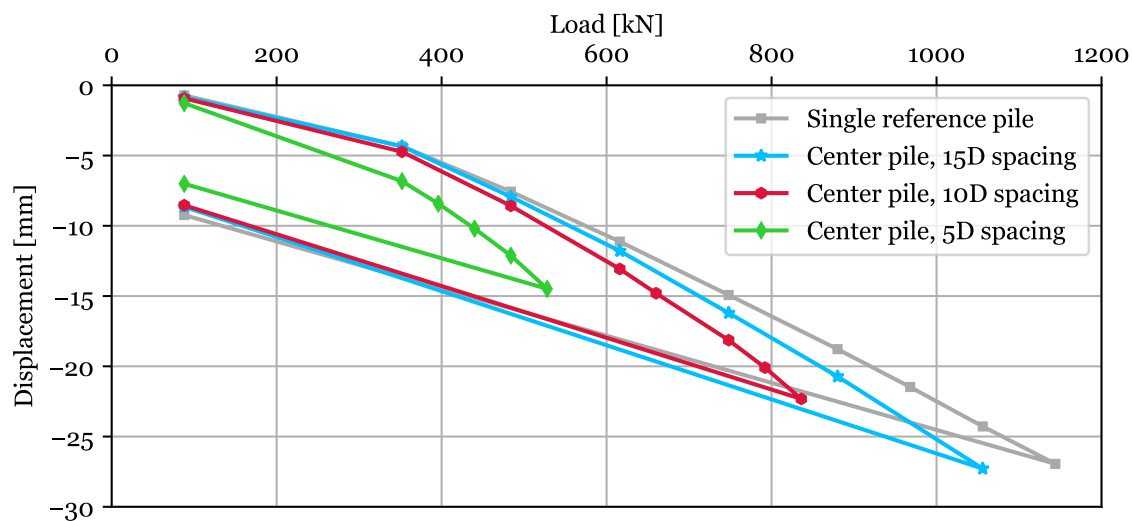
Figure 4.17: The load-displacement behaviour of the three different pile group spacings compared for the standard case.

Comparing the 10D and 5D spacing cases to the 15D spacing case, the decrease in capacity ($F_{r;t;d}$) and secant stiffness at 70% of the ultimate load ($k_{sec;0.7}$) is clearly visible. The capacity reduction ($P_{cap.}$) of the 5D spacing case is 50% and the stiffness reduction ($P_{stif.}$) in the final stage is 8%. For the 10D spacing case the capacity is reduced with 27% and the stiffness reduction is insignificant. The secant stiffness at 70% of the ultimate load level is determined according to equation (4.5). The capacity and stiffness reductions are calculated with equations (4.3) and (4.4), shown below.

$$P_{cap.} = \frac{F_{r;t;d}^{new} - F_{r;t;d}^{old}}{F_{r;t;d}^{old}} \cdot 100 \tag{4.3}$$

$$P_{stif.} = \frac{k_{sec;0.7}^{new} - k_{sec;0.7}^{old}}{k_{sec;0.7}^{old}} \cdot 100 \tag{4.4}$$

$$k_{sec;0.7} = \frac{\Delta F_{ult;0.7}}{\Delta u_{ult;0.7}} \tag{4.5}$$

Horizontal effective stress development

The tension force applied to the piles is redistributed in the soil, as shown in subsection 4.1.2 figure 4.6 this results in rotation of the principal stresses at the pile-soil interface. But the influence of redistribution of the tension force is not limited to the interface. In the following figures the development of the horizontal effective stress during the different loading stages for the differently spaced pile group models are shown. For each model a cross-section is made parallel to the x-axis, at the center of the pile group.

In the figure below the horizontal effective stress development of the 5D spaced pile group model is shown. The scale used for all figures where the horizontal effective stress development is shown ranges from $0.00\ kN/m^2$ (dark blue) to $-950\ kN/m^2$ (dark red). One can clearly see that the interaction between the piles is strong, at the 60% load stages the horizontal effective stress levels around the high pressure zone of the piles are already significantly reduced.
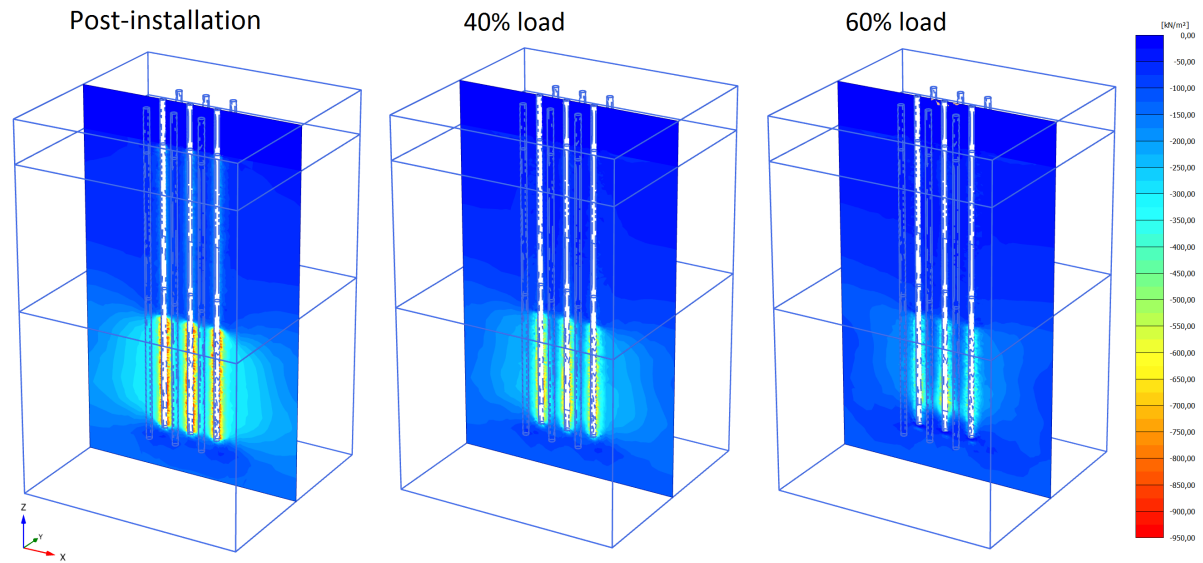
Figure 4.18: The development of the horizontal effective stress at the center of the 5D spaced nine pile group.

As expected for a more widely spaced pile group, the interaction reduces for the pile group with 10D internal spacing, which is presented below in figure 4.19.
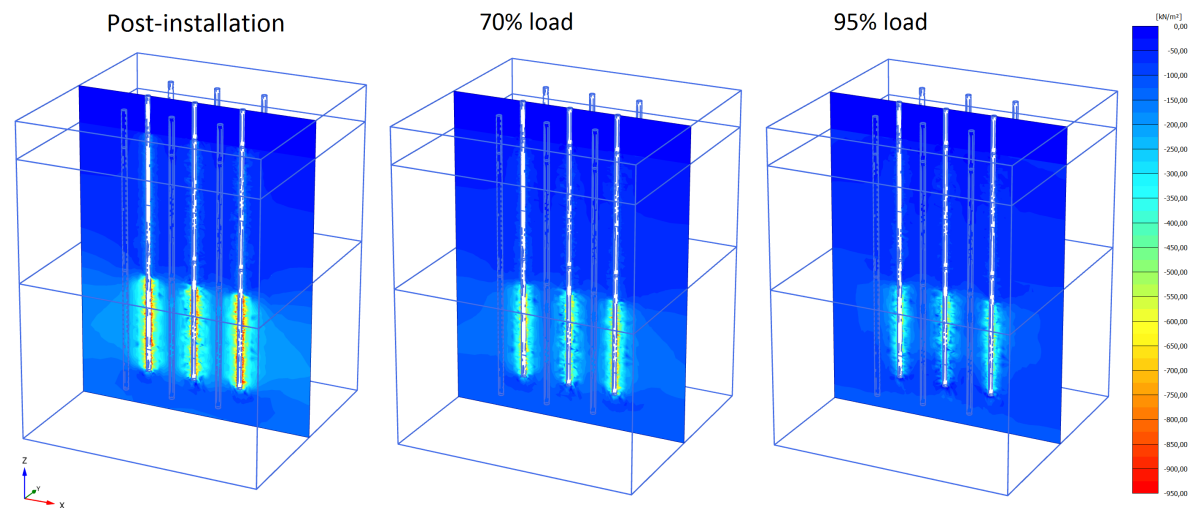
Figure 4.19: The development of the horizontal effective stress at the center of the 10D spaced nine pile group.

The most widely spaced pile group with 15D internal spacing has the least interaction and the highest levels of horizontal effective stress around the individual piles, shown below in figure 4.20.
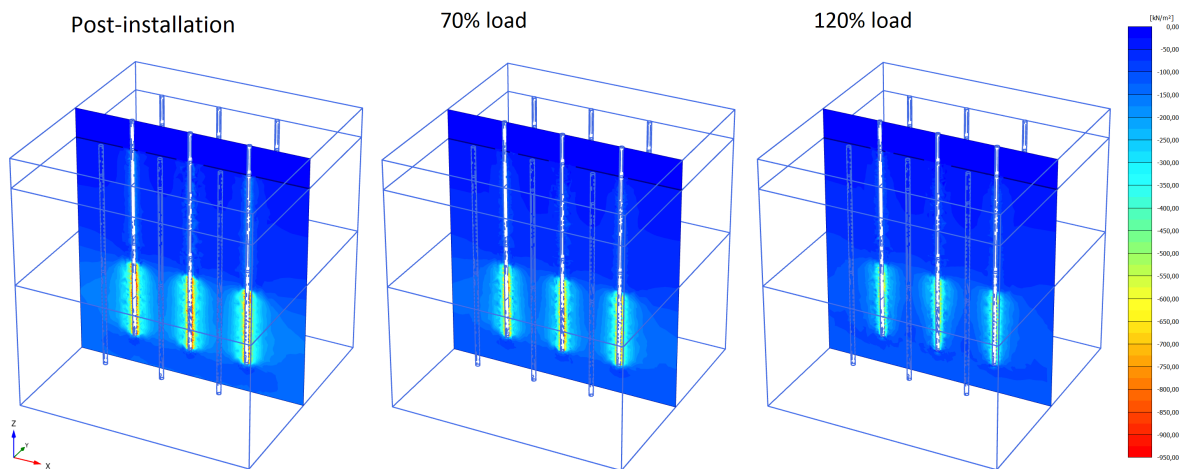
Figure 4.20: The development of the horizontal effective stress at the center of the 15D spaced nine pile group.

Relative shear stress development

On of the possible failure mechanisms is slip of the pile at the interface with the soil. The pile will slip when the shear stress is fully developed at the interface, in Plaxis this can be checked with the development of the relative shear stress (see equation (4.2)) at the interface. The capacity of the micropiles is mainly dependent on the lower section of the pile, where the higher horizontal effective stress levels are present. The relative shear stress development is most relevant for the last few loading stages where the micropile groups approach failure. Therefore the relative shear development will be shown for the interface of the lower pile section, at the higher pressure grouted zone.

Below in figure 4.21 one can see the development of the relative shear stress on the interface of the center pile for the 5D spaced nine pile group. The shear stress is not fully developed at the last loading stage of 60% of the load, therefore it can be concluded that the center pile will not fail by slip. Especially in the middle section of the pile some capacity seems to remain.
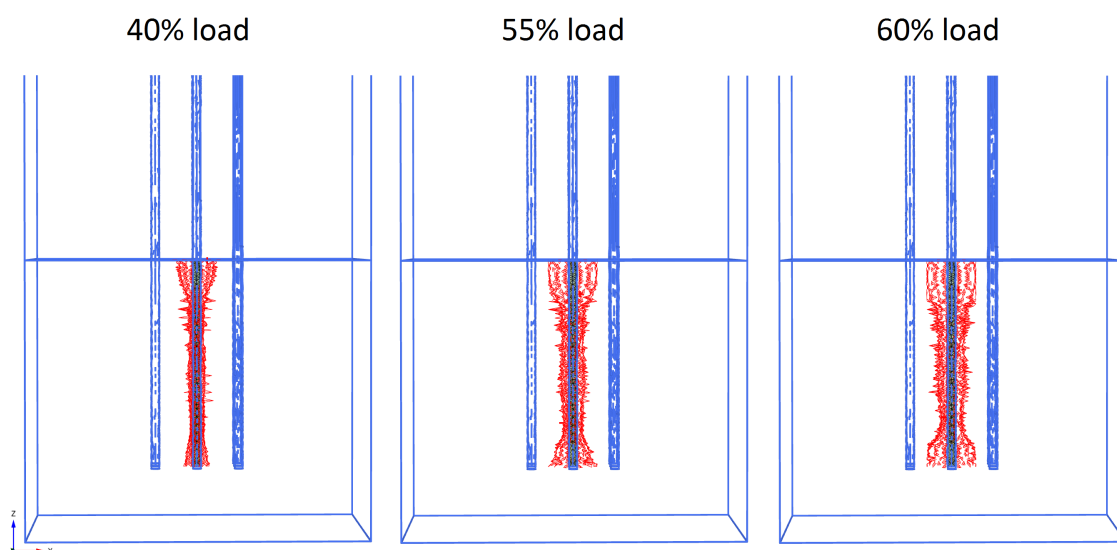
Figure 4.21: The development of the relative shear stress at the interface of the center pile for the 5D spaced nine pile group.

With the 10D spaced pile group a similar trend can be seen, where the shear stress develops fully at the bottom and top of the interface but some capacity remains in the middle. The pattern is less obvious compared to the 5D spaced pile group, but it looks like the center pile will not fail by slip.

| 70% load | 85% load | 95% load |
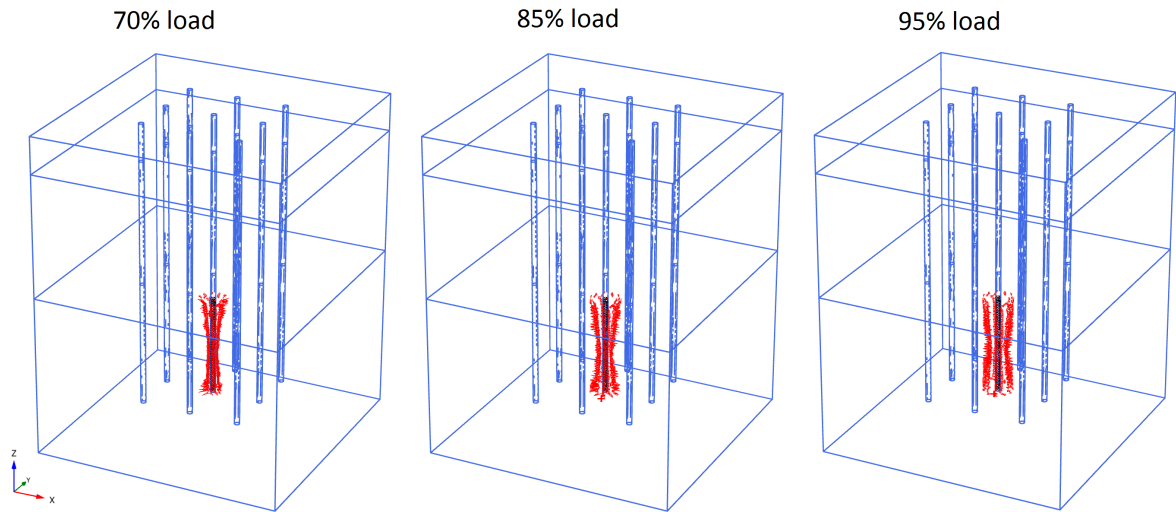
Figure 4.22: The development of the relative shear stress at the interface of the center pile for the 10D spaced nine pile group.

This trend is different for the 15D spaced pile group, where the mobilisation of the shear stress and therefore the development of the relative shear stress resembles the development for the single piles. It can be said the center pile will fail by slip.

| 70% load | 100% load | 120% load |
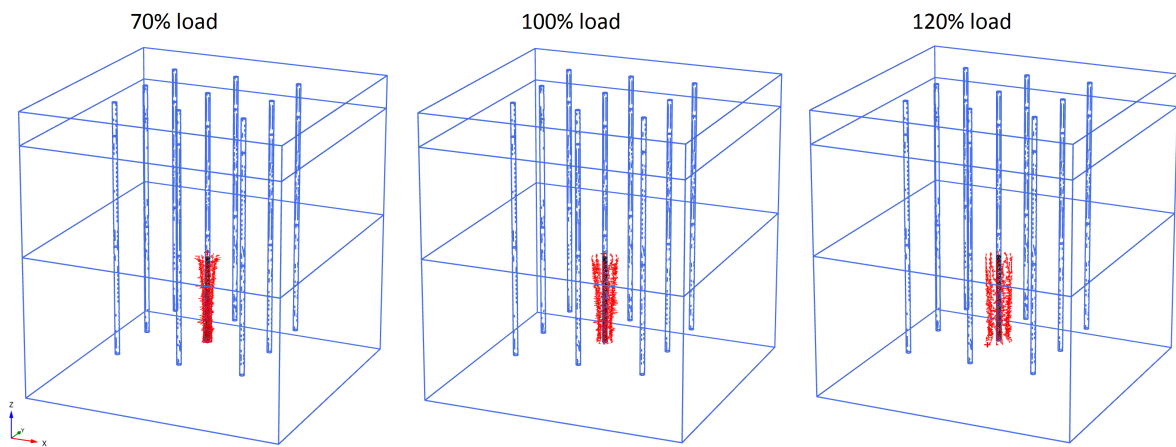
Figure 4.23: The development of the relative shear stress at the interface of the center pile for the 15D spaced nine pile group.

Total vertical displacements - last loading stage

At the level of the high pressure grouting zone the total vertical displacements of the three spacing cases are compared. The scale is the same for each case and ranges from 0.0 mm (dark blue) to 5.0 mm (dark red).
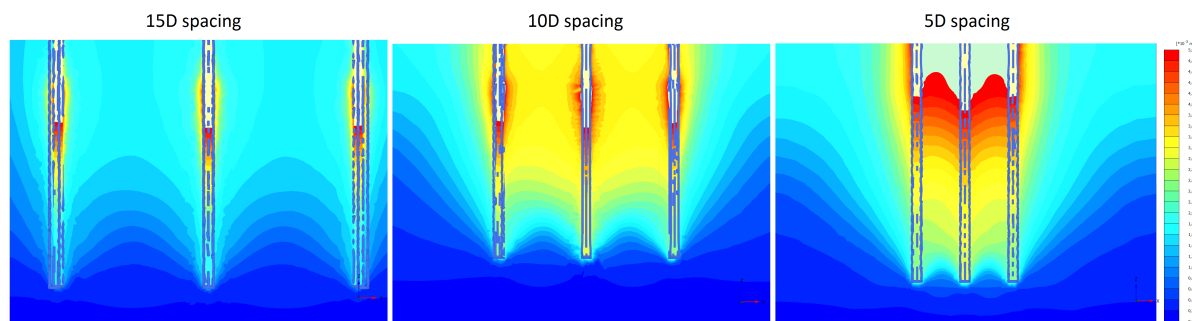
Figure 4.24: A comparison of the total vertical displacements at the last loading stage for the different spacing models.

The displacements in figure 4.24 illustrate the difference in failure mechanism found in the 5D and 15D spacing case. Where the soil displaces more in the 5D spacing case, the displacements in the 15D spacing case are more related to the pile and a very small area around the pile. For the 10D spacing case the failure mechanism tends more towards the 5D spacing case, where a soil plug forms and is pulled out of the soil.

Phase deviatoric strains - last stage

The failure mechanisms that were found for the different spacing cases upon inspection of the vertical displacement and relative shear stress are confirmed by the phase deviatoric strains. The deviatoric strains are shown on a scale from 0.0 (dark blue) to 1.0×10^{-3} (dark red). Zones where the deviatoric strain levels are higher than 1.0×10^{-3} are transparent, for example the high strain levels closely around the individual piles for the 15D spacing case.
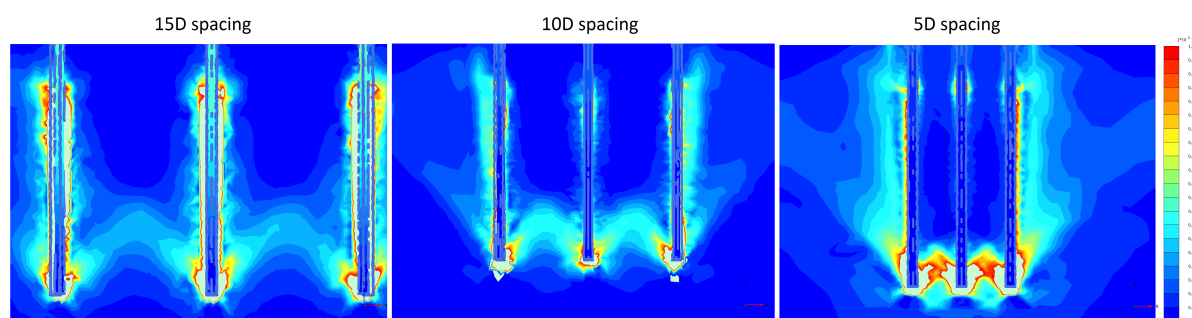
Figure 4.25: A comparison of the phase deviatoric strains at the last loading stage for the different spacing models.

In figure 4.25 above the highest strain levels are found either around the pile, for the 15D spacing case, or in a soil contour around the pile group, for the 5D and 10D spacing case.

4.3.2. Stiff case vs. standard case

For all model results of the stiff case the reader is referred to Appendix B.6.1. In this subsection the results of the stiff and standard case are compared. Firstly the difference in displacements at the same load levels is compared for each spacing case. Below in figure 4.26 the percentage change of the displacement are presented when comparing the stiff case to the standard case. The percentage change, P, is calculated with equation (4.6).

$$P = \frac{u_z^{(stiff)} - u_z^{(standard)}}{u_z^{(standard)}} \cdot 100 \tag{4.6}$$

In figure 4.26 it can be seen that the soil stiffness, relatively, has the most influence on the displacement of the 5D spacing case and the influence decreases for the more widely spaced pile groups. For the absolute difference in displacements between the different stiff spacing cases the reader is referred to Appendix B.6.1.

Percentage change of the displacements, comparing the stiff cases to the standard cases
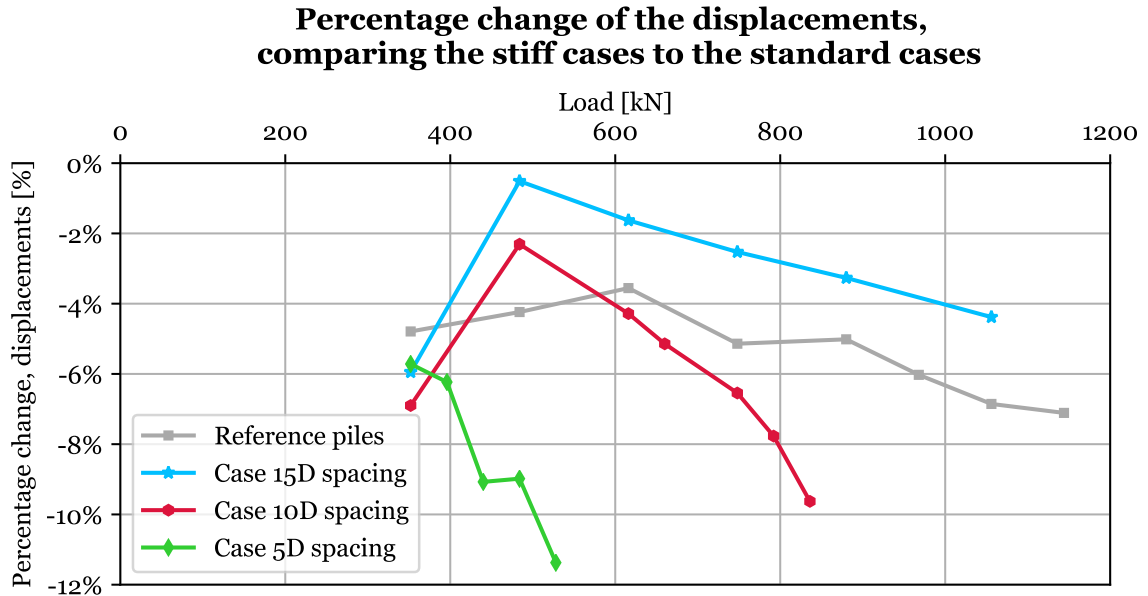
Figure 4.26: The percentage change of the displacements in the standard and stiff case model for the different spacing models.

The difference between the spacing cases in soil stiffness dependency of micropile head displacement might be related to the developing failure mechanism. For the slip failure cases, single pile reference and 15D spacing case, the dependency is less compared to the soil plug failure cases. In the paragraphs below the developing failure mechanisms in the standard and stiff cases are compared for the different spacings.

5D pile group spacing

Below in figure 4.27 the relative shear stress in the final loading stage at the bottom of the group center pile are compared for the standard and stiff case. It can be seen that for both pile groups the shear stress is not fully mobilised at the interface, but more mobilisation is seen for the stiff case. Since the cases only differ in stiffness, the fact that the maximum shear stress is reached sooner for the stiff case is as expected.
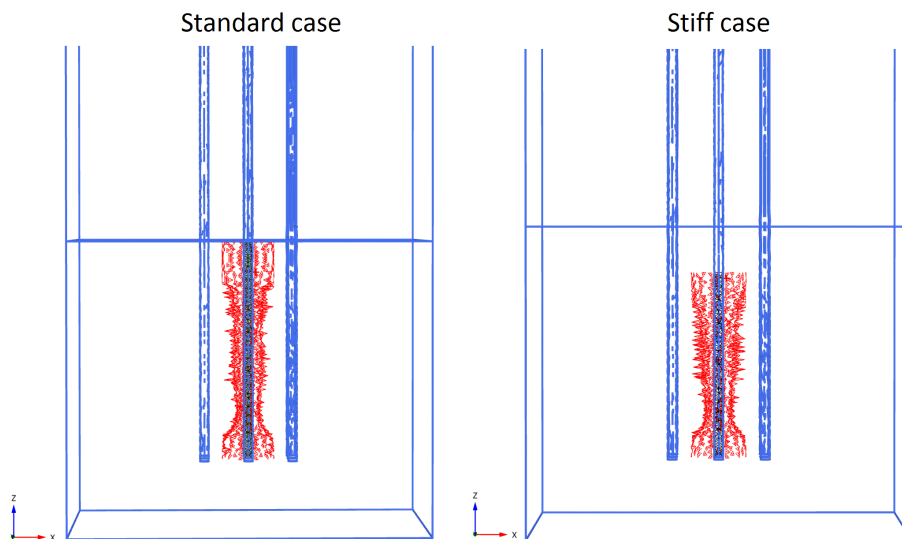
Figure 4.27: The relative shear stress at the interface for the last loading stage of the standard and stiff case model for the 5D spaced pile group compared.

In the comparison of the phase deviatoric strains below in figure 4.28 the developing failure mechanism, soil plug pull-out is the same for both cases, but the contours of both soil plugs are different. The cause of this difference is unknown, but for the case with a higher soil stiffness the development of a smaller soil plug seems likely to occur due to a smaller mobilised volume.
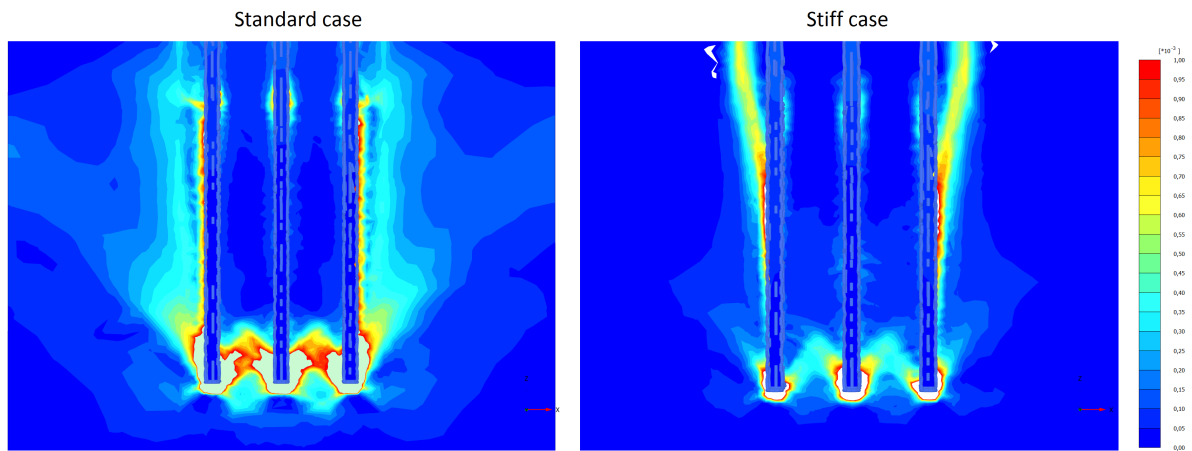
Figure 4.28: The phase deviatoric strain at the last loading stage of the standard and stiff case model for the 5D spaced pile group compared.

10D pile group spacing

For the 10D spacing case the relative shear stress shows less difference than for the 5D spacing case. Again the shear stress is slightly more mobilised for the stiff case, where a larger area at the top of the interface has reached a relative shear stress of 1.0.
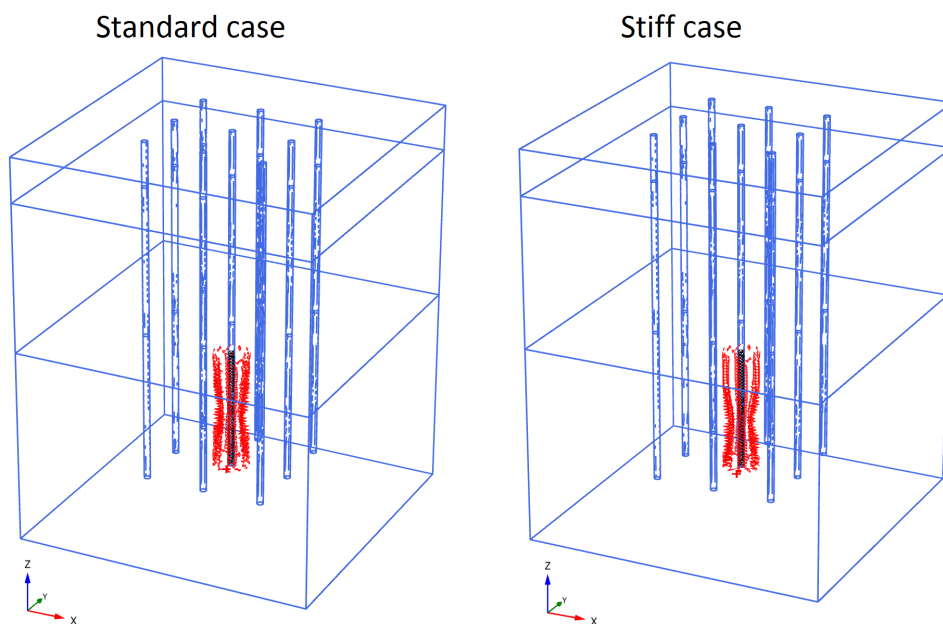
Figure 4.29: The relative shear stress at the interface for the last loading stage of the standard and stiff case model for the 10D spaced pile group compared.

The comparison of the phase deviatoric strains shows a similar trend is developing for the 10D spacing cases, but that the strain levels are lower for the stiff case. The strain levels for the piles on the side of the group look more like individual slip is developing, see figure 4.30. Despite the individual slip of the piles on the side, the lower strain levels around the center pile and arches at the bottom of the pile group are clearly visible as well, which indicate soil plug failure.
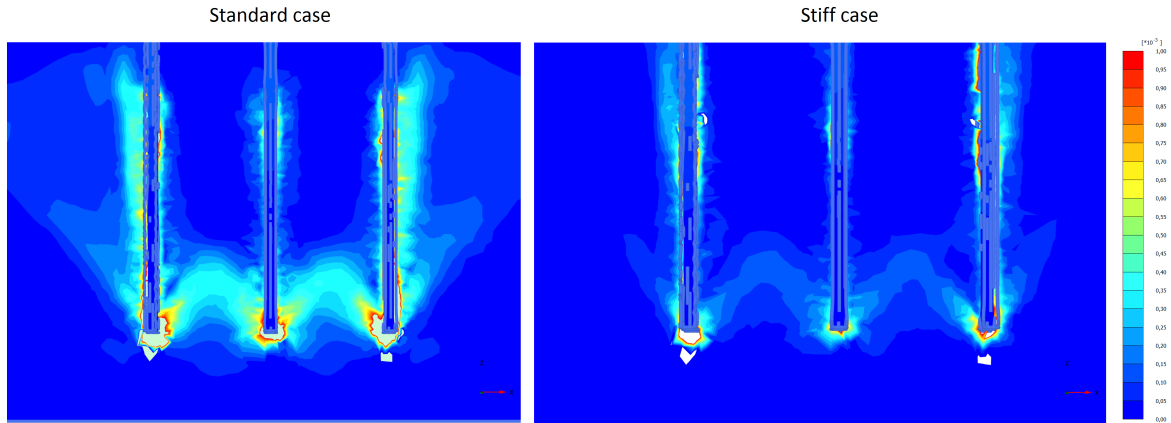
Figure 4.30: The phase deviatoric strain at the last loading stage of the standard and stiff case model for the 10D spaced pile group compared.

15D pile group spacing

The 15D spacing case does not deviate from the earlier mentioned differences between the standard and stiff case: some more shear stress mobilisation at the top of the interface is seen for the stiff case.
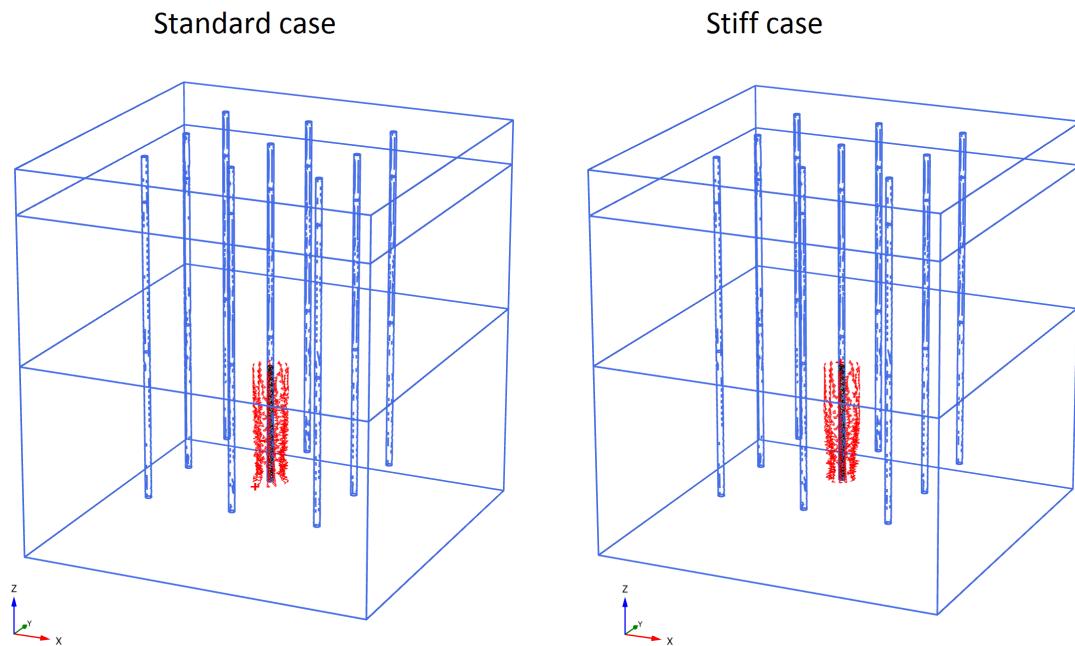
Figure 4.31: The relative shear stress at the interface for the last loading stage of the standard and stiff case model for the 15D spaced pile group compared.

In the phase deviatoric strain comparison in figure 4.32 the individual pile slip failure is clearly developing for both cases, the arches forming at the bottom of the pile group are less significant for the stiff case.

Standard case   Stiff case
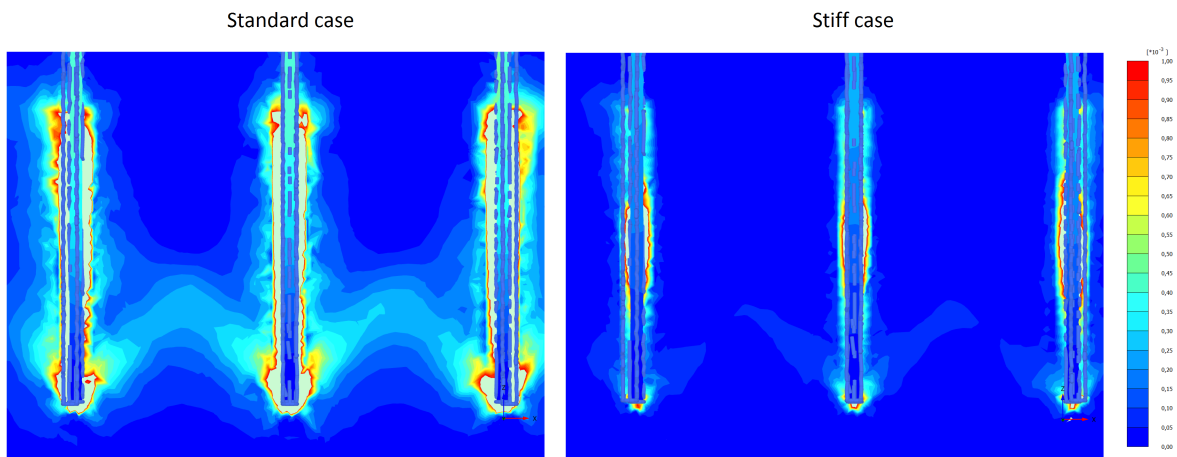
Figure 4.32: The phase deviatoric strain at the last loading stage of the standard and stiff case model for the 15D spaced pile group compared.

Overall one can say that, obviously, the strain levels and displacements are lower for the stiff case. The failure mechanism developing for the stiff cases does not seem to deviate from the failure mechanism developing in the standard cases, although some small differences are seen. The soil stiffness affects the pile group displacement most for the lay-outs that fail by pull-out of the soil plug, in the case of this research the 5D spacing and 10D spacing cases.

5

Discussion and limitations

The modelling approach for the individual micropiles and micropile groups has practical limitations. Next to the practical limitations of the modelling approach several assumptions were made during the research. In this chapter the varying assumptions and simplifications of the modelling approach are listed and explained. Furthermore, the most relevant findings and limitations of the research are discussed.

5.1. Assumptions, simplifications and limitations

Below the assumptions and simplifications made in this research are listed together with the practical limitations of the research.

Assumptions and simplifications

⋄ The modelled soil layers behave according to the stress-strain relationships of the Hardening Soil small strain stiffness (HSs) model. Softening and non-linear unloading/reloading behaviour, for example, is therefore not included.

⋄ The soil present at the test site is modelled by three homogeneous layers. The natural variation and heterogeneous behaviour in the subsurface is therefore not included.

⋄ A micropile consists of two sections: an unbounded section and bounded section. The unbounded section is modelled as very stiff, linear elastic, volume elements that fail on slip in the interface. The stiffness of the bounded section is used as fitting parameter and within the range of 4.0 to 16.0 GPa, again with linear elastic volume elements.

⋄ The groutbody has reached its full stiffness directly after installation.

⋄ The micropiles are loaded at the top of the pressurized groutbody with a surface load.

⋄ The interface of the pressurized groutbody behaves according to the Mohr-Coulomb model, with parameters directly correlated to the parameters of the surrounding soil.

⋄ Stress redistribution between group piles by the means of a stiff structural element, such as an underwater concrete floor, is not modelled.

Limitations

⋄ The pile group model is limited in its practical use due to the computationally expensive procedure for relatively small pile groups.

⋄ The model does not include the variation in positive and negative effects of the installation process found in practice. An example of the variation in micropile performance can be found in Appendix B.8.

⋄ The pile group model is not validated through comparison with field data.

5.2. Discussed aspects

The most significant findings, assumptions, simplifications and limitations of this research are discussed in this section.

5.2.1. Literature review

The literature review showed the limited amount of physical research performed to determine the group effect for tension piles. The Dutch standards and guidelines for the group effect of micropile groups originate from the driven pile standards and therefore experiments that were performed with driven piles. The installation effects are different for micropiles. Since the installation process affects the soil stress state in a pile group significantly, the applicability of driven pile research for micropiles is limited. Research on micropile group behaviour did not result in a general outcome so far. Various researchers found contradicting results, with either positive or negative installation effects, see subsection 2.3.1. But is has to be stated that several comprehensive researches into micropile behaviour, such as the FOREVER project, were not completely reviewed. The focus of the literature study was Dutch micropile practice. Moreover, the numerical results found in other researches using Plaxis software had the focus. Therefore some literature investigating group behaviour for other practices with different numerical software packages might not be present in the current literature study.

5.2.2. Development of 2D and 3D models

During the development of the final 2D plane strain and 3D single pile models several modelling approaches were considered. In this subsection the assumptions made during the 2D plane strain modelling phase are described first, afterwards the assumptions made during the development of the 3D single pile models are explained.

In the 2D plane strain modelling phase the use of long plates and volume elements was discarded because of the limited applicability for single piles, but the use of node-to-node (N2N) anchors and embedded beam row (EBR) models is not without limitations either. Both the N2N and EBR are directly connected to the mesh at only two nodes, namely the starting and end point of the structure. Loads applied at these nodes directly result in displacements of the soil at that node: slip behaviour of the pile is not possible at those nodes. To overcome this problem, small plate elements were used to provoke the slip behaviour and exclude the unrealistic soil displacements at the location where the load is introduced in the system. Since the load is applied to the pile and not the soil this workaround improves the validity of the model and represents reality more closely.

Another important aspect of the 2D plane strain EBR models is the interface stiffness factor (ISF). Since the pile row stiffness in plane strain is an average stiffness of the piles and the soil, the pile row spacing and pile diameter affect the load-displacement behaviour [47]. This is taken into account for the EBR: the ISF calibrates the interface stiffness and is dependent on the pile row spacing and pile diameter as well. For micropiles, with a relatively low pile stiffness, this factor has not been validated yet. For the 2D models an ISF of 1.0 was assumed, to model a relatively stiff interface that has a limited effect on the displacements of the system. This makes the chosen pile and soil stiffness dominant for the displacements of the system and for the load transfer from the micropile to the soil. For a validated ISF value for single micropiles in the 2D plane strain EBR models, comparison with field data and validated 3D models should be made.

Thirdly, the layer dependent EBR 2D models derive their capacity from the surrounding soil state. The horizontal effective stress level is the most significant parameter and is adjusted in the 2D models with the K_0-parameter. The values used for the K_0-parameter are not realistic and are illustrative for the horizontal effective stress levels that can be back calculated from the field data. More on the limits of the K_0-parameter can be found in Appendix B.2.

For the 3D single pile models used for validation five approaches were discarded, see figures B.1 and B.2 in Appendix B.1. The three embedded beam element (EBE) models include the same discussion points about the N2N and K_0-parameter of the 2D EBR models. A third point of discussion is the way the capacity is determined for the 3D layer dependent EBE. Again the Mohr-Coulomb criterion in equation (2.14) is used for the limit state, but than for 3D conditions. The actual 3D normal effective stress σ'_n is approximated with the mean effective stress p' at the EBE interface. This means the vertical effective stress level affects the capacity directly and not only through the lateral earth pressure coefficient correlation. The three mentioned limitations to the 3D EBE are the main reasons the EBE was discarded for the final 3D model.

For the two models with volume elements the first model was discarded because of the unrealistic shear stress mobilisation at the top of the volume element, resembling the behaviour of an anchor instead of a tension pile. For the second model several line elements such as distributed loads, EBE's, beams and geogrids were used to model the GEWI bar. Because of the large stiffness differences occuring in the modelled systems these models did not produce realistic stress or strain distributions and varying numerical issues were encountered. When one considers the group effect in micropile groups, the GEWI bar is not the most essential part of the micropile model and the simplifications applied in the final 3D models are considered valid. Without the GEWI a realistic load redistribution from the pile via the interface to the soil was achieved, as shown in section 4.1.2.

5.2.3. Final 3D models

In the paragraphs below several aspects of the final 3D models are discussed. The discussion of the final 3D models focusses on the simplifications and assumptions that had to be done for the numerical model and what consequences this has for the results of this research.

Mesh size and quality

The 3D individual pile models have a different mesh fineness and quality than the 3D group models. The comparison of the 3D single pile validation models with the 2D axisymmetric models shows the relevance of the mesh size and quality for the accuracy of the output. Moreover, the comparison shows the consequences of the mesh size and quality for the input parameters chosen for the validation of these single pile 3D models. For practical reasons, such as calculation time and the limited duration of this research, the meshes of the group models were not further refined. This affects the displacement of the micropile head and the distribution of stresses in the soil body. Since no quantitative comparison was made between the displacements in the numerical 3D pile group models and displacements measured in the field the relevance of such an improvement is limited for the current research, but it is vital for validation of the research with field data. The distribution of stress in the soil were only used to qualitatively show developing trends in the soil, again further refinement of the meshes is not expected to be relevant for this research.

Groutbody stiffness

The interaction between the GEWI bar and groutbody are not present in the modelling approach. These elements are replaced by a linear elastic volume with one linear stiffness: the groutbody stiffness. In reality the stiffness is neither linear elastic nor constant throughout the groutbody. Furthermore, the stiffness varies during all loading phases. The groutbody is known to crack with the introduction of higher tension loads, these cracks develop during the different loading stages affecting the stiffness [35]. This leads to a difference in the way the load is redistributed in the numerical model and the way this occurs in reality. A different load distribution would lead to a different shear stress mobilisation at the interface and therefore influences the stiffness and possibly the strength of the micropile. The results could be improved if a new material model would be developed that captures the non-linear stiffness of the groutbody in tension.

Loading of the system

In the current modelling approach, as explained in the previous paragraph, the GEWI bar is not included. Next to the simplified interaction in the groutbody, the load is not introduced at the top of the pile. The current choice for the introduction of a surface load at the top of the groutbody leads to the exclusion of the GEWI elongation in the free or unbounded length of the micropile. For the group models this is only 1.5 meters of unbounded GEWI, the influence on the model results will therefore be limited. The surface load was chosen to spread the load evenly over the nodes representing the top of the groutbody, introducing the load at one node is more likely to lead to numerical issues or inaccuracies. In reality a stiff element such as an underwater concrete floor will be present, this will lead to the redistribution of stresses and unequal loading of the different piles in a pile group. If the element is very stiff, the stress level will be fairly equally distributed and the current approach is sufficiently accurate.

Interface parameters and behaviour

One of the crucial elements of the micropile models is the interface. At the interface the load in the pile is transferred from the pile shaft to the soil. The deformation and parameters of the interface are of great influence on the micropile behaviour. Issues were encountered when deformations of the interface became

relatively large, approximately > 10 mm, and the shear stress at parts of the interface was fully mobilised while even higher loads were introduced in the model. Stiffness differences between the pile and the soil, the mesh fineness and the shape of the interface are all contributing to the deformation of the interface and the stress levels present at the interface. The current set of interface parameters were derived after several trial runs, but were still not fully satisfactory. Below some limitations of the current interface modelling are explained in more detail.

Dilation
A manual dilation cut-off was implemented after stress concentrations on the interface were seen for the section where the shear stress was fully mobilised. It is known that the amount of dilation that can occur is physically limited. Since the HS model has infinite dilation this cut-off is seen a realistic model adjustment.

2nd order elements
The shaft capacity of the micropile model is dependent on the normal force at the interface, which is derived from the horizontal effective stress level at the interface. The horizontal effective stress level at the interface is determined by interpolation between the different nodes and stress points that represent the interface. In Plaxis 3D, this interpolation is done with a second order precision. The curved surface of the interface is therefore represented by a hyperbola between two nodes. This is a relatively accurate approximation but might cause issues with the stress level normal to the nodes where two hyperbolas meet. This is illustrated in figure 5.1, the effective stress level at the node is an average of the effective stress levels resulting from the hyperbolas. This leads to stress concentrations at the nodes.
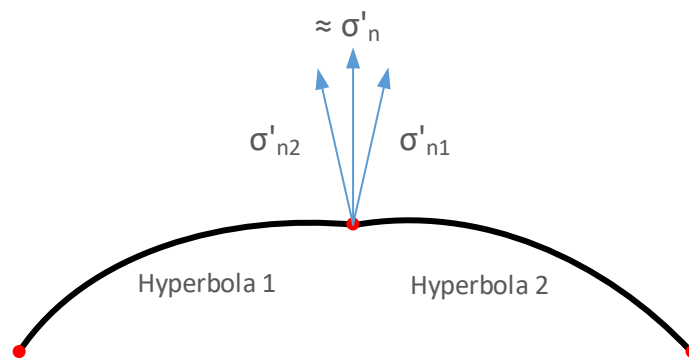
Figure 5.1: An conceptual visualisation of the determination of the normal effective stress on a node at the interface.

Installation simulation

The installation process of a micropile type A is simulated in a simple three-step approach where conditions are idealised. With the activation of the full stiffness of the groutbody after the introduction of the grout pressure, the increased horizontal stress levels remain almost fully present at the interface after the surface loads are deactivated in the third step.

The differences between the simulated installation process and the actual process in practice are discussed in this paragraph. The installation effects of pile type A are most significant during the high pressure grouting phase (step five mentioned in the introduction of Chapter 3). For simplicity the effect of the boring process with the double casing is considered negligible in the 2D and 3D analyses. The high pressure grouting has two possible effects on the surrounding soil. The outcome depends on the development of the grout seal around the borehole, which is determined by the duration of the boring and pressure grouting phase.

Pore water over-pressure
With high pressure grouting quickly after the boring process the grout mixture is still very fluid and has not hardened yet, therefore high pressure grouting results in additional pore water pressures. This process might cause blow-out along the shaft. Depending on the permeability of the soil and the water tightness along the shaft, additional pore water pressures might develop in the soil or the water may freely drain into the soil. In the case of pore water pressure increase effective stresses decreases, weakening the soil and possibly causing liquefaction. It has to be noted that blow out or free draining is expected to happen before liquefaction can occur. Liquefaction is not expected because water follows "the path of least resistance" and a leak is more likely to occur than the build-up of high pressures. When free draining is assumed, the water cement ratio is lowered by the high pressure grouting phase, resulting in a stronger groutbody.

Radial effective stress increase
When some time is taken between the boring phase and high pressure grouting phase the groutbody can harden over time. This results in a less permeable seal forming around the borehole. The additional pressure from the high pressure grouting phase now effects the radial effective stress in the soil due to the groutbody expansion. In this case the capacity of the groutbody is increased due to increased radial effective stresses, whether these stress levels remain at the same level during the lifetime of a micropile is unknown. In the current modelling approach it is assumed that the stiffness of the groutbody is fully developed after the pressure grouting phase has ended.

Residual strength

It is known that the capacity of micropiles installed in dense sands with a relatively high length (> 5.0 meter) might be affected by the lose of shear resistance due to residual strength in the soil/interface. To mobilise peak shear strength displacements of 2.0 mm to 10 mm are needed [19]. Longer micropiles are likely to displace more than 10 mm around the top of the micropile. In this zone the residual strength level of the soil or interface might be reached and the shear resistance drops. Since the soil is modelled with the HSs model, no residual strength behaviour is included in the current modelling approach. For the group models with 10 meter long piles the effect of excluding residual strength behaviour is expected to be limited. Most of the capacity of these piles is derived from the deeper second sand layer, where the displacements are relatively small.

Validation group model

No comparison was made between field or experimental data and the group modelling results. The behaviour found in the group model therefore remains invalidated. The single pile models were validated and the constitutive models used in this research, such as the Hardening Soil model, have been used for several years and their behaviour has been validated for numerous cases. Since the single pile behaviour is confirmed and the HS model is known to be a good approximation of the soil behaviour the modelling approach can be reviewed as reliable and the trends found in the results are theoretically sound, yet not validated with field data.

5.2.4. Field data and final model parameters
The available geotechnical field data for two sites was used to determine the input parameters for the various numerical models. For the Amsterdam case the validated Hardening Soil (HS) parameter set of a nearby project was used by identifying the same geological layers at the test site. The small strain parameters were found with rules of thumb, relating the small strain stiffness to the unloading/reloading stiffness of the soil. For the The Hague case only CPT data was used to correlate the Amsterdam soil data to the test site in The Hague. The used parameters in the models of this research have a limited validity and could be improved by fitting soil tests such as oedometers, direct shear and triaxial tests performed at samples of both sites. In the field data fitting process, the K_0-parameter and the effective internal friction angle ϕ' used in the numerical models were adjusted within bandwidths found in literature. Again the choice of these parameters were not determined with geotechnical laboratory testing and could be improved by doing so. The heterogeneity found in soils in reality is not represented by the modelling of three homogeneous soil layers for the Amsterdam case and one homogeneous soil layer for the The Hague case.

5.2.5. Capacity comparison with the Dutch standards
In section 1.1 subquestion five is formulated: "How can the findings of the research be validated and implemented in practice?". In the current subsection a comparison between the standards available in Dutch practice and the 3D pile group model results is made, see figure 5.2 on the next page. This comparison gives a first idea of the consequences of the implementation of the research results in practice. For recommendations on the validation of the 3D pile group model the reader is referred to Chapter 7.

In figure 5.2 the capacities of an individual micropile in the middle of a micropile group are presented for different pile group spacings. In CUR 236 the capacity is calculated for two different failure mechanisms: slip and soil plug pull-out. Two scenarios are presented for the soil plug pull-out since there is some discussion whether micropiles should be defined as soil displacement or non-displacement piles. The Excel sheets made for the CUR 236 calculations are presented in Appendix B.7.

Capacity reduction due to group effects, CUR 236 vs. Plaxis 3D model
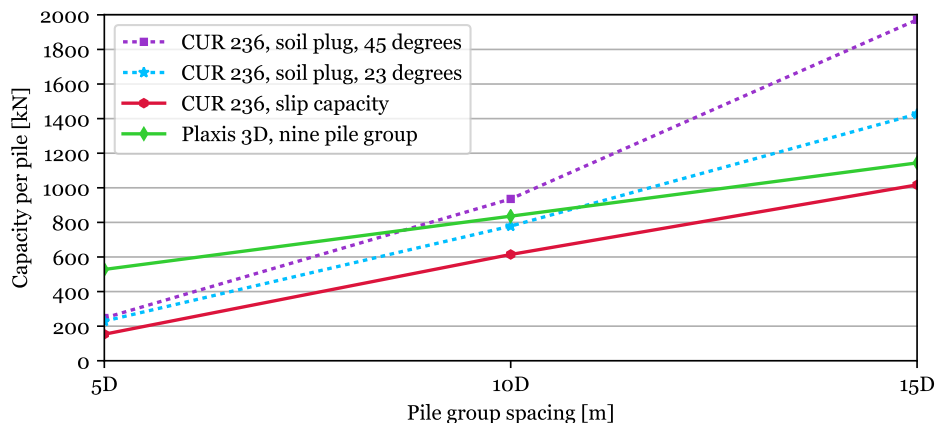
Figure 5.2: Individual micropile capacity according to CUR 236 and Plaxis calculations comparing the three different pile group spacings.

The definition of maximum capacity for the Plaxis models and the standards are not necessarily similar. The models were run until no further load could be introduced. The standards work with safety factors to account for uncertainty in input parameters, these safety factors are not explicitly taken into account in Plaxis. The comparison must therefore be reviewed with great care and should be seen as an indication of the difference between both methods regarding single group pile capacities. The capacity determination of both the CUR236 and the Plaxis 3D model is governed by the horizontal effective stress level around the micropiles. The Mohr-Coulomb failure criterion presented in equation (2.14) is used for the limit state in the Plaxis 3D calculations, for the CUR 236 calculations the CPT related method from equation (2.3) is applied. The horizontal effective stress level in the Plaxis calculations is dominated by the installation simulation, with this approach the model outcome was fitted with the data from the pile load tests for single piles. The CPT profile was not used to determine the at rest horizontal effective stress state in the Plaxis models. For the CUR 236 the pile load test data was used to determine the α_t value, related to the CPT's presented in Appendix A.1. The maximum design shear stress is then determined with the CPT data after excavation, see Appendix B.7.1, divided by a partial safety factor of 1.35.

In figure 5.2 a clear difference between the standards and the Plaxis model for the 5D spacing case is seen. The 5D spacing case is unlikely to occur in practice and the standards are not made to predict the capacity accurately for such a case. Therefore the standards are relatively conservative with a reason: such closely spaced pile groups must be avoided in practice.

For the 10D spacing case the capacity determined in Plaxis is closer to the soil plug capacities determined with the CUR 236. This coincides with the failure mechanism found in the previously presented 3D pile group modelling results. For the 15D spacing case the Plaxis capacity is close to the maximum slip capacity determined with the CUR 236. The trends shown in figure 5.2 look linear for the capacity determined with Plaxis 3D and the CUR 236 slip capacity. However, the capacity of the single piles are theoretically limited around 1400-1500 kN. This limit is found if the CUR 236 calculations are checked with a large pile group spacing (>8.0 m) where the f_2 factor increases to 1.0. The graph shown in figure 5.2 focusses on the pile group spacing where the interaction is significant. The slope of the Plaxis and CUR 236 limit trends decreases drastically after the 15D spacing case: for these spacings the interaction is increasingly less relevant.

With validation of the current 3D modelling approach an improvement of the CUR 236 could be proposed. Based on the current results this might improve the design for pile groups spaced around 10D, where it is more likely that soil plug pull-out will occur and slip failure will not be the limiting state. The level of safety for soil plug pull-out is lower than the level of safety used for the slip failure mechanisms. If the standards were to be adjusted, additional safety should be included in the capacities determined with the soil plug pull-out mechanism to keep the safety level sufficient for design calculations.

6

Conclusion

In this chapter the main research question and subquestions are answered and subsequent conclusions are drawn.

I What is an appropriate model for a single micropile under axial tensile loading?

The load-displacement behaviour of a micropile can accurately be modelled in both Plaxis 2D and 3D. The 2D plane strain embedded beam row model is limited in its use since displacements and stress redistribution in the soil are not calibrated and the interface stiffness factor (ISF) is introduced. The 2D axisymmetric model and 3D model with volume elements include realistically modelled installation effects and have a more realistic stress and displacement distribution in the soil. The stress and distribution is more realistic for the models with installation simulation because of the prestressed zone around the groutbody of which the magnitude of horizontal effective stresses can be back-calculated from the micropile tensile capacities reached in pile load tests. The displacement distribution is more realistic due to the absence of the plane strain assumptions. Since the displacements are calculated in three directions (x, y and z) for both the 2D axisymmetric and 3D model, no average pile row stiffness has to be determined.

II How does pile spacing influence the size of the group effect?

Comparing the 15D spaced and 5D spaced pile group for both the standard and stiff case, the capacity of the 5D spaced pile group is reduced by 50%. The stiffness is reduced by approximately 8% for the standard case and 4% for the stiff case. This shows the significant impact of spacing on the size of the group effect. For pile groups spaced more widely than the 15D case the influence of the group effect will decay and the capacity becomes equal to the capacity of single piles. For more narrowly spaced pile groups the group effect becomes more intense, but such a scenario is not realistic as a 5D spacing is already not applied in practice.

III How can installation effects be included?

All five types of micropiles, defined according to the Dutch classification system, have different installation effects. In this research the effect of pressure grouting for pile type A has been simulated. The boring process of pile type A has a relatively limited effect on the soil state in both stress and strain terms. Therefore only the effect of the pressure grouting is included. Installation effects of pressure grouted micropiles can be included by introducing a three-phase installation simulation. First surface loads are introduced at the pressure grouting zone, then the linear elastic, stiff groutbody is activated. Thirdly, the surface loads are deactivated and the displacements are reset. The stresses induced with the surface loads remain in the soil body and act perpendicular to the micropile interface. This installation simulation process has some limitations in its approach, see Chapter 5 'Installation simulation'.

IV What is an appropriate 3D model?

A realistic 3D micropile model can be made of linear elastic volume elements, a three step installation simulation process, soil property dependent interfaces and a sufficiently fine mesh. The mesh fineness has been determined by comparing the 3D single pile modelling results with a 2D axisymmetric model with a very fine mesh and more nodes per element compared to 3D. Especially for single micropiles this modelling approach is appropriate: it is both sufficiently accurate as efficient. The modelling approach with embedded beam elements is regarded as inappropriate if the capacity of the micropile is not yet accurately determined. The embedded beam element approach is not suitable for the modelling of micropile groups and the influence of the group effect on the capacity of the micropiles. The modelling approach with volume elements for pile groups is theoretically appropriate, but has significant drawbacks in terms of general applicability and computational efficiency. For the limitations of the 3D pile group models with volume elements, see Chapter 5.

V How can the findings of the research be validated and included in the design code?

For a more elaborated explanation on the validation possibilities for the group models used in this research the reader is referred to Chapter 7. The results of this research show a lower slip capacity reduction than currently determined in the standards. With the comparison between the capacities determined in practice and the Plaxis 3D modelling results the differences in the various assumptions and the level of safety must be considered. The main parameter for the determination of the micropile slip capacity (maximum shear stress) is the horizontal effective stress level. For the Plaxis 3D model the horizontal effective stress level is dominated by the installation simulation process, for the CUR 236 calculations the maximum shear stress is determined directly from CPT data and a predetermined α_t value from the pile load tests at the same site. With this difference in approach, the level of safety of a new group effect factor that would originate from this research must be investigated before implementation in the design code can be considered.

Next to the answers of the subquestions two more general conclusions were found, which explain the influence of the group effect on the behaviour of micropiles for strength, stiffness and failure mechanism.

1. The two known failures modes for micropile tension pile groups, slip failure and soil plug pull-out, are seen in the final loading stages of the 3D group models. Failure by soil plug pull-out means that the mobilised shear stress in the soil in a contour around the pile group has reached its maximum earlier than the shear stress that is mobilised around the surface of the micropiles. Further deformations follow the contour of the forming shear band and the soil plug is pulled out of the surrounding soil. This means that the horizontal effective stress levels within the pile group remain high enough: the soil is clamped between the piles. At the bottom of the pile group the developing shear bands between the piles form arches through the soil, as can be seen in subsection 4.3.1, figure 4.25. Failure by individual slip means that the maximum mobilised shear stress is first reached around all individual surfaces of the micropiles. Each pile will therefore move up, only interfering with a relatively limited volume of soil directly around the interface. For the 15D meter pile group it is seen that the displacement in between the piles of the pile group is higher than outside of the pile group but this is limited in magnitude. It is concluded that the 5D and 10D spacing cases fail by soil plug pull-out, the 15D spacing case and single reference pile fail by slip.

2. The group effect reduces the capacity per micropile and stiffness of the system significantly. The pile group spacing is negatively correlated to the group effect: decreasing the pile group spacing from 15D to 5D resulted in a capacity decrease of 50% and stiffness decrease of 8%. No direct correlation of the group effect with the soil stiffness was found, but the stiffness of the pile groups was more strongly affected for the 5D and 10D cases where the soil plug failure mechanism occurred. This can be explained by the fact that the failure state surface is relatively large where the soil plug failure mechanism occurs, since it is a contour around the pile group where the maximum shear stress is mobilised. For single piles and the 15D case the failure occurs directly at the pile-soil interface.

7

Recommendations

The modelling approach and validity of the pile group model can be improved in several ways. In the Discussion the limitations of the researched were discussed, in this Chapter some improvements on the limitations, assumptions and simplifications of the research are presented.

Validation of the pile group model

It is highly recommended that the pile group modelling results are validated using for example experimental, geocentrifuge modelling test data or a full scale group loading test. With a geocentrifuge experiment the development of effective stress levels in the soil might be reviewed, for example including a simulated installation procedure. The transfer of the applied grout pressure to the soil skeleton can be determined to improve the installation simulation in the numerical model. To determine these resulting effective stress levels pore water pressure must be measured to calculate effective stress levels from total stress levels.

With a full scale group loading test the parameters of the numerical models could be calibrated to fit the load-displacement behaviour found in the full-scale test, as done in the single pile model validation of this research. Load and displacement measurements are needed for a full scale micropile group loading test. The load per pile and the displacement of the pile head must be collected in such a test. To confirm shear stress development found at the interface of the numerical model, strain measurements of the rebar might be applied in the full scale test. Shear stress development can be back-calculated with the strain measurements and a known micropile stiffness EA. Small scale experiments at 1g are not deemed useful due to the importance of a realistic magnitude of the stress levels on the group effect and interaction phenomena.

Improvement of numerical model

Most of the recommendations are done for the improvement of the numerical model since the 3D pile group model is the core of this research.

Mesh and interface

First of all, with a more elaborate mesh investigation the mesh sensitivity of the results can be investigated. With a mesh sensitivity analysis an optimal mesh can be chosen, which is needed for the group model validation. The mesh sensitivity can be determined by running model variations where all parameters are constant and only the mesh coarseness is varied. The optimal mesh can be chosen when for example the final vertical displacements are plotted against the mesh coarseness, see figure 7.1 to the right for a qualitative example. If the plot reaches an asymptote for the displacements, the most coarse mesh with sufficient accuracy is chosen. The required level of accuracy must be determined based on the context of the research.
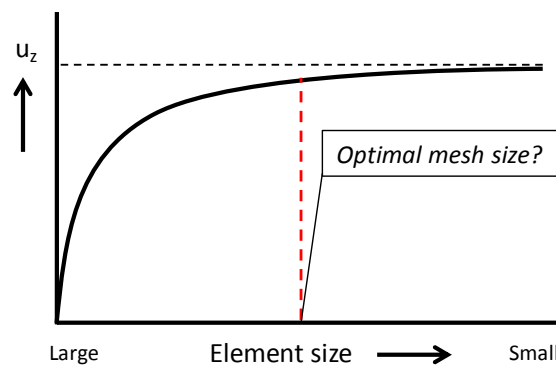
Figure 7.1: A qualitative illustration of the procedure for a mesh sensitivity analysis.

Secondly, the interface behaviour can be improved with the implementation of a dilatancy cut-off based on the void ratio and the determination of a limit state and appropriate R_{inter} values for the interface sections that failed at slip. This is needed to limit the deformations of the interface and therefore unrealistic normal effective stress levels on the interface. The current HS constitutive model provides the dilatancy cut-off option to the user. To use this dilatancy cut-off based on void ratio, more information about the soil properties of the material present at the site that is modelled must be known. At least the minimum and maximum void ratio of the soil must be determined and the in-situ relative density must be estimated. The implementation of a reduced R_{inter} value cannot be directly determined in practice but could be derived from lab shear box tests and then correlated to the situation in practice.

Installation effects and single pile model validity
Thirdly, different approaches to include installation effects can be compared to check the validity of the current approach. Next to recommendations given for the execution of centrifuge experiments a numerical study of installation effects can be done. Other ways to model installation effects are for example fixed displacements around the pressurized groutbody or an increase of local water head values and a consolidation phase. Both methods will result in an increase of local horizontal effective stress levels. Another improvement of the model validity would be the extension of the field data used for the single pile validation. Currently two cases are reviewed and a relatively wide range of groutbody stiffness values was found to fit the data. With more pile type A load-displacement and installation data appropriate ranges for the model behaviour and groutbody stiffness can be determined.

Boundary effects and model efficiency
In the current approach the model boundaries where set at a minimum of 3.0 meters. These boundaries act as a symmetry boundary, therefore the next pile group is virtually present at 6.0 meters. It is expected that this distance of 30D is sufficient, but this should be confirmed if the research is extended with the validation of the pile group model. This can be done in an analysis similar to the mesh sensitivity analysis: varying the boundaries instead of the element size.

Lastly it is advised to investigate the opportunities for a more efficient model. The current modelling approach is computationally very expensive. It takes up to three/four days (72-96 hours) on a regular commercially available computer to complete the entire calculation for the large and stiff group models and determine the failure phase. The amount of plastic points in the current models is very large and grows towards the failure stages, this strongly affects the calculation time. Options to reduce the amount of plastic points are reducing the number of elements or the implementation of the Mohr-Coulomb (MC) model instead of the HSs model. Both methods would reduce the accuracy of the modelling approach. The MC soil model would be useful for the determination of the ultimate limit state of the micropiles since the failure criterion is the same for the HSs model. Load-displacement behaviour is less accurately modelled with the implementation of a MC model, it is expected that this has a significant influence on the results when a large volume of soil is mobilised.

Monitoring and evaluation of practical cases
By monitoring the loads and displacements of, for example, the underwater concrete floor in a full scale building pit the stiffness of pile groups could be derived from the monitoring data. The loads on a pile group for a full scale building pit can be determined from strain and pore water pressure measurements. With strain measurements the load per micropile can be determined and with pore water pressure measurements the upward load on the underwater concrete floor is calculated. If the vertical displacement of the floor is tracked, the stiffness of the system can be calculated. With constant monitoring in practice a database can be made, the current standards on group effects can be evaluated by comparing the measured and design calculation results from the cases in the monitoring database.

Bibliography

[1] T. Armour, P. Groneck, J. Keeley, and S. Sharma. Micropile Design and Construction Guidelines Implementation Manual. Technical Report June, US Department of Transportation, Federal Highway Administration, 2000.

[2] A. Beijer-Lundberg. *Displacement pile installation effects in sand.* PhD thesis, Delft University of Technology, 2015.

[3] J. W. Bosch and W. Broere. Small incidents, big consequences. Leakage of a building pit casuses major settlement of adjacent historic houses. Amsterdam North-south metro line project., 2008.

[4] R. B. J. Brinkgreve. Hardening Soil model, 2016.

[5] W. Broere and A. F. van Tol. Modelling the bearing capacity of displacement piles in sand. *Proceedings of the ICE - Geotechnical Engineering*, 159(3):195–206, 2006. ISSN 1353-2618. doi: 10.1680/geng.2006.159.3. 195. URL http://www.icevirtuallibrary.com/content/article/10.1680/geng.2006.159.3. 195.

[6] CUR Committee 1690. Addendum to CUR report 236 'Micropiles' - Axial spring stiffness. Technical report, Stichting SBRCURnet, Delft, 2016.

[7] CUR committee C152. CUR report 236 'Micropiles'. Technical report, Stichting CURNET, Gouda, 2011.

[8] CUR committee C98. CUR report 2001-4 'Design rules for tension piles'. Technical report, Stichting CUR, Gouda, 2003.

[9] A. De Nicola and M. F. Randolph. Tensile and compressive shaft capacity of piles in sand. *Journal of Geotechnical Engineering*, 119(12):1952–1973, 1994.

[10] J. Dijkstra. *On the Modelling of Pile Installation.* PhD thesis, Delft University of Technology, 2009.

[11] M. A. El-Reedy. *Offshore Structures: Design, Construction and Maintenance.* Elsevier Science, Oxford, 2012. ISBN 9780123854766.

[12] H. K. Engin. *Modelling Pile Installation Effects: A Numerical Approach.* PhD thesis, Delft University of Technology, 2013.

[13] H. K. Engin, E. G. Septanika, R. B. J. Brinkgreve, and P. G. Bonnier. Modelling piled foundations by means of embedded piles. In Karstunen & Leoni, editor, *Proceedings of the 2nd international workshop on geotechnics of soft soils, Glasgow*, pages 131–136, London, 2008. Taylor & Francis Group.

[14] J. Feda. K0 -Coefficient OF Sand In Triaxial Apparatus. *Journal of Geotechnical Engineering*, 110(4): 519–524, 1984.

[15] B. H. Fellenius. Discussion of "Side resistance in piles and drilled shafts". *Journal of Geotechnical and Geoenvironmental Engineering*, 128(May):446–450, 2002. ISSN 1090-0241. doi: 10.1061/(ASCE) 1090-0241(2002)128:5(448).

[16] V. Fioravante. On the shaft friction modelling of non-displacement piles in sand. *Soils and Foundations*, 42(2):23–33, 2002. ISSN 09168451. doi: 10.1248/cpb.37.3229. URL https://www.jstage.jst.go.jp/article/sandf1995/42/2/42{_}2{_}23/{_}article.

[17] W. G. K. Fleming, A. J. Weltman, M. F. Randolph, and W. K. Elson. *Piling Engineering.* Surrey University Press, John Wiley and Sons., New York, second edition, 1992.

[18] K. E. Gaaver. Uplift capacity of single piles and pile groups embedded in cohesionless soil. *Alexandria Engineering Journal*, 52(3):365–372, 2013. ISSN 11100168. doi: 10.1016/j.aej.2013.01.003. URL `http://dx.doi.org/10.1016/j.aej.2013.01.003`.

[19] C. Gaudin, B. M. Lehane, J. A Schneider, and . Scale effects on tension capacity for rough piles buried in dense sand. *Géotechnique*, 55(10):709–719, 2005. ISSN 0016-8505. doi: 10.1680/geot.2005.55.10.709.

[20] T. Herbst. German practice, micropile groups resisting uplift forces. In *2nd International Workshop on Micropiles*, pages 57–72, Ube, Japan, 1999. ISM.

[21] G.T. Houlsby. How the dilatancy of soils affects their behaviour. In *Proceedings of the 10th European Conference on Soil Mechanics and Foundation Engineering*, pages 1189–1202, 1991. URL `http://www.eng.ox.ac.uk/civil/publications/reports-1/ouel{_}1888{_}91.pdf`.

[22] IBZ. Report: Construction close to built environment. Technical report, Arcadis/Witteveen+Bos, Amsterdam, 2015.

[23] I. Juran, D. A. Bruce, A. F. Dimillio, and A. Benslimane. Micropiles: the state of practice. Part II: design of single micropiles and groups and networks of micropiles. *Proceedings of the ICE-Ground Improvement*, 3(3):89–110, 1999. ISSN 1755-0769.

[24] S. Krabbenhoft, A. Andersen, and L. Damkilde. The tensile capacity of bored piles in frictional soils. *Canadian Geotechnical Journal*, 45(12):1715–1722, 2008. ISSN 0008-3674. doi: 10.1139/T08-086. URL `http://www.nrcresearchpress.com/doi/abs/10.1139/T08-086`.

[25] F. H. Kulhawy. Drilled Shaft Foundations. In Hsai-Yang Fang, editor, *Foundation Engineering Handbook*, pages 537–552. Springer US, Boston, MA, 1991. ISBN 978-1-4757-5271-7.

[26] F. H. Kulhawy and P. W. Mayne. Manual on Estimating Foundation Design Parameter. Technical report, Cornell University, Ithaca, 1990.

[27] A. Lashkari. Prediction of the shaft resistance of nondisplacement piles in sand. *International Journal for Numerical and Analytical Methods in Geomechanics*, 37:904–931, 2013. ISSN 03639061. doi: 10.1002/nag.

[28] B. M. Lehane. Mechanisms of shaft friction in sand from instrumented pile tests. *Journal of Geotechnical Engineering*, 119(1):19–35, 1993.

[29] B. M. Lehane and R. J. Jardine. Shaft capacity of driven piles in sand: a new design approach. In *Conference on the Behaviour of Offshore Structures*, pages 23–36, 1994.

[30] S. S. Liew and C. C. Fong. Design & Construction of Micropiles. Technical Report September, Gue & Partners Sdn Bhd, Kuala Lumpur, 2003.

[31] D. Loukidis and R. Salgado. Analysis of the shaft resistance of non-displacement piles in sand. *Géotechnique*, 58(4):283–296, 2008. ISSN 0016-8505. doi: 10.1680/geot.2008.58.4.283.

[32] K. Maleki. *Contribution a l'Etude des Micropieux Isoles et en Groupe*. PhD thesis, Ecol Nationale des Ponts et Chaussées, 1995.

[33] Y. Mascarucci, S. Miliziano, and A. Mandolini. A numerical approach to estimate shaft friction of bored piles in sands. *Acta Geotechnica*, 9(3):547–560, 2014. ISSN 18611133. doi: 10.1007/s11440-014-0305-4.

[34] P. W. Mayne and F. H. Kulhawy. K0 – OCR relationships in soil. *Journal of Geotechnical Engineering Division*, 108(GT6):851–869, 1982.

[35] L. Meerdink. *Performance of Micropiles Under axial tensile loading*. Master's thesis, Delft University of Technology, 2013.

[36] H. D. Netzel and D. Vink. Prediction of soil deformations during excavation works for the renovation of " Het Nieuwe Rijksmuseum " in Amsterdam , The Netherlands. *Plaxis Bulletin*, 20:16–19, 2006.

[37] Plaxis B.V. Screw pile, 2016. URL `https://www.plaxis.com/kb-tag/screw-pile/`.

[38] Plaxis B.V. Plaxis Material Models Manual, 2016.

[39] M. F. Randolph. Science and empiricism in pile foundation design. *Géotechnique*, 53(10):847–875, 2003. ISSN 0016-8505. doi: 10.1680/geot.2003.53.10.847.

[40] M. F. Randolph and S. Gourvenec. *Offshore Geotechnical Engineering*. CRC Press, first edit edition, 2011.

[41] L. C. Reese and M. W. O'Neill. *Drilled shafts: construction procedures and design methods*. Prepared for US Department of Transportation, Federal Highway Administration, Office of Implementation, Washington, D.C., 1988.

[42] A. F. Rotta Loria, F. Orellana, A. Minardi, J. M. Fürbringer, and L. Laloui. Predicting the axial capacity of piles in sand. *Computers and Geotechnics*, 69:485–495, 2015. ISSN 18737633. doi: 10.1016/j.compgeo. 2015.06.013. URL http://dx.doi.org/10.1016/j.compgeo.2015.06.013.

[43] M. Sadek and I. Shahrour. A three dimensional embedded beam element for reinforced geomaterials. *International Journal for Numerical and Analytical Methods in Geomechanics*, 28(9):931–946, 2004. ISSN 03639061. doi: 10.1002/nag.357.

[44] K. Shanker, P. K. Basudhar, and N. R. Patra. Uplift capacity of pile groups embedded in sands: predictions and performance. *Soils and Foundations*, 46(5):605–612, 2006. ISSN 09168451. doi: 10.1248/cpb.37. 3229.

[45] B. Sharma and P. Buragohain. Behaviour of micropile groups under oblique pull out loads in sand. *Indian Geotechnical Journal*, 44(4):400–408, 2013. ISSN 22773347. doi: 10.1007/s40098-013-0091-1.

[46] A. Shelke and N. R. Patra. Effect of Arching on Uplift Capacity of Pile Groups in Sand. *International Journal of Geomechanics*, 8(6):347–354, 2008.

[47] J. J. M. Sluis. *Validation of Embedded Pile Row in PLAXIS 2D*. Master's thesis, Delft University of Technology, 2012.

[48] F Tschuchnigg and H F Schweiger. Comparison of deep foundation systems using 3D Finite Element analysis. *Geotechnical Engineering Journal of the SEAGS & AGSSEA*, 44(3):40–46, 2013.

[49] F. Tschuchnigg and H. F. Schweiger. The embedded pile concept - Verification of an efficient tool for modelling complex deep foundations. *Computers and Geotechnics*, 63:244–254, 2015. ISSN 18737633. doi: 10.1016/j.compgeo.2014.09.008. URL http://dx.doi.org/10.1016/j.compgeo.2014.09.008.

[50] L. Vanitha, N. R. Patra, and S. Chandra. Uplift capacity of pile group anchors. *Geotechnical and Geological Engineering*, 25(3):339–347, 2007. ISSN 09603182. doi: 10.1007/s10706-006-9114-3.

[51] A. C. Vriend. Veenkade The Hague - report on failure load tests GEWI-micropiles. Technical report, 2013.

A
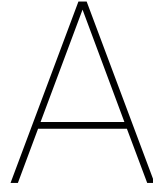
Appendix A

A.1. CPT data pile load tests
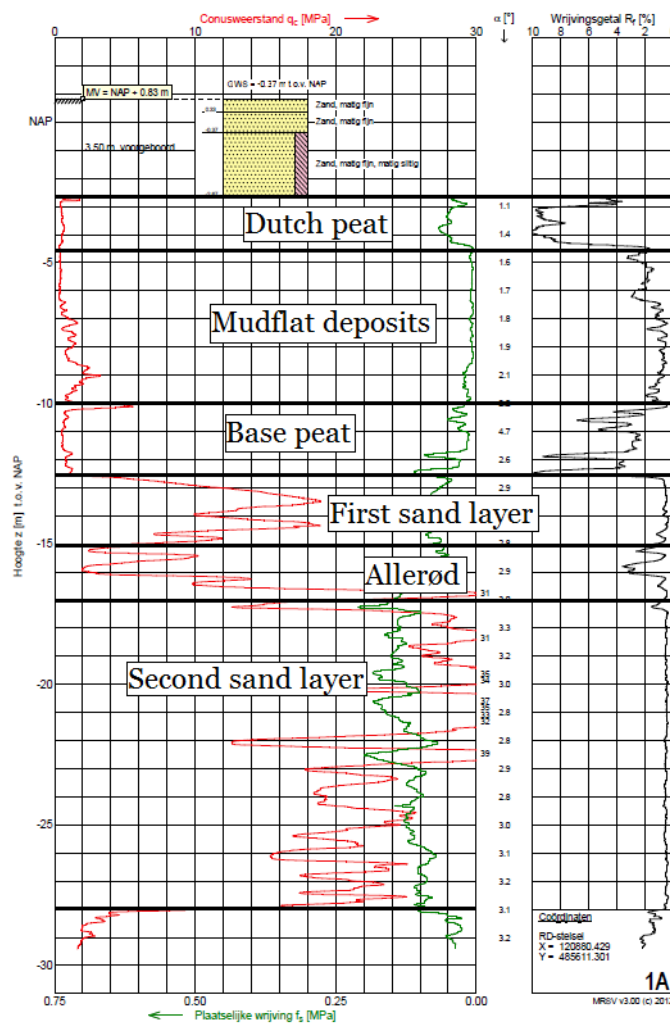
Figure A.1: CPT 1 at the site of the pile load tests.
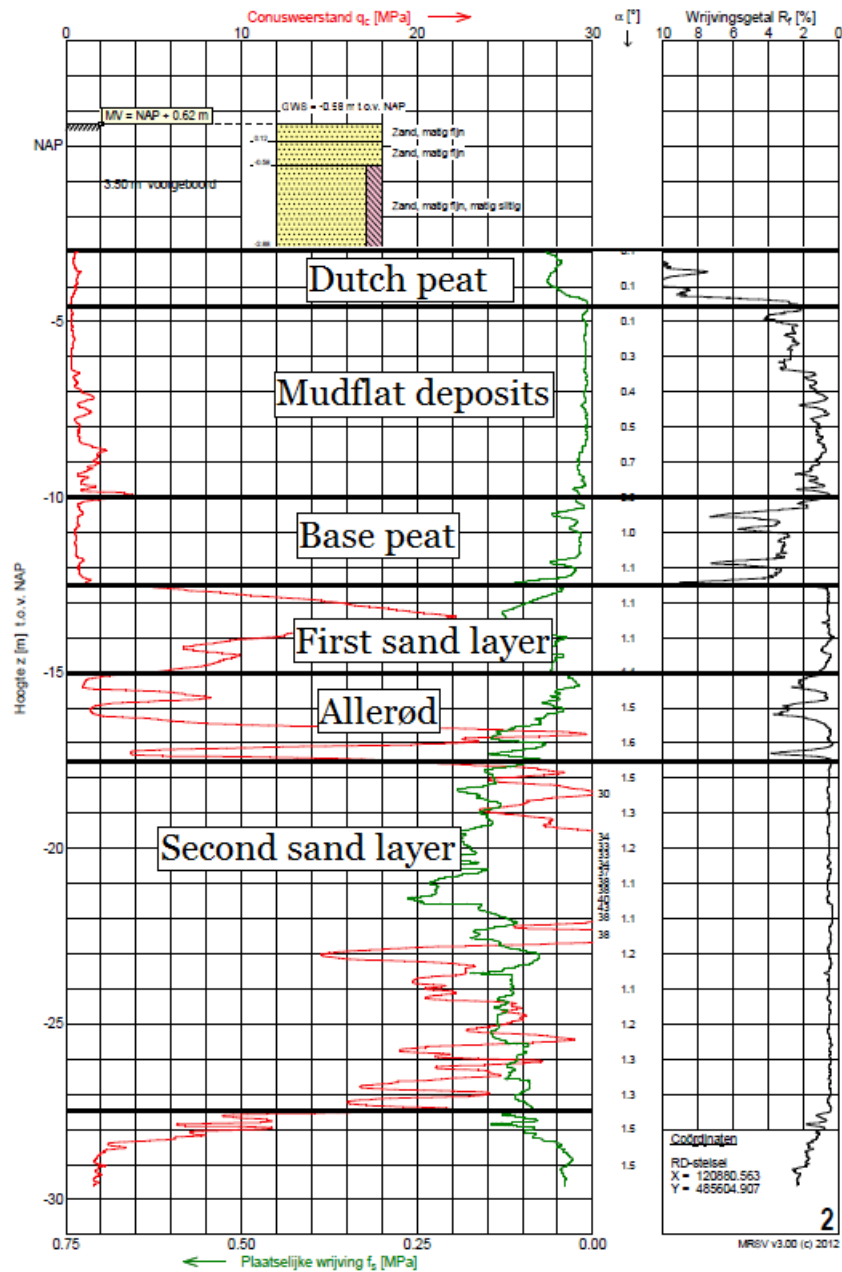
Figure A.2: CPT 2 at the site of the pile load tests.

A.2. Processed load-displacement data pile load tests

Load-displacement diagram, pile 1

Load-displacement diagram, pile 2

Load-displacement diagram, pile 3
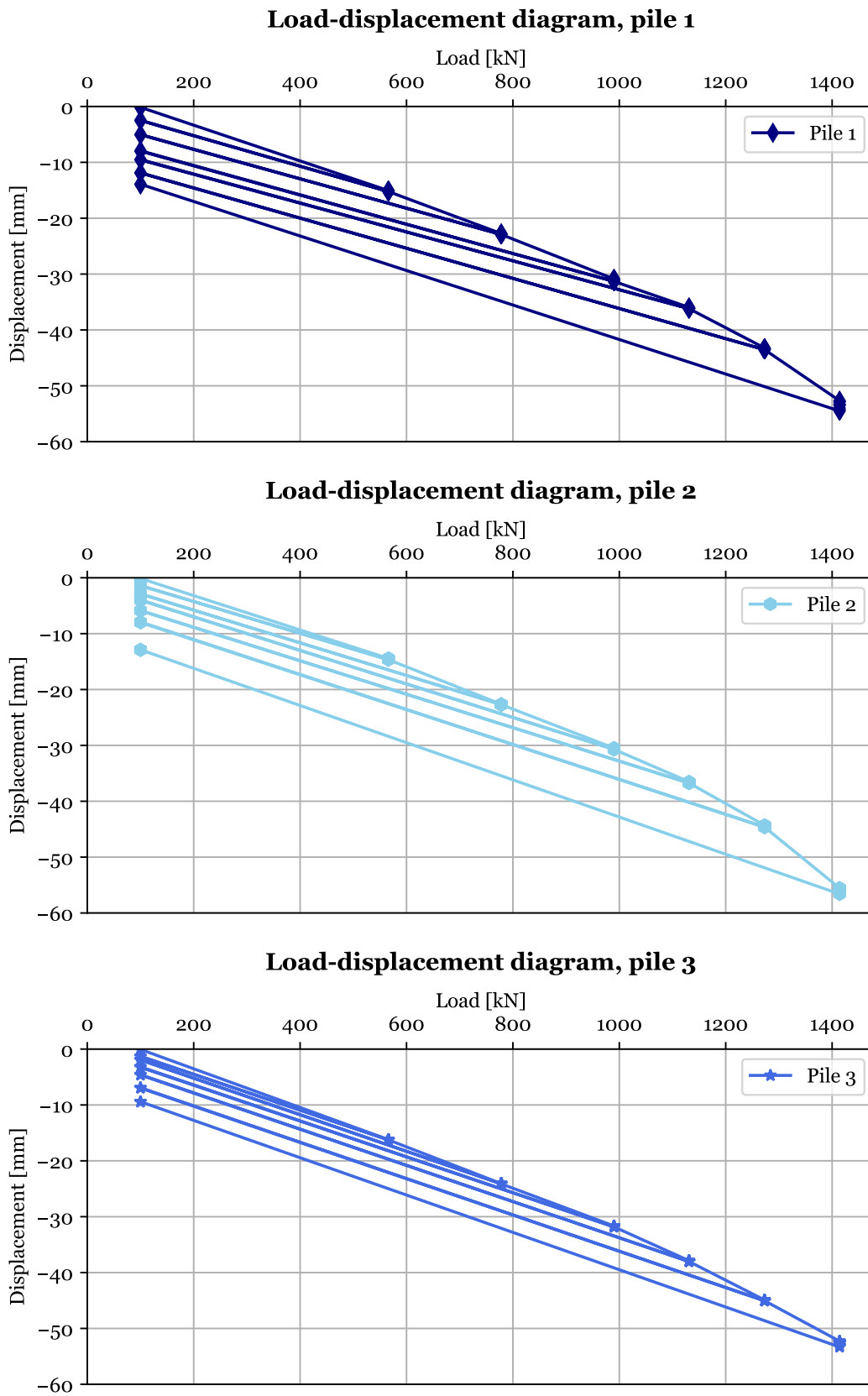
Figure A.3: Load displacement behaviour of test piles 1 to 3.

Load-displacement diagram, pile 4

Load-displacement diagram, pile 5

Load-displacement diagram, pile 6
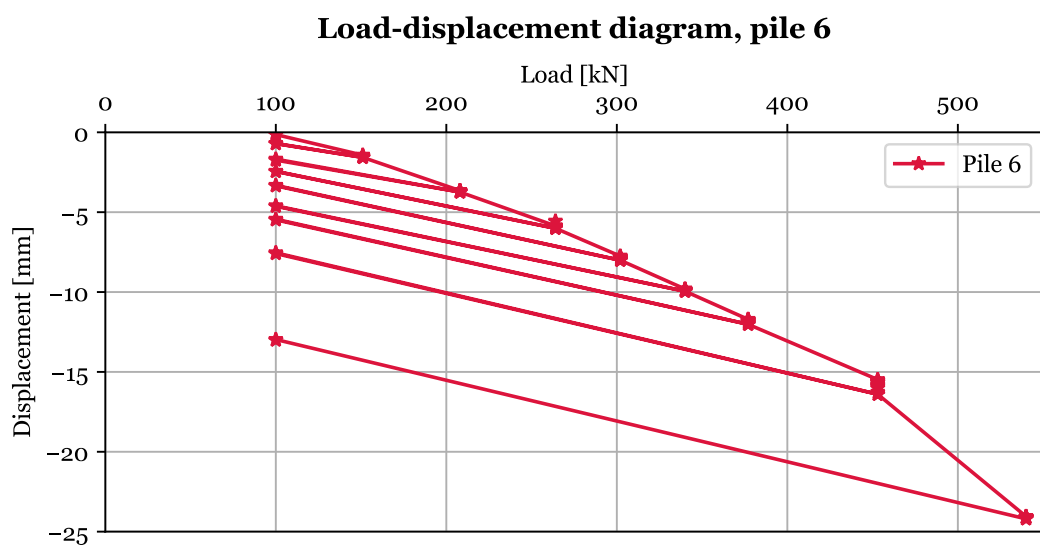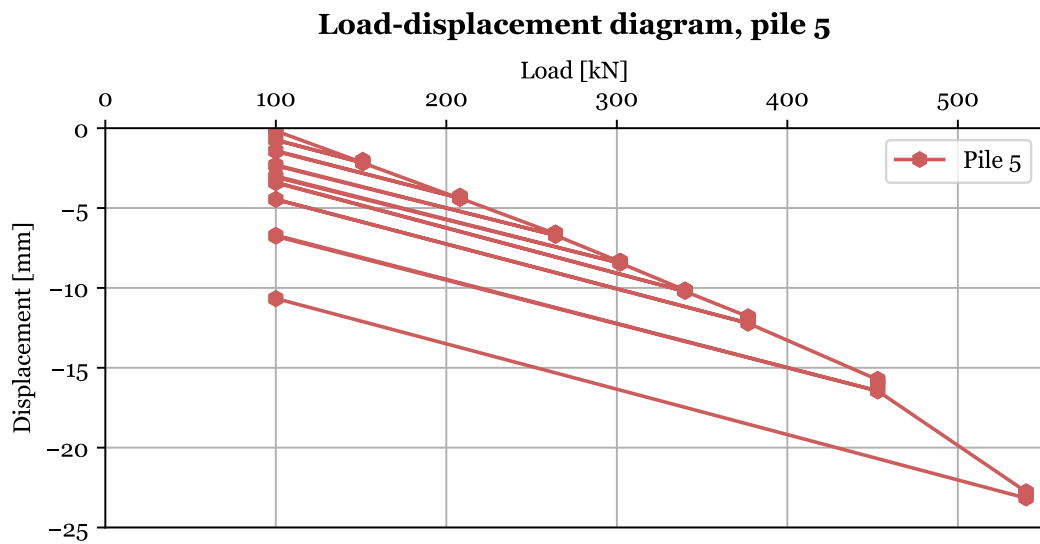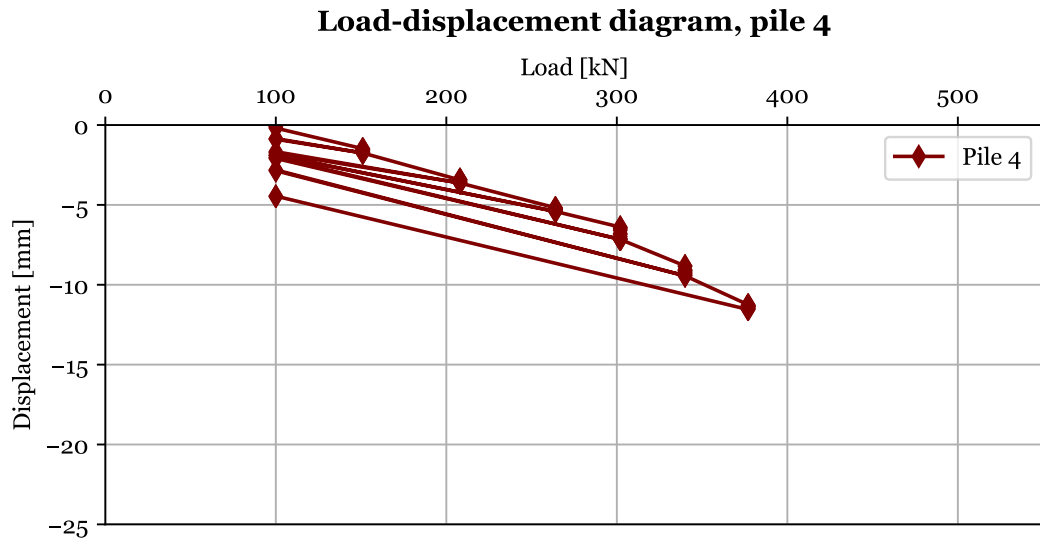
Figure A.4: Load displacement behaviour of test piles 4 to 6.

A.3. 2D FEM models

In this section the chosen 2D model options and input parameters are presented. For the two sets of pile load tests, first and second sand layer, two different models are created. Moreover two modelling options for each groutbody are presented. This results in four different models: two slightly different pile models per sand layer.

A.3.1. Constitutive model

To model the Amsterdam first and second sand layer, the HSs model is selected. Since accurate modelling of the displacements is relevant for modelling the pile load test this non-linear soil model is expected to be more precise than the MC model and the HS model. The biggest disadvantage of this choice is a lower overall efficiency: calculation procedures are more complicated for the HSs model. Due to the limited amount of elements and nodes in the 2D model, efficiency is not yet an issue and therefore accuracy is chosen over efficiency. From the geotechnical data a set of parameters for the HS model is already derived by geotechnical specialists [22]. First estimates of the additional parameters used in the HSs model are obtained with rules of thumb and parameter correlations [4]. The dataset for the HSs model is shown below in table A.1. For the 2D modelling phase the entire soil body is modelled as one soil layer. Only one soil layer is modelled because the load-displacement behaviour of the pile is strongly dependent on the pile stiffness and how the interaction between the groutbody and the second/first sand layer is modelled. Moreover, the GEWI bar that passes all soft top layers is modelled as frictionless making the interaction with the soft top layers less significant.

Table A.1: Plaxis input parameters of the HSs model for the 2D models of both the first and second sand layer.

Hardening Soil small strain - input					
General	**Value**	**Unit**	**Parameters**	**Value**	**Unit**
Drainage type	Drained	-	c'_{ref}	0.10	kN/m^2
γ_{unsat}	17.00	kN/m3	ϕ'	32.00	deg
γ_{sat}	19.00	kN/m3	ψ	2.00	deg
Advanced	Default	-	$\gamma_{0.7}$	0.0002	-
Parameters	**Value**	**Unit**	G_0^{ref}	180,000	kN/m^2
E_{50}^{ref}	30,000	kN/m^2	Advanced	Default	-
E_{oed}^{ref}	30,000	kN/m^2	**Interfaces**	**Value**	**Unit**
E_{ur}^{ref}	90,000	kN/m^2	Strength	Rigid	-
m	0.50	-	R_{inter}	1.00	-

For model 2 the axial skin resistance is 'layer dependent'. Therefore the model behaviour is sensitive to the soil parameters. For the layer dependent model 2, ϕ', ψ and K_0 (tabsheet 'Initial') are adjusted to fit the pile load test data. These adjustments are quantified and discussed in subsections A.3.2 and A.3.3.

A.3.2. Pile models

First, modelling in the axisymmetric environment was reviewed. Modelling with node-to-node anchors or plates in the symmetry axis leads to numerical errors. For both plates and node-to-node anchors, certain geometry input does not match with the concept of the symmetry axis. For example the out-of-plane spacing of the node-to-node anchors is not relevant in axisymmetry. Since it is known that an axisymmetric model is not capable of modelling a square group of piles, no efforts are made to produce a working single pile model in the axisymmetric mode with node-to-node anchors, embedded beam rows (EBR's) and plates.

For a plane strain model the combination of a node-to-node anchor and embedded beam row is the most straight forward choice. The node-to-node anchor does not intersect the soil and has no soil structure interaction between the nodes, ideal for modelling the frictionless GEWI bar. The disadvantage of the node-to-node anchor is the strong anchor-soil interaction at the nodes, where the node-to-node anchor is attached to the node of the soil element. In the first runs of the model this issue proved to cause collapse of the soil body and therefore prematurely ends the calculation. A workaround was found with the implementation of a short plate at the top node of the node-to-node anchor where the load is applied. Disadvantages of the plate element are its continuity in out-of-plane direction and input parameters that do not match the specifications of the actual GEWI 63.5 bar.

The embedded beam row is most capable of modelling the behaviour of the groutbody, this is due to input options such as the diameter, pile spacing and skin resistance. The diameter is chosen to be 0.2 meters, the same as the micropiles in the pile load tests. The pile spacing is set at 20 meters, where almost no pile row interaction is expected [47]. The interface stiffness factor (ISF) is a difficult factor to determine. In the first model run the default values for the ISF were used, which are validated for stiff, bored piles. ISF values for less stiff piles are lower [47], since the ISF values are already very low for a high pile spacing no significant difference is expected. The groutbody stiffness was taken to be the same as the steel GEWI bar. From the pile load test data the axial skin resistance was set at 314 kN/m and 75.4 kN/m respectively.

The results with these parameters proved to show no fit with the pile load test data as presented in figure A.8, section A.4. Therefore it was decided to adjust the groutbody stiffness and the ISF values, the adjustments are motivated in section A.4. The input parameters of the final 2D models are presented in this section. Below in table A.2 the parameters for the embedded beam row model of the groutbody in the first sand layer are shown. Two options are given for the skin resistance of the groutbody model: linear with a predetermined capacity (model 1) and layer dependent (model 2). With the layer dependent model of the groutbody in the first sand layer the ϕ' is adjusted to 33.0 degrees, ψ to 3.0 degrees and the K_0 to 1.50. These adjustments are done after comparing the layer dependent 2D FEM results to the field data.

Table A.2: Plaxis input parameters of the embedded beam row groutbody of the 2D first sand layer model.

Groutbody - first sand layer model 1			Groutbody - first sand layer model 2		
Material set	**Value**	**Unit**	**Material set**	**Value**	**Unit**
E	7.0×10^6	kN/m^2	E	7.0×10^6	kN/m^2
γ	24.00	kN/m^3	γ	24.00	kN/m^3
Pile type	Predefined	-	Pile type	Predefined	-
Predefined pile type	Mas.circular pile	-	Predefined pile type	Mas. circular pile	-
Diameter	0.20	m	Diameter	0.20	m
$L_{spacing}$	20.00	m	$L_{spacing}$	20.00	m
Axial skin resistance	**Value**	**Unit**	**Axial skin resistance**	**Value**	**Unit**
$T_{skin, start, max}$	75.40	kN/m	Axial skin resistance	Layer dependent	-
$T_{skin, end, max}$	75.40	kN/m	T_{max}	100.00	kN/m
ISF	1.00	-	ISF	1.00	-

Below in table A.3 the parameters for the embedded beam row in the second sand layer are shown. Two options are given for skin resistance of the groutbody model: linear with a predetermined capacity (model 1) and layer dependent (model 2). With the layer dependent model of the second sand layer the ϕ' is adjusted to 36.0 degrees, ψ to 6.0 degrees and the K_0 to 3.40. These adjustments are discussed in subsection A.3.3.

Table A.3: Plaxis input parameters of the embedded beam row groutbody of the 2D second sand layer model.

Groutbody - second sand layer model 1			Groutbody - second sand layer model 2		
Material set	**Value**	**Unit**	**Material set**	**Value**	**Unit**
E	5.0×10^6	kN/m^2	E	5.0×10^6	kN/m^2
γ	24.00	kN/m^3	γ	24.00	kN/m^3
Pile type	Predefined	-	Pile type	Predefined	-
Predefined pile type	Mas. circular pile	-	Predefined pile type	Mas. circular pile	-
Diameter	0.20	m	Diameter	0.20	m
$L_{spacing}$	20.00	m	$L_{spacing}$	20.00	m
Axial skin resistance	**Value**	**Unit**	**Axial skin resistance**	**Value**	**Unit**
$T_{skin, start, max}$	314.00	kN/m	Axial skin resistance	Layer dependent	-
$T_{skin, end, max}$	314.00	kN/m	T_{max}	500.00	kN/m
ISF	1.00	-	ISF	1.00	-

The embedded beam row can also be used for modelling the GEWI bar, for this purpose the skin resistance is set at zero and the diameter is set at 0.0635 meter. A comparison between the GEWI bar modelled as embedded beam row and the GEWI bar modelled as node-to-node anchor + plate proved that both choices result in very similar pile head displacements. The author has chosen for the embedded beam row option because of the higher flexibility of the embedded beam row (potential skin resistance and self-weight) and more straightforward geometry.

Table A.4: Plaxis input parameters of the embedded beam row GEWI bar in the 2D model.

GEWI 63.5		
Material set	**Value**	**Unit**
E	210×10^6	kN/m^2
γ	78.00	kN/m^3
Pile type	Predefined	-
Predefined pile type	Mas. circular pile	-
Diameter	0.0635	m
Axial skin resistance	**Value**	**Unit**
$T_{skin, start, max}$	0.00	kN/m
$T_{skin, end, max}$	0.00	kN/m
$L_{spacing}$	20.00	m
ISF	Default	-

A.3.3. Complete models and mesh

The general mesh of all models is presented below in figure A.5. The mesh is 50 meters wide, 27 meters high for the second sand layer models and 22 meters high for the first sand layer models. The embedded beam row is placed in the middle of the mesh at (25 ; 0.0), the EBR groutbodies are at -12.5 m and -17.5 m respectively. The mesh dependency of the results is relatively low, several runs with medium coarse to very fine meshes and local mesh refinements resulted in the same displacement and stress distributions. The point load is not visible in the mesh, but is applied at the top of the upper embedded beam row. The point load is actually an out-of-plane line load in 2D plane strain conditions. Since the pile spacing of the embedded beam row is 20.0 meters, the line load over 20.0 meters must be equal to the point load applied in the pile load tests. The preload of 100 kN, for example, is therefore implemented in the model as a 5.00 kN/m line load.
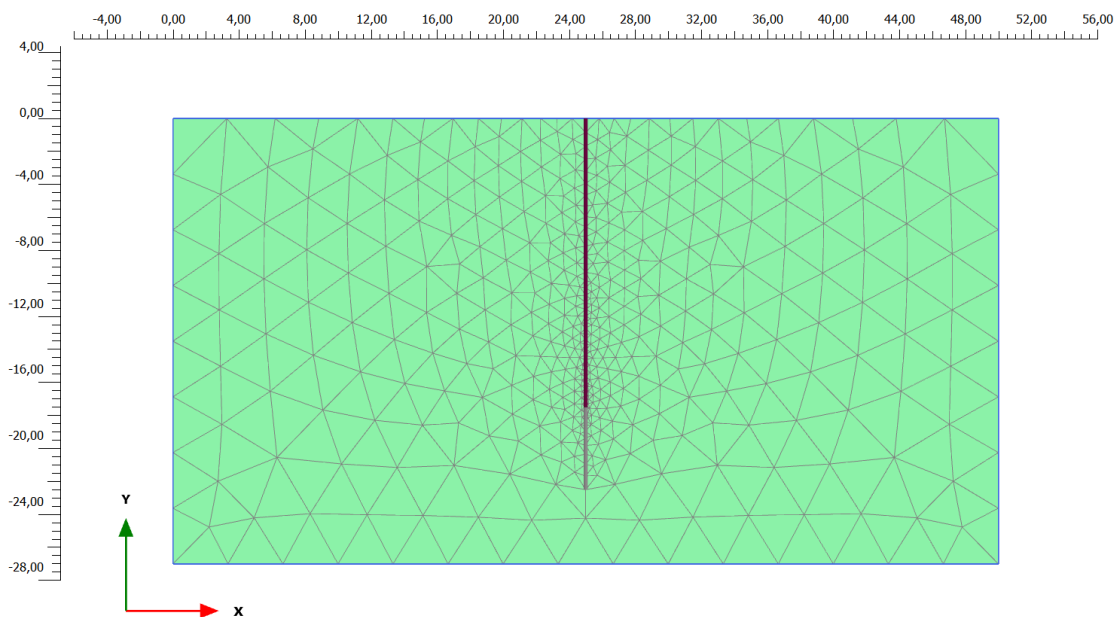
Figure A.5: Medium coarse mesh of the Plaxis 2D linear capacity model, automatically refined around the embedded beam row. The rulers show the dimensions of the model in meters, the comma should be interpreted as a decimal seperator in this case.

Since the behaviour of the embedded beam row (EBR) is dominant in the model, the EBR is presented with more detail as a spring system in figure A.6 to the right. The formulation of the EBR is based on the 3D embedded beam element [43]. The user-defined E-modulus of the EBR is assigned to to entire elastic zone of the EBR and the axial and lateral springs within the dashed lines. The size of this area is determined by the user with the specification of a pile shape and diameter. The elastic behaviour of the interface is determined with the soil shear stiffness parameter, pile spacing and the ISF. The plastic slider is limited by a user input value (for example the 'linear' option) or calculated by Plaxis (the 'layer dependent' option). Both options are used in the 2D modelling phase to gain insight in the differences in strain and stress levels around the EBR for both options.
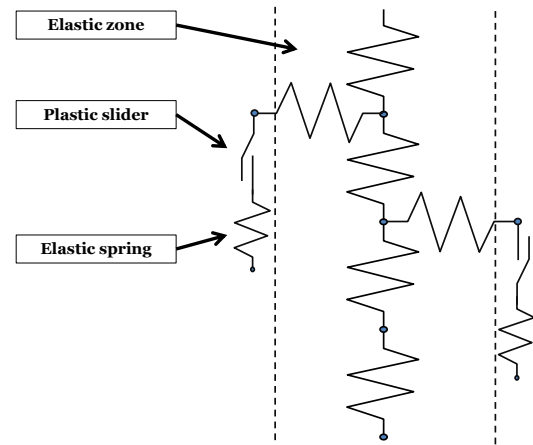
Figure A.6: The embedded beam rows representation in more detail.

The capacity of the layer dependent piles is calculated with the Mohr-Coulomb failure criterion, see equation (2.14). This capacity determines at which stress level the plastic slider, shown in figure A.6, is activated. By adjusting the soil input parameter values for the friction angle ϕ' or the lateral earth pressure coefficient at rest K_0, the capacity of the layer dependent EBR's is increased or decreased. In the current 'layer dependent' model this adjustment of the soil parameters accounts for the entire second sand layer, shown as the light blue layer in figure A.7. These adjustments cause a very sudden increase in strength and horizontal effective stress at the boundary of the soil layers. This situation is not realistic when compared to the results of CPT's at the site. Nevertheless, the default effective stress level calculation procedure of Plaxis does not take the local conditions into account as well. The new values could be realistic for a zone close to the groutbody: this zone both being over-consolidated in at rest conditions and influenced by the installation process of the pile. In a later stage of this research when group effects are investigated, the soil stress and strength distribution is a crucial factor and must therefore be determined more accurate.
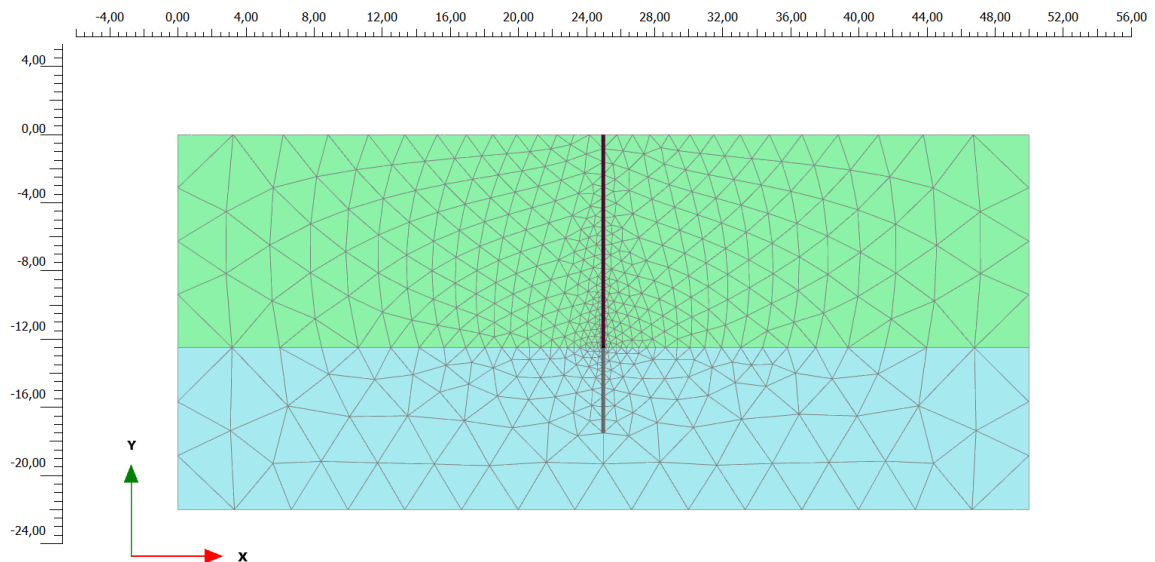
Figure A.7: Medium coarse mesh of the Plaxis 2D layer dependent model, automatically refined around the embedded beam row. The rulers show the dimensions of the model in meters, the comma should be interpreted as a decimal seperator in this case.

A.4. FEM 2D model results

In this section the model results of the different 2D FEM models are presented. The results from the first input set, with a high groutbody stiffness and default ISF, the unloading-reloading behaviour of the pile is elastic and no significant plastic strains are produced during the six different loading stages. Next to the pile behaviour, the interface behaviour is mainly elastic. This behaviour is presented below in figure A.8.
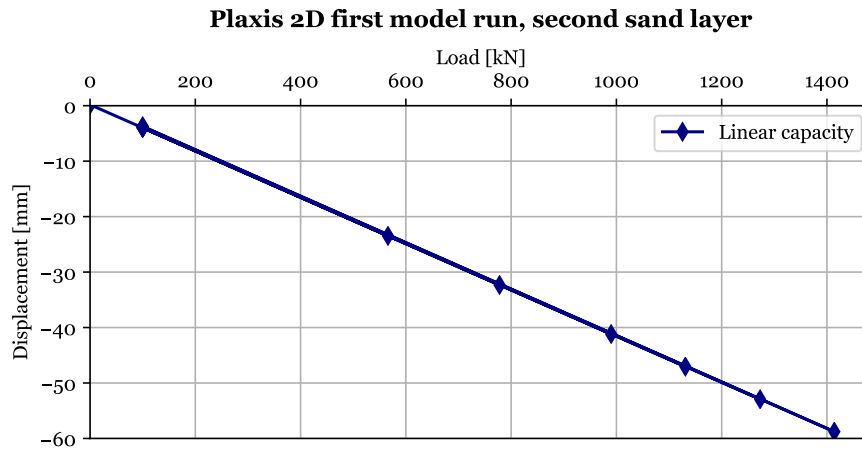
Figure A.8: Load-displacement behaviour of a micropile in the second sandlayer, modelled in Plaxis 2D.

A closer look at these output results shows that the pile head displacement at unloading stages even decreases compared to the pre loading stage of 100 kN. From theory the opposite behaviour is expected: during the loading stage plastic strains develop which means the total vertical displacement should increase after each loading stage. The author expects this behaviour to be due to the soft, fully elastic behaviour of the interface. Upon the final unloading stage the maximum displacement is equal to 3.7 mm, slightly lower than the maximum displacement after pre loading. From a brief sensitivity study of the input parameters, the Young's modulus (E-modulus) of the pile and the ISF of the pile interface appear to be the most significant parameters. In figure A.9 below, the significance of the E-modulus and pile spacing (directly affecting the default ISF) can be clearly distinguished. The E-modulus governs the elastic deformation of the pile. The elongation of the GEWI bar is visible in all three cases: it determines the slope of the displacements in the upper part of the pile, see figure A.9. The three cases have different input parameters for the pile spacing: 5.0 m, 20 m and 40m. These three different spacings result in different default ISF values and therefore in significant differences in the pile-soil interface stiffness. The difference in pile-soil interface stiffness leads to different vertical displacements of the interface in each case.
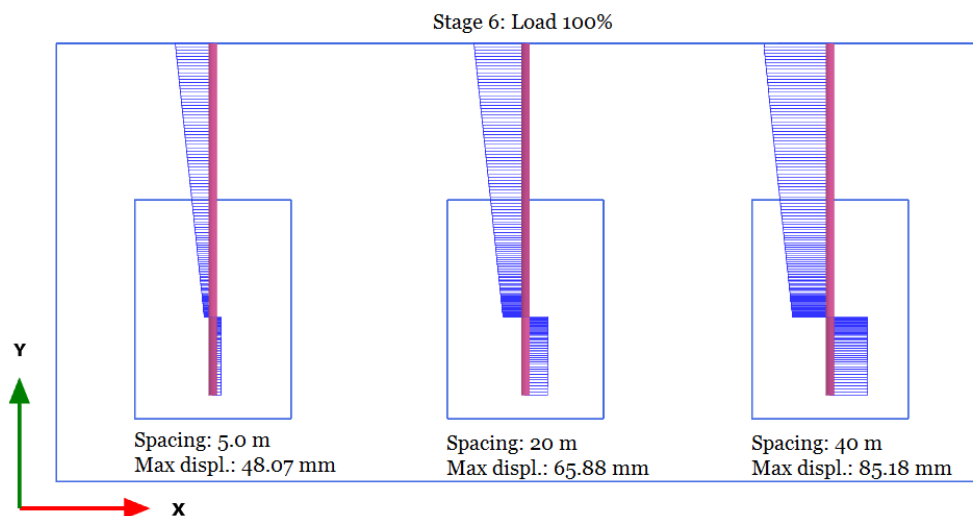
Figure A.9: Significance of the E-modulus and ISF in the displacement behaviour of the EBR.

The elastic deformation of the pile body during the final loading stage is equal to approximately 35 mm, which is a significant portion of the total displacement. The elastic deformation of the interface accounts for the remaining displacement of the pile, its significance increasing with higher pile spacing as visible in figure A.9. After these results it was concluded that the E-modulus of the groutbody and the stiffness of the interface (ISF) had to be adjusted in order for the 2D model to capture the non-linear load-displacement behaviour found in the pile load tests.

In the set of final input parameters presented in subsection A.3.2, the groutbody stiffness is reduced and the ISF is set at 1.0. The reduction of the groutbody stiffness is done for two reasons: in reality the stiffness of the groutbody will be lower than the stiffness of steel which was used for the first model run. Moreover, a lower stiffness makes partial plastic behaviour of the groutbody interface possible. A reduced stiffness leads to different displacements at the top and the bottom of the groutbody and therefore different levels of shear mobilisation at different loads. This partially plastic behaviour is visible in the pile load test data and is expected to represent the real groutbody interface behaviour more closely. The new stiffness value of the groutbody was determined iteratively by comparison with the plastic and elastic deformations measured in the pile load tests. As shown in table A.2 and A.3 the stiffness is determined at $5.0 \times 10^6 \, kN/m^2$ to $7.0 \times 10^6 \, kN/m^2$. This new value is relatively low when compared to the stiffness of for example the steel GEWI bar (210 GPa) or cracked reinforced concrete (approx. 10 GPa).

The adjustment of the ISF was based on the observed high elastic displacements at the bottom of the groutbody, see A.9. This shows a significant influence of a relatively soft interface that never reaches plastic behaviour. To reduce the influence of the elastic displacements of the interface, the ISF is determined at 1.0. A value of 1.0 means that the interface stiffness is equal to the shear stiffness of the soil divided by the pile spacing [47].

In figure A.10 it can be seen that the groutbody is mobilised from the top down. At the top of the grout body the maximum skin friction that can be mobilised is reached already at a load of 40%, therefore this part of the groutbody slides plastically in the model. The plastic zone increases at each load step, some margin in the capacity remains at the 100% load since the skin friction is not yet completely mobilized.
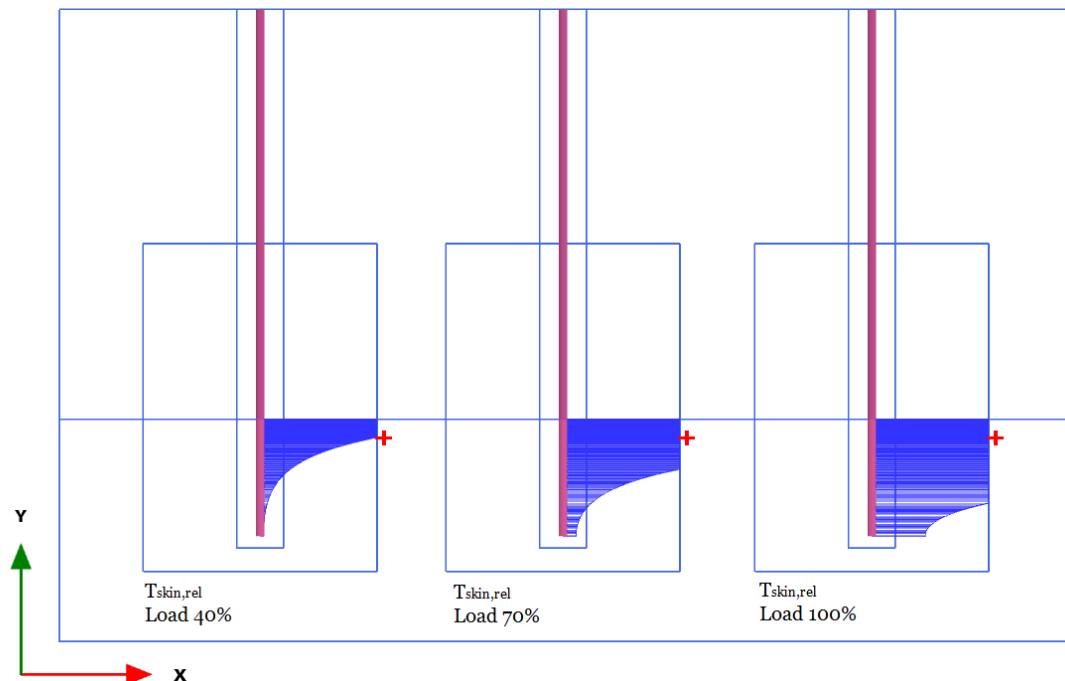
Figure A.10: The skin friction mobilisation of the groutbody for load levels 40%, 70% and 100%.

With the final parameters the load-displacement behaviour of the 2D model shows plastic deformations in all models. Below in figure A.11 and A.12 the load-displacement behaviour of the linear capacity models (model 1) for both sand layers is presented. For the micropile in the second sand layer the maximum load reached in the model is 1414 kN, corresponding to a displacement of 58 mm. The displacement after the final unloading step is approximately 12 mm.
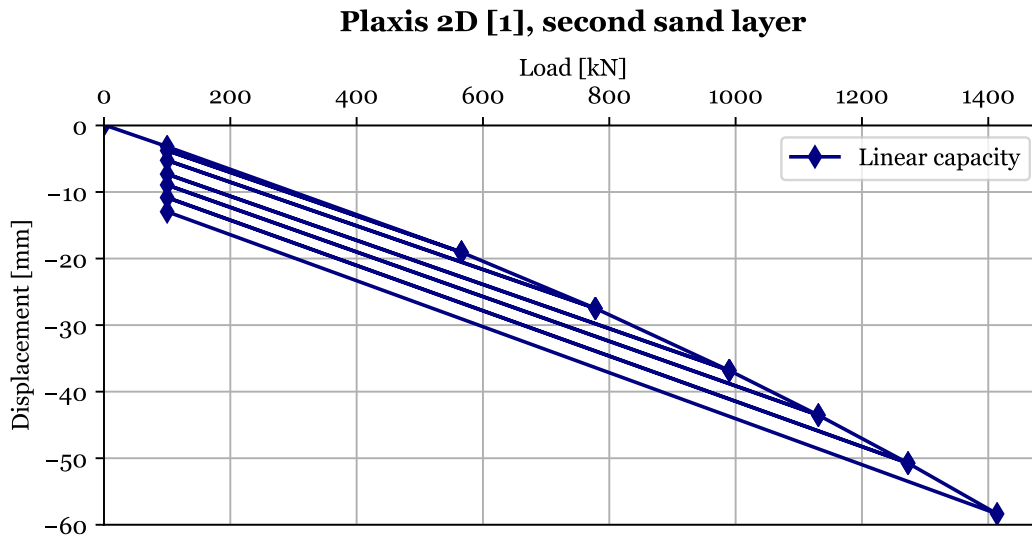
Figure A.11: Load-displacement behaviour of a single micropile in the second sandlayer, model [1].

The behaviour of a single micropile in the first sand layer is presented in figure A.12 below. For the micropile in the first sand layer the maximum load reached is 377 kN, corresponding to a displacement of approximately 12 mm. The displacement after the final unloading step is approximately 4.5 mm.
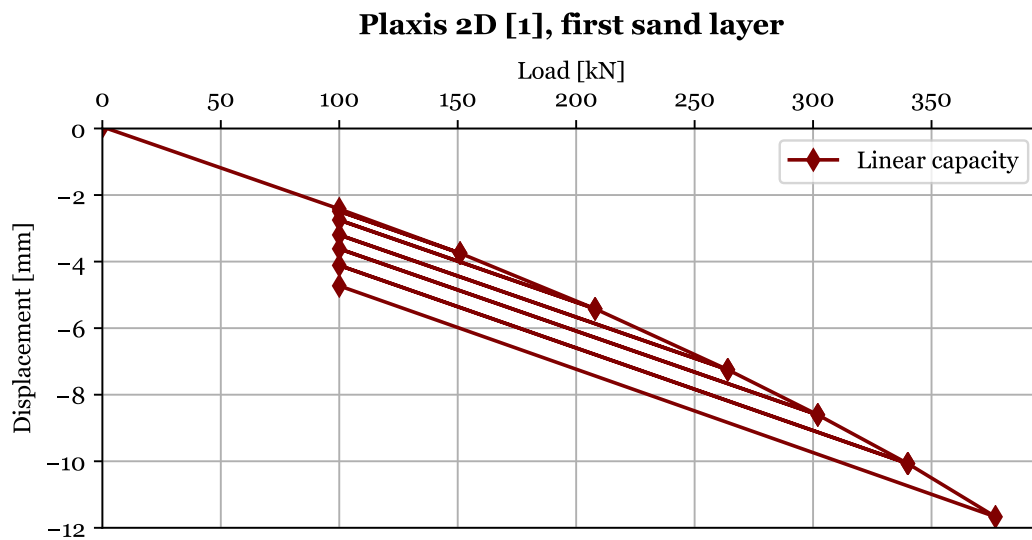
Figure A.12: Load-displacement behaviour of a single micropile in the first sandlayer, model [1].

A.4.1. Model 2, load-displacement behaviour

The load-displacement behaviour of the layer dependent models (model 2) differs insignificantly from the models with a linear capacity. The results of these models are presented below.
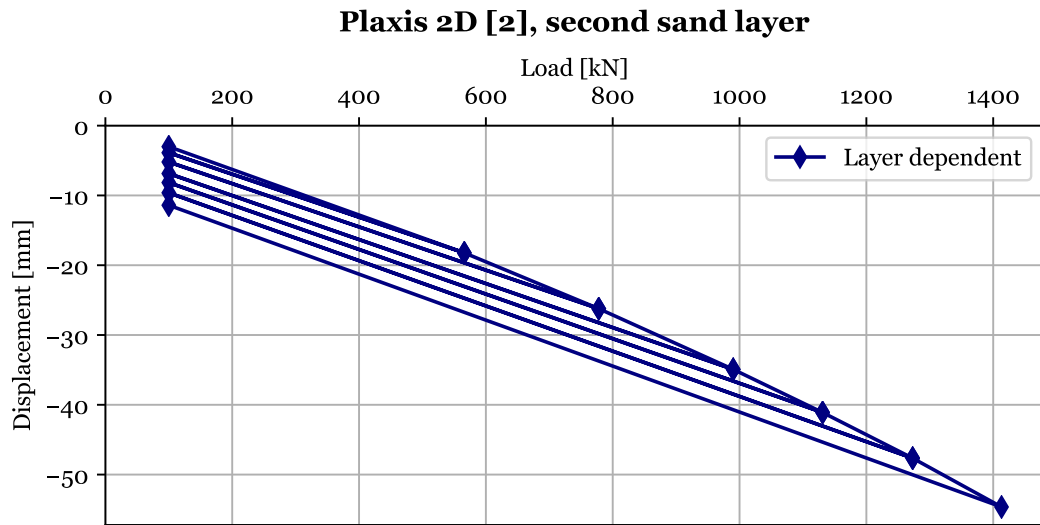
Figure A.13: Load displacement behaviour of model 2 for a single micropile in the second sand layer.
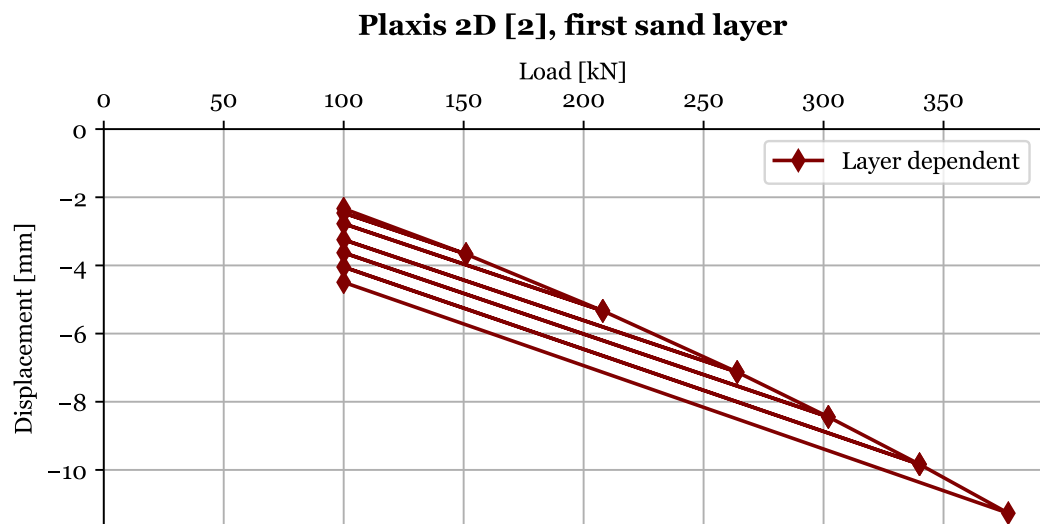
Figure A.14: Load displacement behaviour of model 2 for a single micropile in the first sand layer.

A.5. 2D model and field data comparison

The modelled behaviour found in the first model run does not stroke with the behaviour observed in the pile load test, since significant plastic strains are observed in the pile load test data. The model data from this first input set is therefore not compared with the field data and not further discussed in this section.

In figures A.15 and A.16 below the results from model 1 (linear capacity of the EBR groutbody) of both sand layers are compared to the field data. First the comparison of the data for the second sand layer is presented. For a neat presentation of the comparison, only the data points of the field data are presented, the interpolation is omitted.
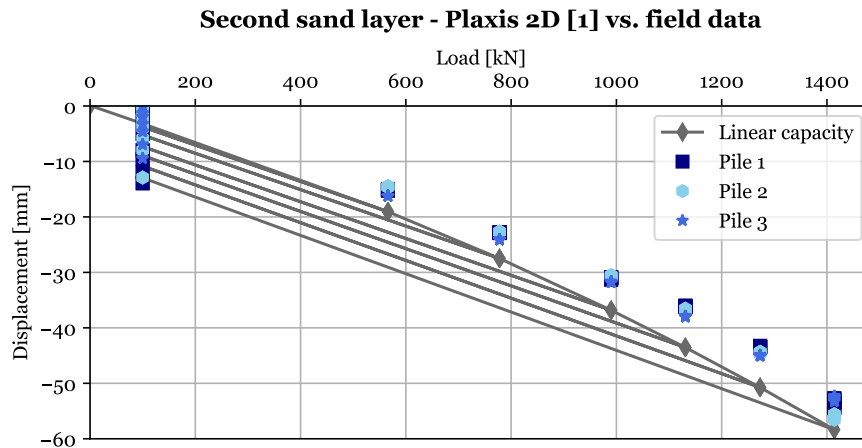
Figure A.15: The Plaxis 2D model 1 results versus the field data for the second sand layer.

For the first sand layer only the data from the six loading stages of all three piles is presented. The fifth and the sixth pile were loaded up to two additional loading stages. Modelling the more gradual failure, visible in the pile load test data of pile 5 and 6, in Plaxis is inconsistent with the currently used axial capacity and groutbody stiffness of the model. Failure in the Plaxis model happens instantly, just after the 100% load level is reached. For consistency in the comparison of the pile load tests in the first sand layer with the numerical results, the two additional loading stages of pile 5 and 6 are omitted.
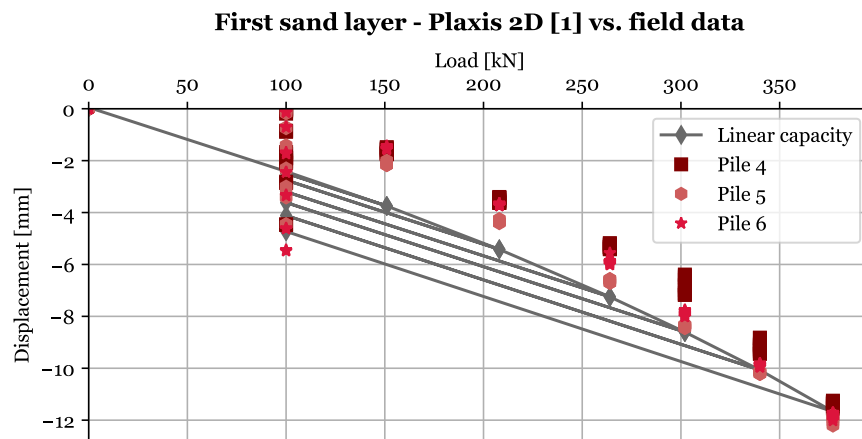
Figure A.16: The Plaxis 2D model 1 results versus the field data for the first sand layer.

There is still an overestimation of the elastic deformation visible, despite the relatively high stiffness of 210 GPa that is used for the GEWI bar. The overestimation of the deformation decreases with higher loads, especially in the first loading stages the overestimation is significant. The overestimation is due to the pre loading phase which is used as calibration for the instruments in the pile load tests. The fit for both pile load test data sets is improved by resetting the displacements after the 100 kN pre loading phase in the Plaxis 2D model. Moreover the fit of the data from the first sand layer is further improved by choosing a lower

groutbody stiffness of $4.0 \times 10^6 \, kN/m^2$. The stiffness of the groutbody in the second sand layer is adjusted to $4.5 \times 10^6 \, kN/m^2$. The final fits with the field data are shown in the main report: section 3.3, figure 3.7 and 3.8. The model used for the final fits is defined as 'model 3'. Model 3 is almost identical to model 1, since it includes the linear capacity option for the groutbody. As described above there are two major differences between these models: a displacement-reset after the preloading phase and an adjustment of the groutbody stiffness to compensate for overestimation of the stiffness in model 1 and 2. This overestimation of the stiffness is because of displacements in the preloading phase: a higher stiffness of the groutbody was chosen to fit the displacements at the final loading stages.

B

Appendix B

B.1. 3D single pile models, development process

For the development of a 3D model, the lessons learned from the 2D modelling phase are used as a starting point. In the 2D model the GEWI bar is modelled with an embedded beam row (EBR), the same strategy is chosen for the 3D models. The residual grout/betonite/soil mixture surrounding the GEWI bar above the groutbody is ignored in this first approach.

Two different structural input elements are investigated for the groutbody: an embedded beam element (EBE) and volume elements. For both elements different options are investigated to determine the strength and stiffness of the interface behaviour. Modelling the interface behaviour correctly is a significant part of the 3D model. The interface behaviour largely dictates the load transfer from the pile to the surrounding soil, strongly influencing the redistribution of the load in the soil body. With the embedded beam element, the linear capacity and layer dependent capacity options are investigated. For the interface behaviour of the model with volume elements two procedures are investigated: adjustment of the soil parameters and simulation of the installation procedure. First the models consisting of EBE's are described, afterwards the models consisting out of volume elements are presented.

B.1.1. Embedded beam element models

In figure B.1 three types of EBE models are shown, the two models on the right are more extensively investigated and elaborated in this subsection. The model on the left, with a N2N representing the GEWI bar proved to cause to much issues with soil displacements at the top. This experience was similar as in the 2D modelling phase.
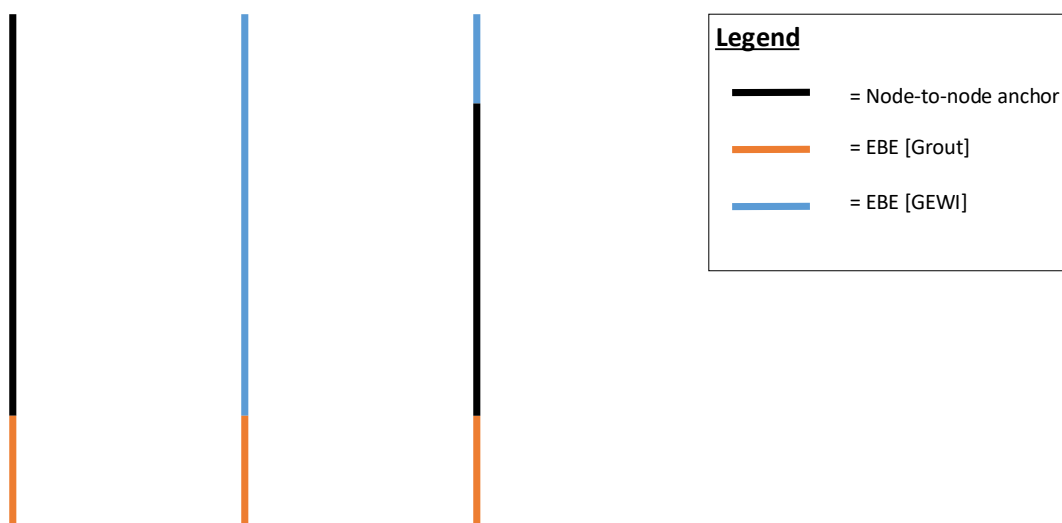
Figure B.1: 3D models consisting of embedded beam elements visualized in a simplified manner.

The second model, where the GEWI bar is modelled with a frictionless EBE, does work. Nevertheless the results show issues: without any lateral force introduced, lateral displacements do occur. Several options were tried, such as using a small axial skin resistance or refining the mesh, but this did not solve the problem. The problem did not occur when the groutbody was modelled as a very stiff element.

To minimize the internal relative displacements of the EBE, but still make use of the 'slip' behaviour, a node-to-node (N2N) anchor is introduced and the EBE is only used for the upper two meters of the GEWI bar. The length of two meters is chosen to limit the influence on the 3D meshing procedure for a coarse mesh. This third model produced stable results and was easily fit with the data from the pile load tests. The capacity of the EBE groutbody was set to 'linear capacity' and therefore a user input value. Since the capacity is a user input value this option is not suitable to investigate the capacity of a micropile in a group. Therefore the layer dependent option was used, with this option the capacity is dependent on the friction angle, lateral earth pressure coefficient and mean effective stress level at the interface of the pile. The mean effective stress level was chosen by Plaxis to be a good estimate of the effective stress level normal to the pile interface. For this investigation, where the horizontal stress level at the pile soil interface is relatively high compared to the vertical stress level, this approximation would be very crude. Moreover, due to the elastic zone created by the EBE it is unclear whether installation effects could be implemented at the interface of the embedded beam. The elastic zone keeps all soil elements within the user specified diameter elastic, but the interface behaviour of the pile is numerically determined at the centerline of the pile. It is decided that the research can best be carried out with volume elements for the groutbody, despite the strongly increased calculation time.

B.1.2. Volume element models

In figure B.2 three types of models with a volume element as groutbody are shown. The left model consists of the N2N-EBE combination for the GEWI bar. After analysing the output of the pile load tests it was found that for this model the most resistance against pull-out develops at the top of the groutbody. In reality some resistance will develop at the top of the groutbody, but after the installation process the gap around the GEWI in the soft layers will mostly be filled with a mixture of soil, grout and bentonite. It is known that most resistance develops along the shaft of the pressure grouted groutbody. To capture this behaviour, another volume is created starting from level to the top of the groutbody. Inside both volumes different line elements such as beams and EBE's were tested to model the behaviour of the GEWI bar. This investigation showed that none of the line elements added additional accuracy or realism to the behaviour of the micropile model. The interaction between the GEWI bar and grout or residual grout is very difficult to model in a 3D numerical program. The calculation procedure became slow and unexpected stress concentrations and numerical issues appeared due to the high stiffness differences in closely spaced nodes. The third model is the final model and the structural details are described in the main report, see section 4.1.1. Compared to the single soil layer in the 2D plane strain models the final model does include a distinction between the soft top layers and the two sand layers. This was done to make sure no load transfer takes plays at the upper section of the micropile model. Moreover, the horizontal stress levels and soil stiffness are relevant for the model behaviour in this modelling approach, a single sand layer is a too crude estimation of the field conditions.
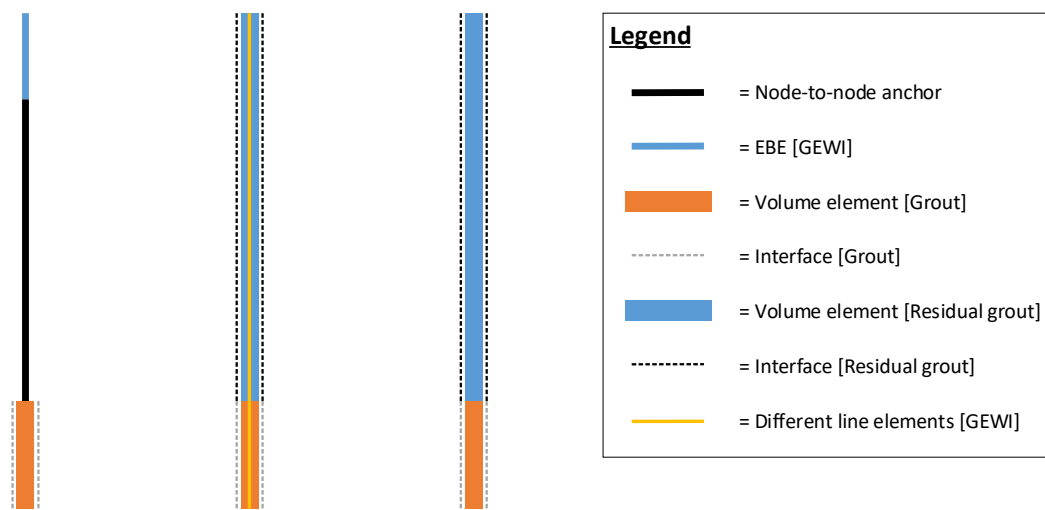
Figure B.2: 3D models consisting of volume elements visualized in a simplified manner.

B.2. 3D final single pile models, input parameters

The fitting of the results from the pile load tests is mainly done by adjusting the groutbody stiffness, the soil strength (ϕ' and ψ) and the K_0-parameter. The internal friction angle used in numerical models of the second sand layer varies between 32.0 and 35.0 degrees in different researches [3, 22, 36]. During the fitting an internal friction angle was tried in this range, the dilatancy angle was derived according to the approximation $\phi' - 30$. The K_0-parameter can vary between the active and passive earth pressure coefficient, depending on the OCR of the soil [14, 34]. From the CPT data it is seen that both the first and second sand layer have relatively high cone resistance values for layers at such depth. From practical experience with these soil layers it is known that they are over consolidated, to what extent is unknown. As a lower boundary the Jaky formula is taken, also the default value used in Plaxis. The upper boundary is more difficult to determine since the OCR of the soil is unknown, but a conservative maximum of 2.0 is assumed [14]. The stiffness of the groutbody is another uncertainty, the difficult interaction between the grout, steel and the soil determines the stiffness of the pile during pile load tests. The value is selected in such a way that partial failure (resulting in plastic displacements) occurs in the interface to fit the plastic displacements found in the field tests. This parameter is the most significant parameter in fitting the model outcome to the field data. Lastly the virgin soil stiffness parameter E_{50} was used to improve the fit. In the 80%, 90% and 100% loading stages the model displacements were unsatisfying: the Plaxis model behaved to soft. Due to the greater soil plug that is mobilised during these loading stages it was decided that an increase in the E_{50} parameter would improve the overall fit. The adjustment of the virgin soil stiffness is also physically defensible. The first estimate was based on parameter determination done for a different project and location, where limited tests were performed to determine the virgin stiffness of the second sand layer. Based on the high cone resistance values and the over consolidated nature of the second sand layer, the newly selected value of 45,000 kPa is realistic. In tables B.1 to B.5 below the input parameters for the different structural elements and soil layers are presented.

Table B.1: Plaxis 3D input parameters for the linear elastic model for the residual grout body and the MC model of the interface.

Linear elastic - input residual grout					
General	**Value**	**Unit**	**Parameters**	**Value**	**Unit**
Drainage type	Non-Porous	-	E	185×10^6	kN/m^2
γ_{unsat}	0.00	kN/m^3	v (nu)	0.01	-
γ_{sat}	0.00	kN/m^3	Advanced	Default	-
Mohr-Coulomb - input interface residual grout					
General	**Value**	**Unit**	**Parameters**	**Value**	**Unit**
Drainage type	Drained	-	v (nu)	0.01	-
γ_{unsat}	17.00	kN/m^3	c'$_{ref}$	0.10	kN/m^2
γ_{sat}	19.00	kN/m^3	ϕ'	10.00	deg
Parameters	**Value**	**Unit**	ψ	0.00	deg
E	5,000	kN/m^2	Advanced	Default	-

Table B.2: Plaxis 3D input parameters for the linear elastic model of the groutbody.

Linear elastic - input groutbody pile 4-6					
General	**Value**	**Unit**	**Parameters**	**Value**	**Unit**
Drainage type	Non-Porous	-	E	4.5×10^6	kN/m^2
γ_{unsat}	24.00	kN/m^3	v (nu)	0.01	-
γ_{sat}	24.00	kN/m^3	Advanced	Default	-
Linear elastic - input groutbody pile 1-3					
General	**Value**	**Unit**	**Parameters**	**Value**	**Unit**
Drainage type	Non-Porous	-	E	5.0×10^6	kN/m^2
γ_{unsat}	24.00	kN/m^3	v (nu)	0.01	-
γ_{sat}	24.00	kN/m^3	Advanced	Default	-

Table B.3: Plaxis 3D input parameters for the HSs model for the mudflat deposits.

Hardening Soil small strain - input Mudflat deposits					
General	**Value**	**Unit**	**Parameters**	**Value**	**Unit**
Drainage type	Drained	-	ϕ'	25.00	deg
γ_{unsat}	16.00	kN/m^3	ψ	0.00	deg
γ_{sat}	16.00	kN/m^3	$\gamma_{0.7}$	0.0001	-
Advanced	Default	-	$G_0{}^{ref}$	30,000	kN/m^2
Parameters	**Value**	**Unit**	Advanced	Default	-
$E_{50}{}^{ref}$	5000	kN/m^2	**Interfaces**	**Value**	**Unit**
$E_{oed}{}^{ref}$	5000	kN/m^2	Strength	Rigid	-
$E_{ur}{}^{ref}$	20,000	kN/m^2	R_{inter}	1.00	-
m	0.80	-	**Initial**	**Value**	**Unit**
c'_{ref}	2.00	kN/m^2	POP	10.00	kN/m^2

Table B.4: Plaxis 3D input parameters for the HSs model for the first sand layer.

Hardening Soil small strain - input first sand layer OC					
General	**Value**	**Unit**	**Parameters**	**Value**	**Unit**
Drainage type	Drained	-	ψ	2.00	deg
γ_{unsat}	17.00	kN/m^3	$\gamma_{0.7}$	0.0002	-
γ_{sat}	19.00	kN/m^3	$G_0{}^{ref}$	180,000	kN/m^2
Advanced	Default	-	Advanced	Default	-
Parameters	**Value**	**Unit**	**Interfaces**	**Value**	**Unit**
$E_{50}{}^{ref}$	30,000	kN/m^2	Strength	Rigid	-
$E_{oed}{}^{ref}$	30,000	kN/m^2	R_{inter}	1.00	-
$E_{ur}{}^{ref}$	90,000	kN/m^2	**Initial**	**Value**	**Unit**
m	0.50	-	K_0	Manual	-
c'_{ref}	0.10	kN/m^2	$K_{0,x} = K_{0,z}$	Yes	-
ϕ'	32.00	deg	$K_{0,x}$	1.00	-

Table B.5: Plaxis 3D input parameters for the HSs model for the second sand layer.

Hardening Soil small strain - input second sand layer OC					
General	**Value**	**Unit**	**Parameters**	**Value**	**Unit**
Drainage type	Drained	-	ψ	4.00	deg
γ_{unsat}	17.00	kN/m^3	$\gamma_{0.7}$	0.0002	-
γ_{sat}	19.00	kN/m^3	$G_0{}^{ref}$	180,000	kN/m^2
Advanced	Default	-	Advanced	Default	-
Parameters	**Value**	**Unit**	**Interfaces**	**Value**	**Unit**
$E_{50}{}^{ref}$	45,000	kN/m^2	Strength	Rigid	-
$E_{oed}{}^{ref}$	30,000	kN/m^2	R_{inter}	1.00	-
$E_{ur}{}^{ref}$	90,000	kN/m^2	**Initial**	**Value**	**Unit**
m	0.50	-	K_0	Manual	-
c'_{ref}	0.10	kN/m^2	$K_{0,x} = K_{0,z}$	Yes	-
ϕ'	34.00	deg	$K_{0,x}$	1.00	-

B.3. 2D axisymmetric models

In this section the 2D axisymmetric models with volume elements, used as comparison for the 3D single pile models, are described in more detail. These models were developed because of the higher accuracy of the 15-noded 2D triangular elements and the lower calulation time. The installation simulation and the loading stages are the same as for the final 3D models, which are described in the main report. The mesh and model input parameters deviate and are therefore elaborated in the subsections below.

B.3.1. 2D axisymmetric models mesh

Below in figures B.3 to B.6 the meshes of the axisymmetric models for the pile load tests performed in the first and second sand layer are shown. For both models the overall mesh coarseness is set to very fine. An additional zone around the groutbody, with a length of 6.0 meters and width 1.0 meters, is refined. The coarseness factors for the different parts of the model are shown in table B.6, the different zones can be seen in figures B.3 and B.4.

Table B.6: The coarsenessfactors of the different volumes and lines in the 2D axisymmetric models.

Volume/surface	Coarsenessfactor
Residual grout volume	4.0
Residual grout interface	1.0
Grout volume	0.5
Grout interfaces	0.0625
Volumes at corner of groutbody	0.125
Volume to the right of the groutbody	0.25

The model of the first sand layer is 6.0 meters by 20 meters, the model of the second sand layer is 6.0 meters by 25 meters. Next to the complete model overview a zoom is provided of the groutbody volume where the mesh gets very fine in figures B.5 and B.6
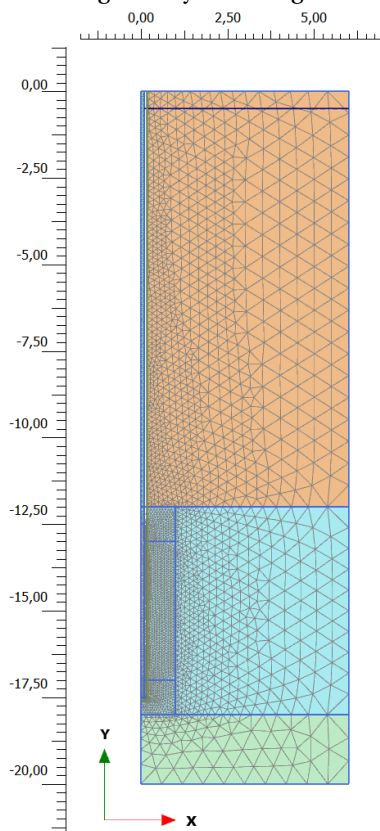
Figure B.3: Full mesh, 2D axisymmetric model of the micropiles in the first sand layer.
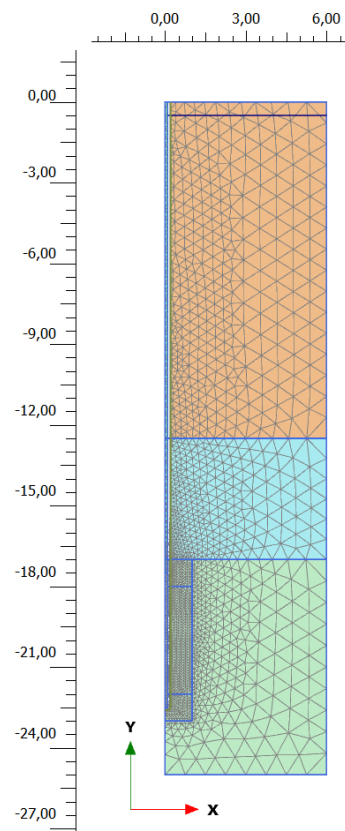
Figure B.4: Full mesh, 2D axisymmetric model of the micropiles in the second sand layer.
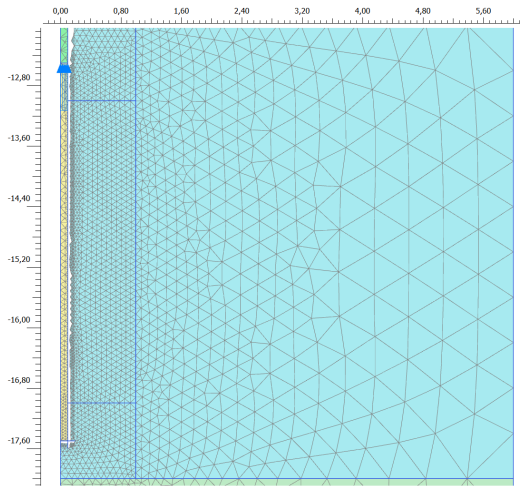
Figure B.5: Zoom of the groutbody, 2D axisymmetric model of the micropiles in the first sand layer.
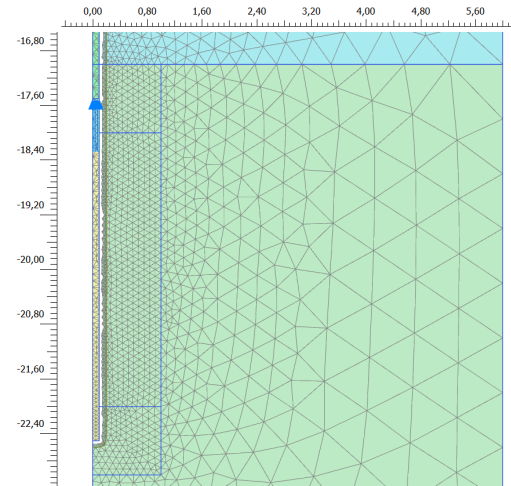
Figure B.6: Zoom of the groutbody, 2D axisymmetric model of the micropiles in the second sand layer.

B.3.2. 2D axisymmetric models, input parameters

In the tables below all input parameters of the different structural and soil volumes and interfaces are presented. First of all the parameters of the groutbodies can be found in B.7. The input parameters of the mudflat deposits and the residual groutbody and residual grout interface are the same as for the 3D model, see section B.2. Secondly the input parameters for the first and second sand layer are presented in tables B.8 and B.9.

Table B.7: Groutbody inputparameters

Linear elastic - input groutbody pile 4-6					
General	**Value**	**Unit**	**Parameters**	**Value**	**Unit**
Drainage type	Non-Porous	-	E	5.0×10^6	kN/m^2
γ_{unsat}	24.00	kN/m^3	v (nu)	0.01	-
γ_{sat}	24.00	kN/m^3	Advanced	Default	-
Linear elastic - input groutbody pile 1-3					
General	**Value**	**Unit**	**Parameters**	**Value**	**Unit**
Drainage type	Non-Porous	-	E	6.0×10^6	kN/m^2
γ_{unsat}	24.00	kN/m^3	v (nu)	0.01	-
γ_{sat}	24.00	kN/m^3	Advanced	Default	-

Table B.8: Input parameters for the HSs model for the OC first sand layer

Hardening Soil small strain - input first sand layer OC					
General	**Value**	**Unit**	**Parameters**	**Value**	**Unit**
Drainage type	Drained	-	ψ	2.00	deg
γ_{unsat}	17.00	kN/m^3	$\gamma_{0.7}$	0.0002	-
γ_{sat}	19.00	kN/m^3	$G_0{}^{ref}$	180,000	kN/m^2
Advanced	Default	-	Advanced	Default	-
Parameters	**Value**	**Unit**	**Interfaces**	**Value**	**Unit**
$E_{50}{}^{ref}$	30,000	kN/m^2	Strength	Rigid	-
$E_{oed}{}^{ref}$	30,000	kN/m^2	R_{inter}	1.00	-
$E_{ur}{}^{ref}$	90,000	kN/m^2	**Initial**	**Value**	**Unit**
m	0.50	-	K_0	Manual	-
c'_{ref}	0.10	kN/m^2	$K_{0,x} = K_{0,z}$	Yes	-
ϕ'	32.00	deg	$K_{0,x}$	0.60	-

Table B.9: Input parameters for the HSs model for the OC second sand layer

Hardening Soil small strain - input second sand layer OC					
General	**Value**	**Unit**	**Parameters**	**Value**	**Unit**
Drainage type	Drained	-	ψ	2.00	deg
γ_{unsat}	17.00	kN/m^3	$\gamma_{0.7}$	0.0002	-
γ_{sat}	19.00	kN/m^3	$G_0{}^{ref}$	180,000	kN/m^2
Advanced	Default	-	Advanced	Default	-
Parameters	**Value**	**Unit**	**Interfaces**	**Value**	**Unit**
$E_{50}{}^{ref}$	45,000	kN/m^2	Strength	Rigid	-
$E_{oed}{}^{ref}$	30,000	kN/m^2	R_{inter}	1.00	-
$E_{ur}{}^{ref}$	90,000	kN/m^2	**Initial**	**Value**	**Unit**
m	0.50	-	K_0	Manual	-
c'_{ref}	0.10	kN/m^2	$K_{0,x} = K_{0,z}$	Yes	-
ϕ'	32.00	deg	$K_{0,x}$	1.00	-

B.4. Extended validation, 2D axisymmetric

The field data used for the validation is extended with a case in The Hague. This is done to prove the modelling concept with volume elements and the installation simulation procedure to be a generally applicable modelling procedure for well-installed micropiles.

B.4.1. Geotechnical parameters, The Hague

For project Veenkade The Hague three micropiles were installed to be tested until failure [51]. The estimation of the soil parameters is entirely based on the correlation between the CPT profiles at the test sites in The Hague and Amsterdam. Because of the limited availability of site investigation data the reliability of the chosen soil parameters must be interpreted with care. The average q_c-value at the location of the test piles in The Hague is similar to the average q_c-value at the Amsterdam test site, the stiffness parameters for the engineering strain levels are therefore not adjusted. From the previous validation research it was found that the influence of the soil parameters on the fit is relatively limited, the current adopted approach for the soil parameter determination is therefore regarded as sufficient. The sand layer in Amsterdam is known to be overconsolidated, this led to the selection of higher K_0-values and small strain stiffness parameters. The 'Haagsche Zand' layer is assumed not to be overconsolidated, therefore the Jaky formula is used for the K_0-value and the lower range of the correlations for the small strain stiffness parameters is used: $\gamma_{0.7}$ is 0.1×10^{-3} and G_0 is 1.5 times E_{ur} [4]. The representative CPT profile for the The Hague case is shown on the next page.

Practical experience with the local sand layer, referred to as 'Haagsche Zand', was used additionally to the correlation between the CPT profiles. It is known that the sand layer in The Hague consists of more rounded sand particles when compared to the sand layer in Amsterdam [51]. Because of the more rounded shape there is less particle interlocking and the internal friction angle is likely to be lower. Therefore a value of 30.0 degrees for the effective internal friction angle is chosen. In the CPT profile, shown in figure B.7, three layers with a significantly lower cone resistance and higher friction ratio are distinguished:

1. From 0.0 m NAP to -1.0 m NAP

2. From -6.0 m NAP to -9.0 m NAP

3. From -14.0 m NAP to -16.0 m NAP

The influence of these three softer layers on the strength, stiffness and stress levels in the soil profile is likely to be insignificant for the displacements in the pile load tests. Therefore the soil profile is modelled with one soil layer: 'Haagsche Zand'.
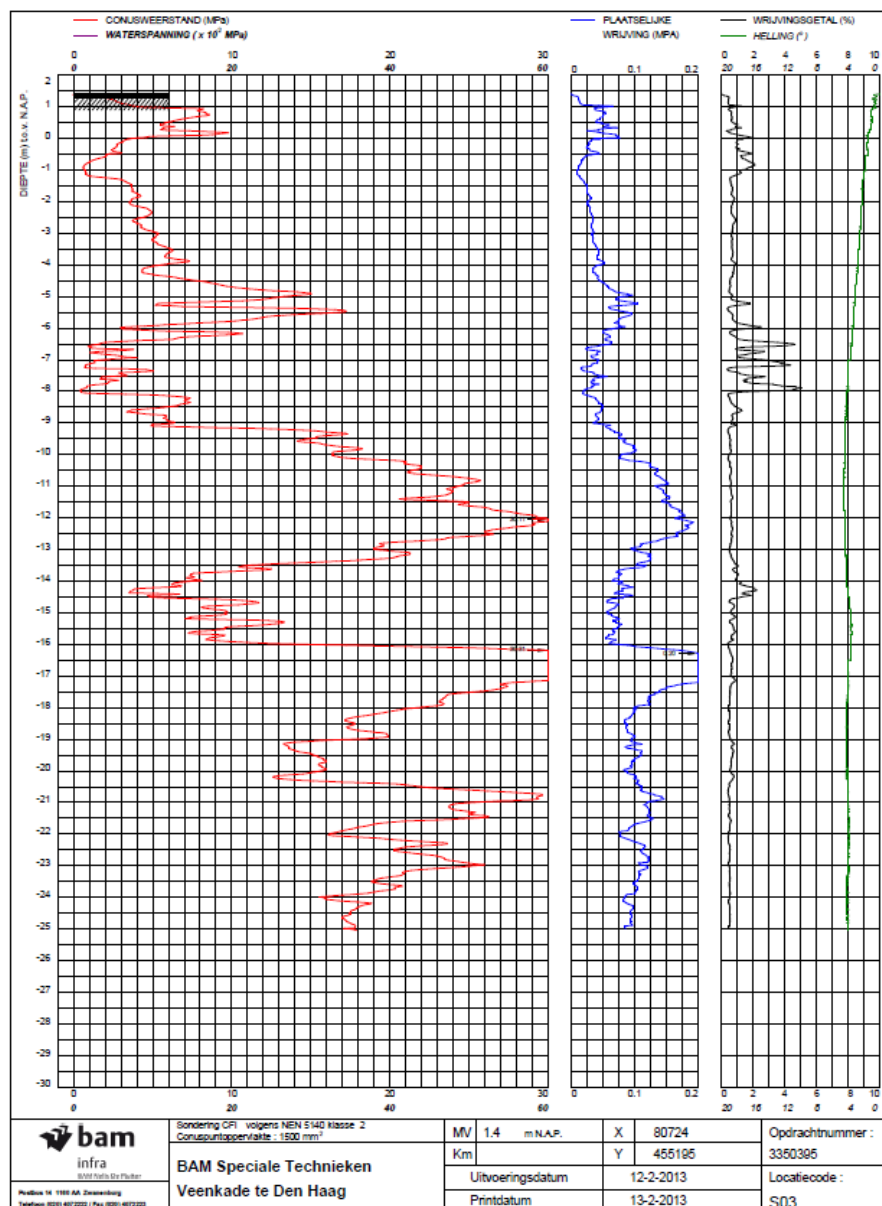
Figure B.7: A representative CPT profile of the soil conditions at the test site for the The Hague micropile failure load tests [51].

B.4.2. Pile load tests, The Hague

The pile load tests performed in The Hague were done according to the standards from the CUR236 [7]. For more details on the loading procedure described in this report, the reader is referred to subsection 3.2.2.

The three micropiles for the load tests consist of a GEWI 75.0 mm bar and a groutbody of 10.0 meters in length. The unbounded residual grout length of the micropile is 11.0 meters and the total length of the GEWI bar 22.0 meters: 12.0 meters of free length and 10.0 meters of bounded length. The lower four meters, from -17.0 m NAP to -21.0 m NAP, are installed with a grout pressure of 10 bar. The upper six meters, from -11.0 m NAP to -17.0 m NAP are installed with a grout pressure of 4 bar. The pre-calculated capacity of the micropiles is equal to 1950 kN. Below in figure B.8 the time-displacement diagram of the three micropile load tests is presented. All three micropiles failed relatively early in the loading procedure and were accepted as stable at the 70% loading stage. Pile 2 and 3 failed geotechnically during the test, pile 1 failed according to the predefined creep measure for failure load tests [7]. It can be seen that pile 2 showed higher displacements in earlier loading stages when compared to pile 1 and 3.
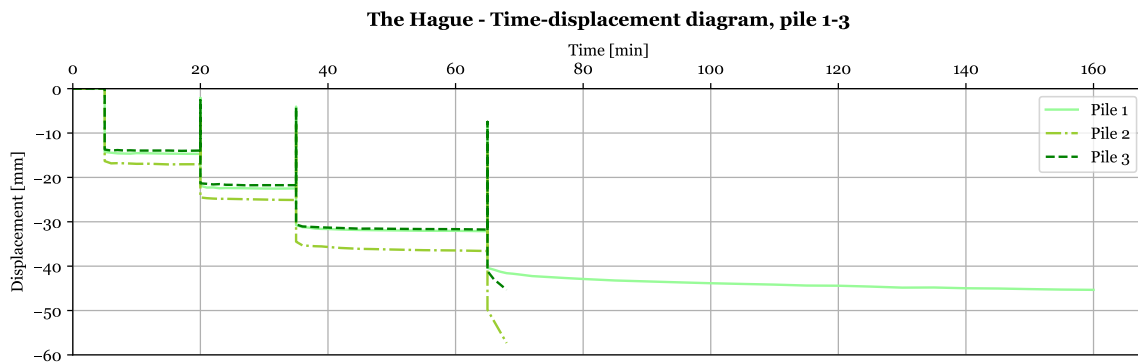
Figure B.8: The time-displacement diagram for the three micropile load tests performed in the 'Haagsche Zand' layer.

In figure B.9 the load-displacement diagram of the pile load tests in The Hague is shown. Pile 2 shows much greater displacements and fails at a lower load than piles 1 and 3. Due to the significant deviation of pile 2, only the load-displacement behaviour of pile 1 and 3 is taken into account for the validation. Since the performance of micropiles is strongly execution dependent pile 2 might have underperformed due to insufficient installation quality. The load-displacement diagram is different from the diagrams presented for the Amsterdam case since the reloading stages were recorded in more detail for the The Hague case. For example when the 70% loading stage is considered: the displacements for the intermediate 40% and 55% (reloading) stages are recorded as well, as shown in figure B.9 below.
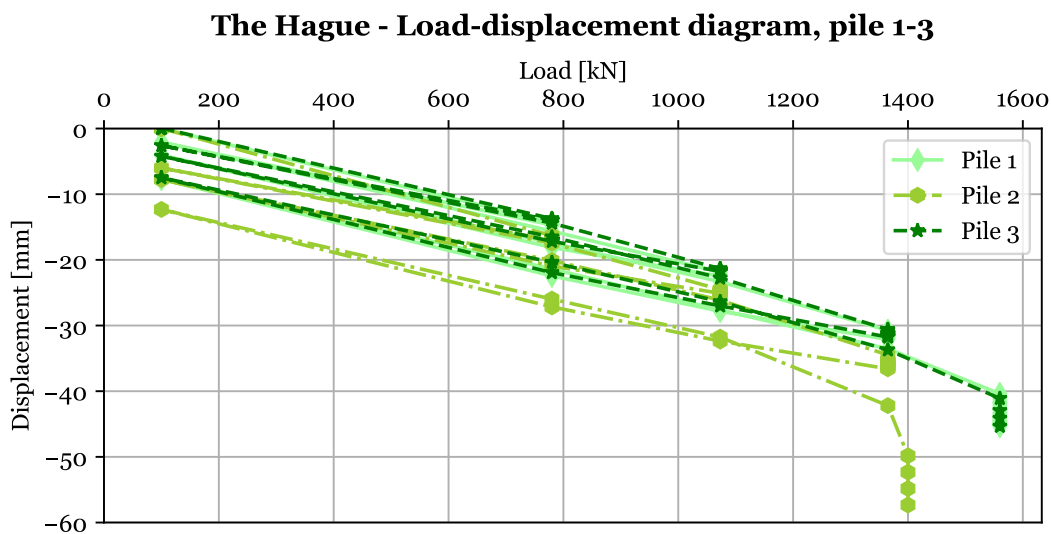
Figure B.9: The load-displacement diagram for the three micropile load tests performed in the 'Haagsche Zand' layer.

B.4.3. 2D axisymmetric model, The Hague

The modelling concept for the 2D axisymmetric model for the The Hague pile load tests is the same as for the previous models. For more details on the modelling concept the reader is referred to subsection 4.1.1.

2D axisymmetric model mesh, The Hague

Below the mesh and a zoom at the level of the groutbody of the micropiles in the 'Haagsche Zand' layer are shown in figure B.10 and B.11. The mesh coarseness factors for the different zones are the same as for the other 2D axisymmetric models, see table B.6. The refined zone for this model has a length of 12.0 meters and a width of 1.0 meter.
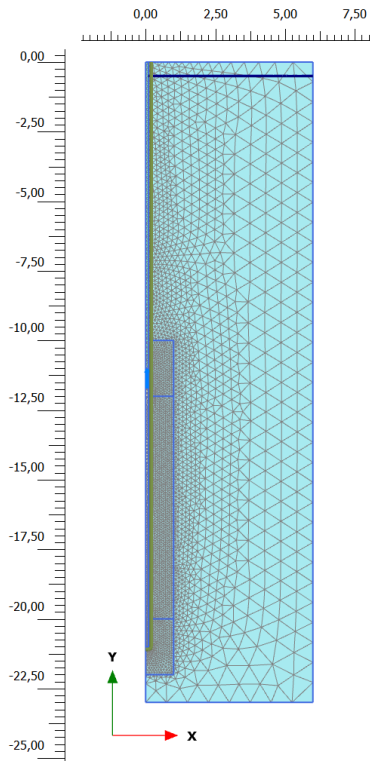
Figure B.10: Full mesh, 2D axisymmetric model of the micropiles the 'Haagsche Zand' layer.
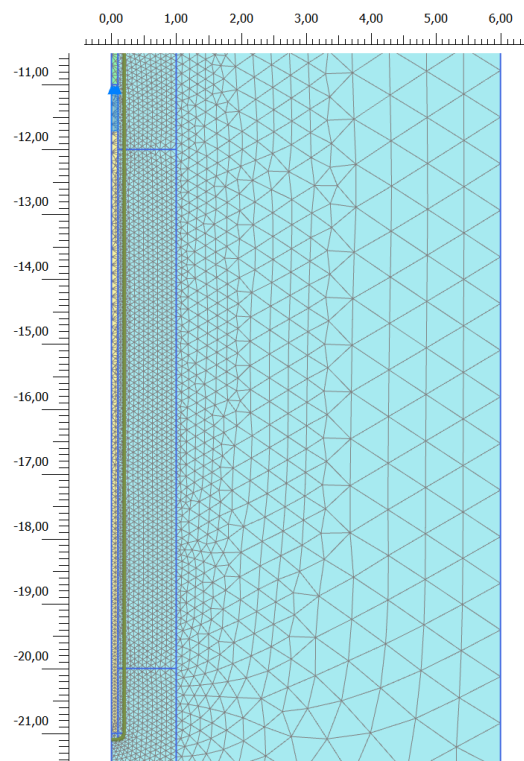
Figure B.11: Zoom of the mesh, 2D axisymmetric model of the micropiles in the 'Haagsche Zand' layer.

Input parameters

The input parameters for the groutbody and 'Haagsche Zand' soil layer are presented in tables B.10 and B.11. The soil input parameter choices were explained in section B.4.1. The residual groutbody and the interface of the residual groutbody in this model have the same input parameters as presented in section B.2.

Table B.10: The HSs input parameters for the soil layer 'Haagsche Zand'

Hardening Soil small strain - input 'Haagsche Zand' NC					
General	**Value**	**Unit**	**Parameters**	**Value**	**Unit**
Drainage type	Drained	-	c'_{ref}	0.00	kN/m^2
γ_{unsat}	17.00	kN/m^3	ϕ'	30.00	deg
γ_{sat}	19.00	kN/m^3	ψ	0.00	deg
Advanced	Default	-	$\gamma_{0.7}$	0.0001	-
Parameters	**Value**	**Unit**	G_0^{ref}	135,000	kN/m^2
E_{50}^{ref}	30,000	kN/m^2	Advanced	Default	-
E_{oed}^{ref}	30,000	kN/m^2	**Interfaces**	**Value**	**Unit**
E_{ur}^{ref}	90,000	kN/m^2	Strength	Rigid	-
m	0.50	-	R_{inter}	1.00	-

The groutbody of the The Hague model is modelled as much stiffer than the groutbodies modelled in the Amsterdam case. The GEWI bar used for the pile load tests in The Hague has a larger diameter both absolute and relative to the total pile diameter. Taking into account the much higher stiffness of steel in tension compared to grout, an increase of micropile stiffness of at least 25% is expected in the The Hague case. This does not explain completely the much higher stiffness needed to fit the displacements for the The Hague case. Possibly the local soil stiffness is underestimated and the groutbody stiffness is used to compensate. The groutbody in the The Hague case is 10 meter long, contrary to the 5.0 meter long groutbody for the Amsterdam case. The much longer and possibly stiffer uncracked part of the groutbody in the The Hague case affects the overall stiffness of the groutbody. Considering a relatively small mobilised and cracked part of the groutbody for the first loading stages, the influence of the long uncracked part is another explanation for the higher stiffness chosen in the fitting process of the The Hague case. In the current modelling approach the groutbody stiffness is reviewed as the main 'fitting' parameter since this stiffness has the most significant influence on the plastic and elastic displacements during the loading and unloading stages.

Table B.11: The linear elastic input parameters for the groutbody in the The Hague 2D axisymmetric model.

Linear elastic - input groutbody, The Hague					
General	**Value**	**Unit**	**Parameters**	**Value**	**Unit**
Drainage type	Non-Porous	-	E	16.0×10^6	kN/m^2
γ_{unsat}	24.00	kN/m^3	v (nu)	0.01	-
γ_{sat}	24.00	kN/m^3	Advanced	Default	-

B.4.4. Validation, The Hague

Below in figure B.12 the comparison between the load-displacement behaviour found in the field data and the Plaxis 2D model is shown. All points of the fit are within a margin of 1.0 mm of the field data. The additional data points for the different reloading stages show that the stiffness of the model behaviour in these stages is confirmed by the field data as well.
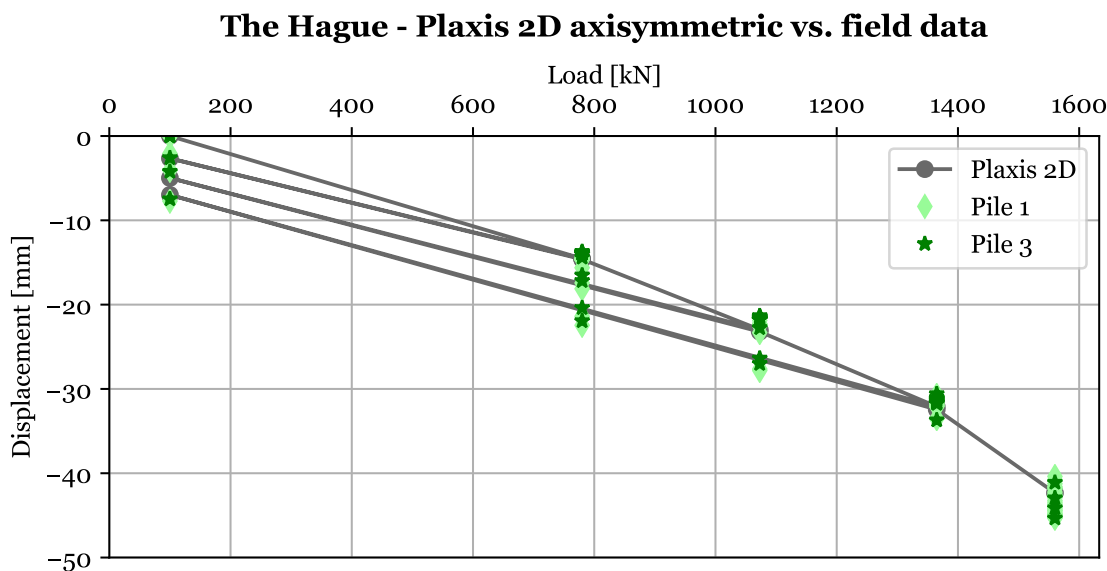
Figure B.12: The 2D axisymmetric model fit for the Veenkade, The Hague case.

B.5. Pile group lay-out investigation

Three basic pile group lay-outs are investigated, a top view of all lay-outs is presented in figure B.13. On the left a pile group lay-out with five piles is presented, in the middle a pile group with nine piles is presented and on the right a symmetry model is shown. The boundaries of the symmetry model are indicated in red, the boundary conditions restrain the displacement normal to the boundary. The resulting stresses and strains of the pile in the soil body can therefore be mirrored at each boundary. Theoretically the mirrored piles can be mirrored at each boundary as well, thus creating an infinite pile group. The boundaries of the five and nine pile groups are at least 3.0 meters away from the piles at the edge of the pile group.
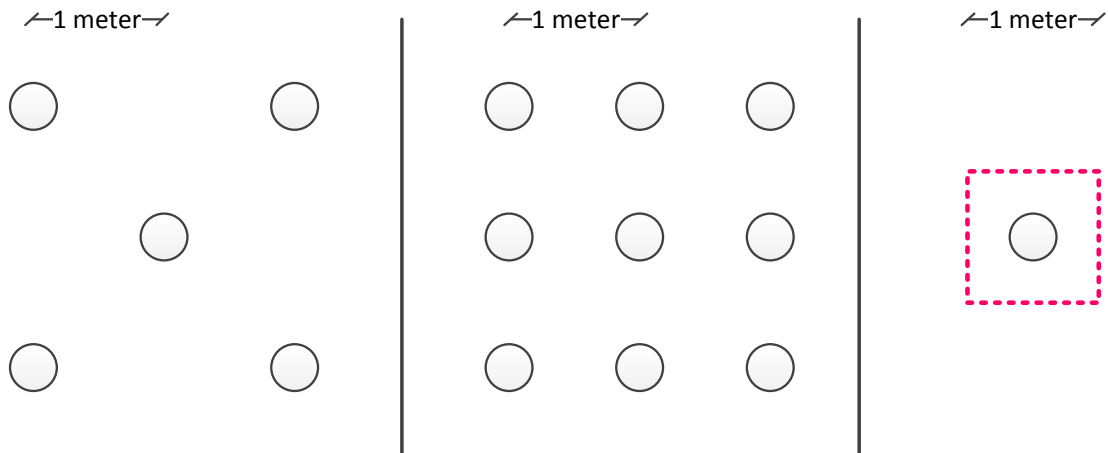
Figure B.13: A top view of the three different pile group lay-outs that are investigated.

All models are run with the same phased construction process: an initial phase, three installation simulation phases and axial loading stages where the tension load increases. The models show different load-displacement behaviour. Below the load-displacement diagrams for the different pile group spacings are shown. First the comparison for the 5D spaced pile groups is presented in figure B.14. The load-displacement behaviour of the symmetry model can not be presented for this case since the model failed after the first installation simulation phase. No equilibrium could be obtained and the soilbody fails in the symmetry model. For the 10D and 15D spacing cases all model results are presented.
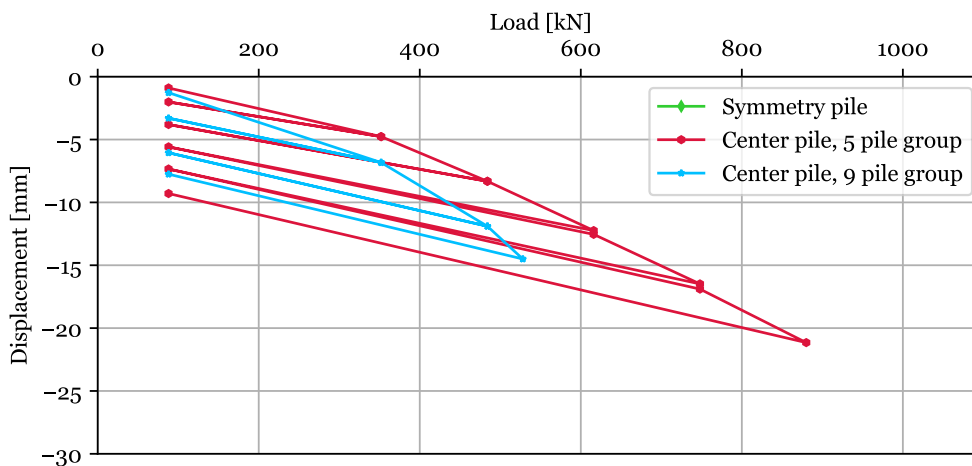
Figure B.14: A comparison of the load-displacement behaviour of the three pile group lay-outs, 5D spacing.

Load-displacement diagram, pile group lay-out comparison, 10D spacing
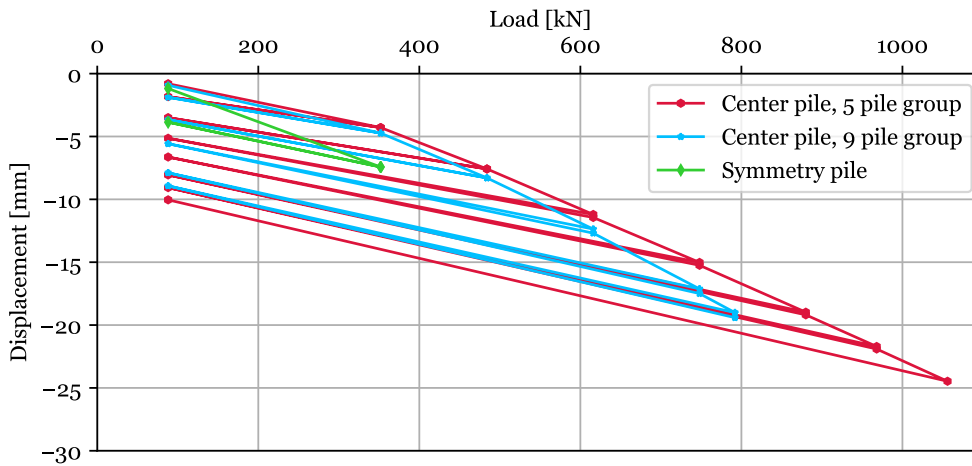
Figure B.15: A comparison of the load-displacement behaviour of the three pile group lay-outs, 10D spacing.

Load-displacement diagram, pile group lay-out comparison, 15D spacing
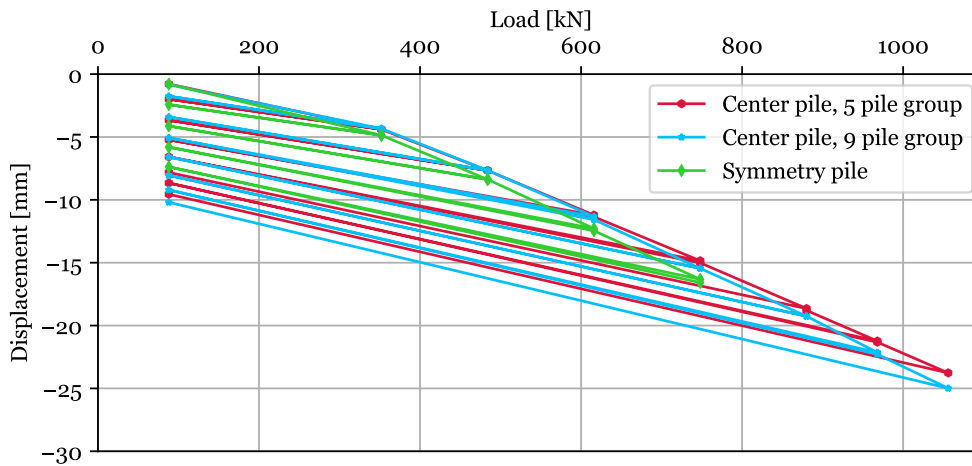
Figure B.16: A comparison of the load-displacement behaviour of the three pile group lay-outs, 15D spacing.

The difference between the five pile group and the nine pile group can be explained by the influence of the additional four piles. When the spacing is increased and the interaction between the piles in the group decreases the differences between the models become smaller. Whether the different behaviour of the symmetry models can be explained by more elaborate interaction effects of the virtually infinite pile group or the strict boundary conditions cannot be said. The symmetry model shows softer behaviour and the model fails at a lower load.

With the five and nine piles group models both the installation loads and loads introduced during the loading stages more soil can be mobilised and the stress is therefore distributed over a larger area. This situation seems more applicable to pile groups in reality, which are almost always larger in number of piles but perfect symmetry is unlikely to occur. Due to interaction with for example the underwater concrete floors attached to the micropiles loads will not be distributed evenly and therefore stress redistribution in the soil is not in perfect symmetry.

The nine pile model is limited in its size and therefore in the pile-soil-pile interaction when compared to larger pile groups, but it is reviewed as sufficient for the current group effect research. For each project the pile group size and load distribution varies, the goal of this research is to identify the influence of spacing and soil stiffness for a general case.

B.5.1. Final group models and mesh

In figure B.17 below the meshes of the final models are shown. The size of the mesh of the different models is 8.0 × 8.0 × 24.0 meters (top left), 10.0 × 10.0 × 24.0 meters (top right) and 12.0 × 12.0 × 24.0 meters (bottom left) respectively.
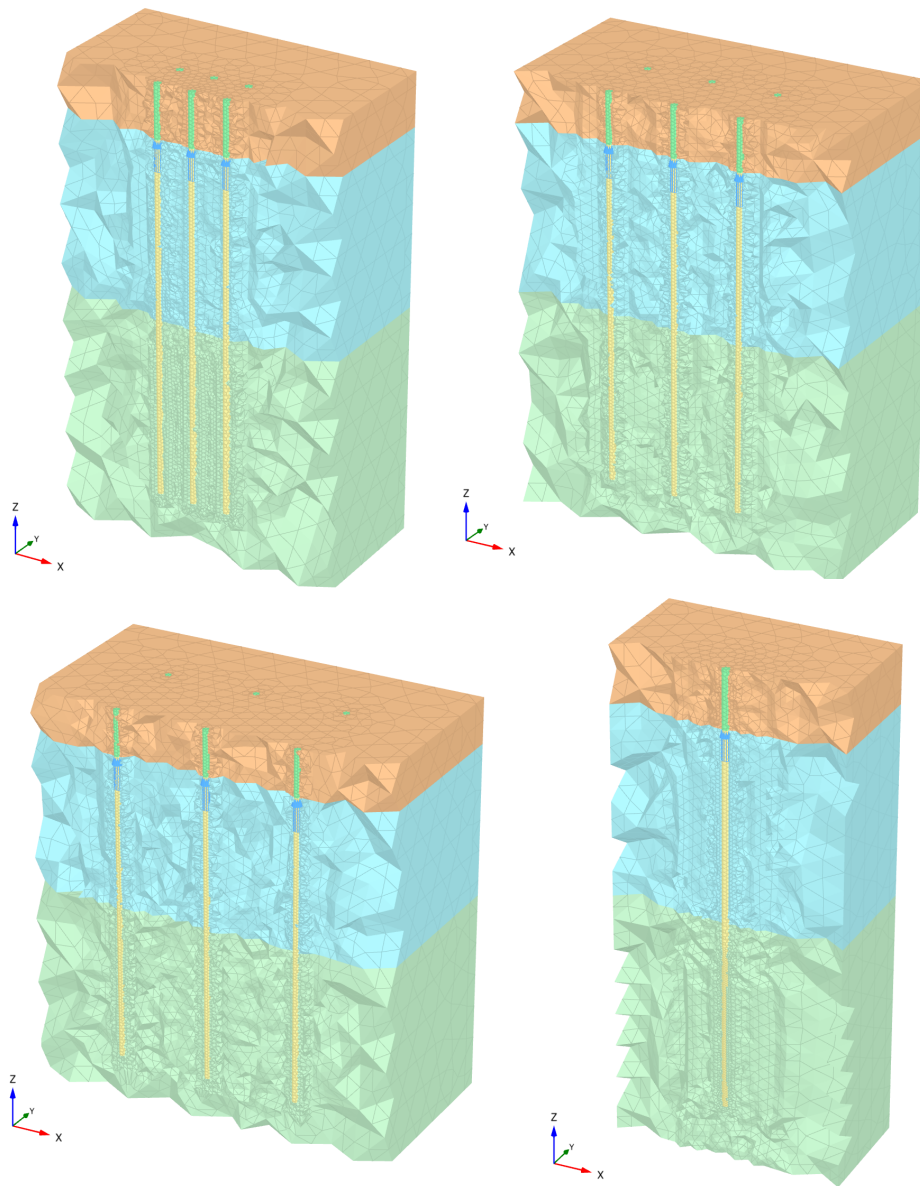
Figure B.17: Meshes of the three different pile group spacing models. Clockwise from top left to bottom left: 5D spacing model, 10D spacing model, single pile reference model and the 15D spacing model.

With the default meshing procedure the mesh size differs strongly for each model and this results in inconsistent mesh quality. Since the results between the different spacing cases are compared, a more consistent mesh quality and element size is demanded. Around the piles different refinement volumes are defined. To limit the size and calculation time of the models, the refinement level is different for the large meshes. On the following pages in tables B.12 to B.15 the coarseness factors of the refinement volumes for the different models are presented.

In the tables the refinement volumes are ordered from large to small, top to bottom. First the volume created around the pile group is presented, lastly the interface at the high pressure grouting zone is defined. The overall coarseness was set to medium, resulting in a target element size of 0.7089 meter. As explained in subsection 4.1.1 paragraph 'Mesh refinement and quality', the coarseness factors indicate the multiplication factor of the target element size for the different volumes and surfaces during the Plaxis meshing procedure.

Table B.12: The coarseness factors of the different volumes and surfaces in the 5D spacing pile group model.

Mesh	Number
Elements	228843
Nodes	316794
Volume/surface	**Coarseness factor**
Volume around pile group	0.5
Residual grout volume	1.0
Residual grout interface	0.3536
Grout volume	1.0
Grout interfaces	0.3536
Volume at the high pressure grouting zone	0.1250
Interface at the high pressure grouting zone	0.0625

Table B.13: The coarseness factors of the different volumes and surfaces in the 10D spacing pile group model.

Mesh	Number
Elements	170047
Nodes	238701
Volume/surface	**Coarseness factor**
Volume around pile group	0.5
Volume around each pile individually	0.3536
Residual grout volume	1.0
Residual grout interface	0.25
Grout volume	1.0
Grout interfaces	0.25
Volume at the high pressure grouting zone	0.1250
Interface at the high pressure grouting zone	0.0625

Table B.14: The coarseness factors of the different volumes and surfaces in the 15D spacing pile group model.

Mesh	Number
Elements	178552
Nodes	250542
Volume/surface	**Coarseness factor**
Volume around pile group	0.7071
Volume around the pile in the first sand layer	0.5
Residual grout volume	1.0
Residual grout interface	0.3536
Volume around the pile in the second sand layer	0.3536
Grout volume	1.0
Grout interfaces	0.25
Volume at the high pressure grouting zone	0.1250
Interface at the high pressure grouting zone	0.1250

Table B.15: The coarseness factors of the different volumes and surfaces in the 3D single pile reference model.

Mesh	Number
Elements	83321
Nodes	115459
Volume/surface	**Coarseness factor**
Volume around pile	0.3536
Residual grout volume	2.0
Residual grout interface	2.0
Grout volume	1.0
Grout interfaces	0.5
Volume at the high pressure grouting zone	0.1250
Interface at the high pressure grouting zone	0.0625

The input parameters used for some materials in the 3D group models differ slightly when compared to the single pile validation model. In the tables below all materials with different input parameters are presented.

In table B.16 below the input parameters of the linear elastic groutbody are shown. The stiffness of the groutbody is the most relevant parameter, the value of $8.5 \times 10^6 \, kN/m^2$ was chosen because of the groutbody stiffness range applied in the validation models and the approximated stiffness of cracked reinforced concrete of $10 \times 10^6 \, kN/m^2$.

Table B.16: Input parameters for the linear elastic groutbody for all pile group models.

Linear elastic - input groutbody, all group models					
General	**Value**	**Unit**	**Parameters**	**Value**	**Unit**
Drainage type	Non-Porous	-	E	8.5×10^6	kN/m^2
γ_{unsat}	24.00	kN/m^3	v (nu)	0.01	-
γ_{sat}	24.00	kN/m^3	Advanced	Default	-

For both the sand layers the pre-overburden pressure (POP) is adjusted to $66 \, kN/m^2$. This is the pressure that was present before removing the 11.0 meters of soft top layers with an effective weight of $6.0 \, kN/m^2$. In tables B.17 and B.18 the input parameters of the sand layers for the standard case are presented, in tables B.19 and B.20 the input parameters of the sand layers for the stiff case are presented.

Table B.17: The input parameters of the second sand layer for the pile group models of the standard case.

Hardening Soil small strain - input second sand layer OC, standard group case					
General	**Value**	**Unit**	**Parameters**	**Value**	**Unit**
Drainage type	Drained	-	$\gamma_{0.7}$	0.0002	-
γ_{unsat}	17.00	kN/m^3	G_0^{ref}	180,000	kN/m^2
γ_{sat}	19.00	kN/m^3	Advanced	Default	-
Advanced	Default	-	**Interfaces**	**Value**	**Unit**
Parameters	**Value**	**Unit**	Strength	Rigid	-
E_{50}^{ref}	45,000	kN/m^2	R_{inter}	1.00	-
E_{oed}^{ref}	30,000	kN/m^2	**Initial**	**Value**	**Unit**
E_{ur}^{ref}	90,000	kN/m^2	K_0	Manual	-
m	0.50	-	$K_{0,x} = K_{0,z}$	Yes	-
c'_{ref}	0.10	kN/m^2	$K_{0,x}$	1.00	-
ϕ'	34.00	deg	OCR	1.00	-
ψ	4.00	deg	POP	66.00	kN/m^2

Table B.18: The input parameters of the first sand layer for the pile group models of the standard case.

Hardening Soil small strain - input first sand layer OC, standard group case					
General	**Value**	**Unit**	**Parameters**	**Value**	**Unit**
Drainage type	Drained	-	$\gamma_{0.7}$	0.0002	-
γ_{unsat}	17.00	kN/m^3	G_0^{ref}	180,000	kN/m^2
γ_{sat}	19.00	kN/m^3	Advanced	Default	-
Advanced	Default	-	**Interfaces**	**Value**	**Unit**
Parameters	**Value**	**Unit**	Strength	Rigid	-
E_{50}^{ref}	30,000	kN/m^2	R_{inter}	1.00	-
E_{oed}^{ref}	30,000	kN/m^2	**Initial**	**Value**	**Unit**
E_{ur}^{ref}	90,000	kN/m^2	K_0	Manual	-
m	0.50	-	$K_{0,x} = K_{0,z}$	Yes	-
c'_{ref}	0.10	kN/m^2	$K_{0,x}$	1.00	-
ϕ'	32.00	deg	OCR	1.00	-
ψ	2.00	deg	POP	66.00	kN/m^2

Table B.19: The input parameters of the second sand layer for the pile group models of the stiff case.

Hardening Soil small strain - input second sand layer OC, stiff group case					
General	**Value**	**Unit**	**Parameters**	**Value**	**Unit**
Drainage type	Drained	-	$\gamma_{0.7}$	0.0002	-
γ_{unsat}	17.00	kN/m^3	G_0^{ref}	360,000	kN/m^2
γ_{sat}	19.00	kN/m^3	Advanced	Default	-
Advanced	Default	-	**Interfaces**	**Value**	**Unit**
Parameters	**Value**	**Unit**	Strength	Rigid	-
E_{50}^{ref}	60,000	kN/m^2	R_{inter}	1.00	-
E_{oed}^{ref}	60,000	kN/m^2	**Initial**	**Value**	**Unit**
E_{ur}^{ref}	180,000	kN/m^2	K_0	Manual	-
m	0.50	-	$K_{0,x} = K_{0,z}$	Yes	-
c'_{ref}	0.10	kN/m^2	$K_{0,x}$	1.00	-
ϕ'	34.00	deg	OCR	1.00	-
ψ	4.00	deg	POP	66.00	kN/m^2

Table B.20: The input parameters of the first sand layer for the pile group models of the stiff case.

Hardening Soil small strain - input first sand layer OC, stiff group case					
General	**Value**	**Unit**	**Parameters**	**Value**	**Unit**
Drainage type	Drained	-	$\gamma_{0.7}$	0.0002	-
γ_{unsat}	17.00	kN/m^3	G_0^{ref}	360,000	kN/m^2
γ_{sat}	19.00	kN/m^3	Advanced	Default	-
Advanced	Default	-	**Interfaces**	**Value**	**Unit**
Parameters	**Value**	**Unit**	Strength	Rigid	-
E_{50}^{ref}	60,000	kN/m^2	R_{inter}	1.00	-
E_{oed}^{ref}	60,000	kN/m^2	**Initial**	**Value**	**Unit**
E_{ur}^{ref}	180,000	kN/m^2	K_0	Manual	-
m	0.50	-	$K_{0,x} = K_{0,z}$	Yes	-
c'$_{ref}$	0.10	kN/m^2	$K_{0,x}$	1.00	-
ϕ'	32.00	deg	OCR	1.00	-
ψ	2.00	deg	POP	66.00	kN/m^2

B.6. 3D pile group model, intermediate results

The results of the first single reference piles and pile group models indicated that the capacity of the idealised piles is higher than the load levels reached in the pile acceptance tests of the Amsterdam case. Part of the pile acceptance test data can be found in Appendix B.8. This difference is expected due the difference in definition between geotechnical failure and the limit state determined in the standards for the pile acceptance tests. Unfortunately, with the introduction of higher loads in the model a not previously found phenomenon was observed in the results. In figure B.18 below the increase in horizontal effective stress levels around the upper pile shaft can be seen. This increase is not observed around the lower pile shaft, where the reduction of horizontal effective stress levels continues. The scale in figure B.18 ranges from 0.00 kN/m^2 (dark blue) to -950 kN/m^2 (dark red).
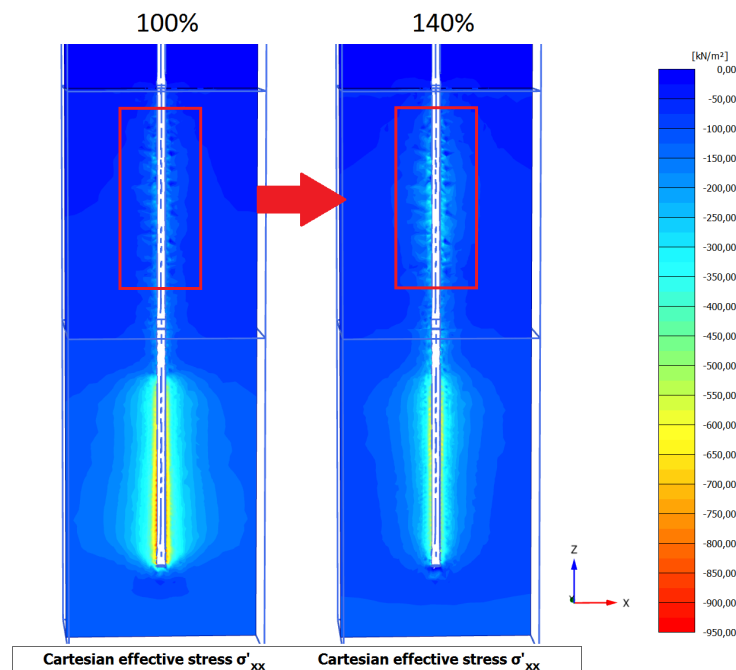
Figure B.18: The horizontal effective stress level in the soil at the 100% and 140% loading stages for the single refernce pile, stiff case.

This increase of horizontal effective stress levels is physically not defensible. In reality a decrease of stress levels is much more likely to occur due to effects as principal stress rotation, see subsection 2.2.1.

The scale used in the previous figure makes the increase of horizontal stress around the upper pile section look limited and possibly irrelevant. Upon inspection of the horizontal effective stress level on the interface of that particular pile section with a different scale, the deviations seem significant and possibly influence the piles global response to increased tensile loading. This is shown in figure B.19. The scale in this figure ranges from 0.00 kN/m^2 (dark blue) to -300 kN/m^2 (dark red).
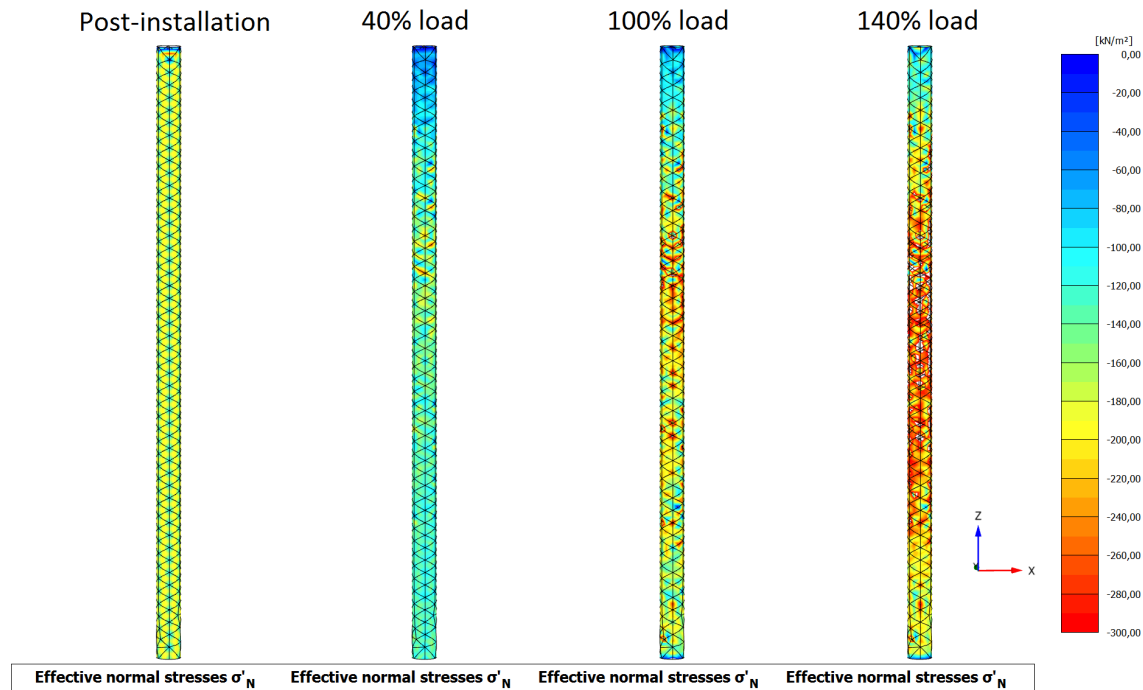
Figure B.19: A comparison of the horizontal effective stress level on the interface of the single pile, high soil stiffness model during different loading phases.

As stated before, the increase in horizontal effective stress levels due to higher tensile loading is something physically inexplicable and is mostly likely due to unrealistic model behaviour. The infinite dilation in the hardening soil model partly explains this behaviour. The interface keeps dilating and therefore generates more horizontal stress around the pile shaft. Since the displacement in the interface of the upper pile section are relatively high compared to the displacements of the interface in the lower pile section, the dilatancy has a significant influence on the behaviour of the upper pile section. To overcome this unrealistic behaviour the dilatancy angle is set to zero for the interface parameter sets of the upper pile section after the first loading stage. This is done to allow for some strength increase in the first loading stage, where a value of 1.0 is reached for the relative shear on almost the entire interface of the upper pile section, but to limit further unrealistic dilation effects for the remaining loading stages. This results in more limited stress concentrations at the higher loading stages, see figure B.20.
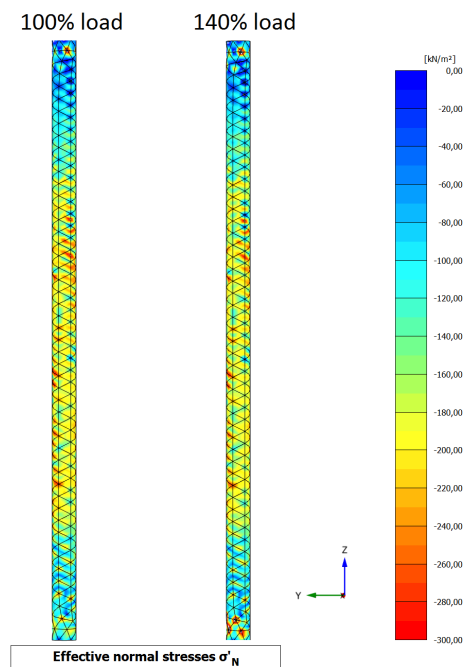
Figure B.20: The horizontal effective stress level on the interface of the single pile, high soil stiffness model, with dilation correction.

All failed calculation stages in Plaxis 3D, the final loading stages found in the model simulations, are presented on the following pages in figures B.21 to B.23.
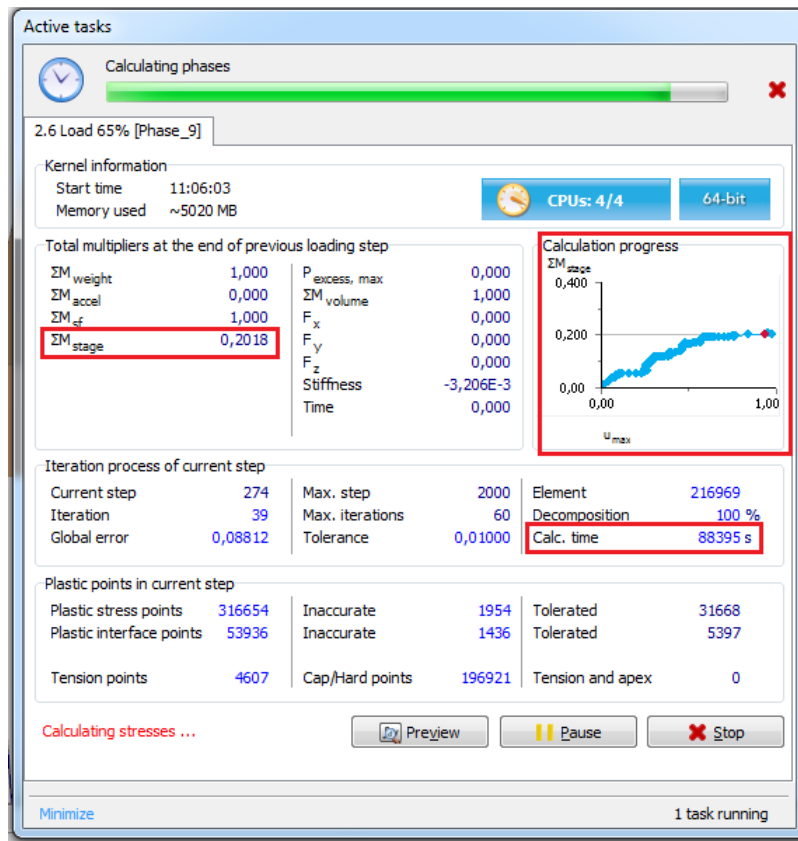
Figure B.21: The limit loading stage for the 5D spacing pile group model.
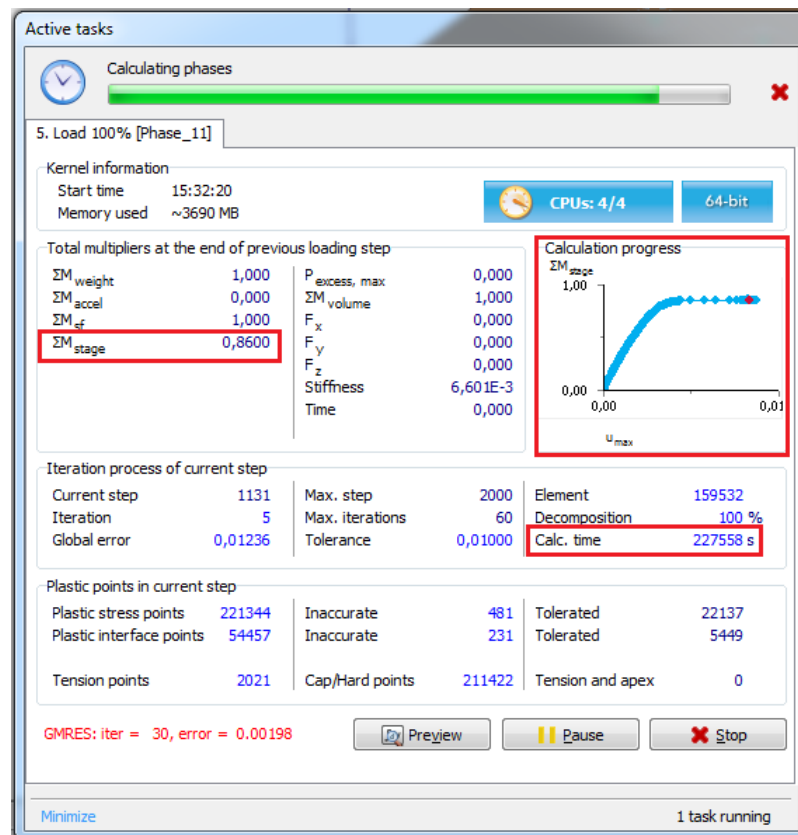
Figure B.22: The limit loading stage for the 10D spacing pile group model.
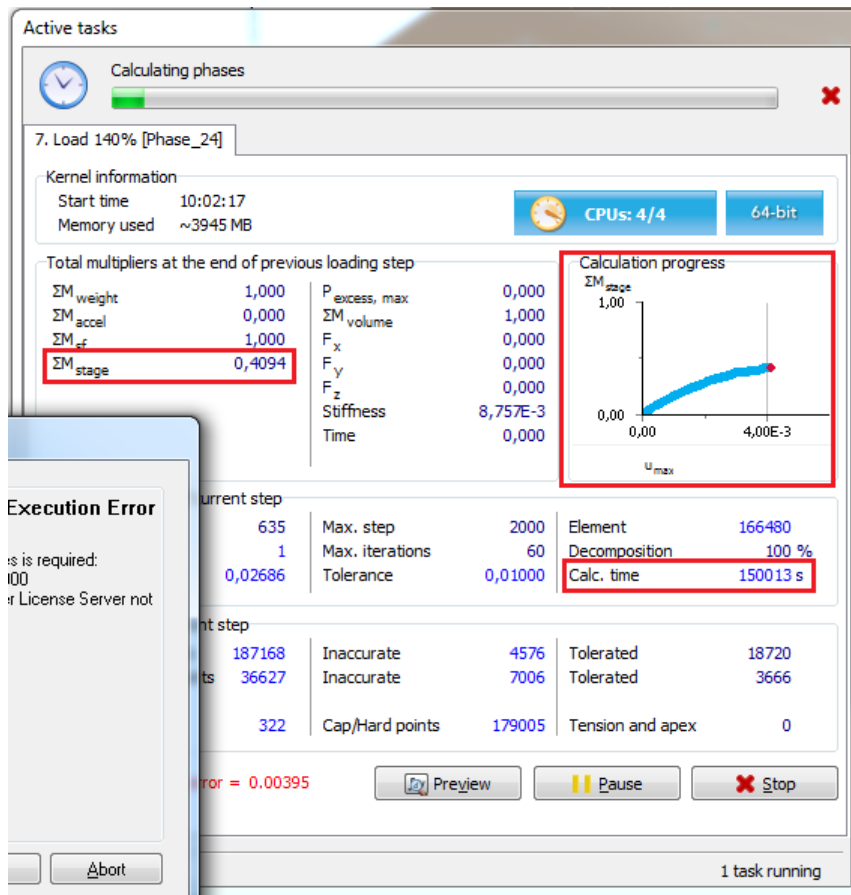
Figure B.23: The limit loading stage for the 15D spacing pile group model.

B.6.1. Stiff case, final results

In this subsection the load-displacement behaviour of the stiff case group models is presented. Below in figure B.24 the load-displacement behaviour of all four stiff case models is shown.
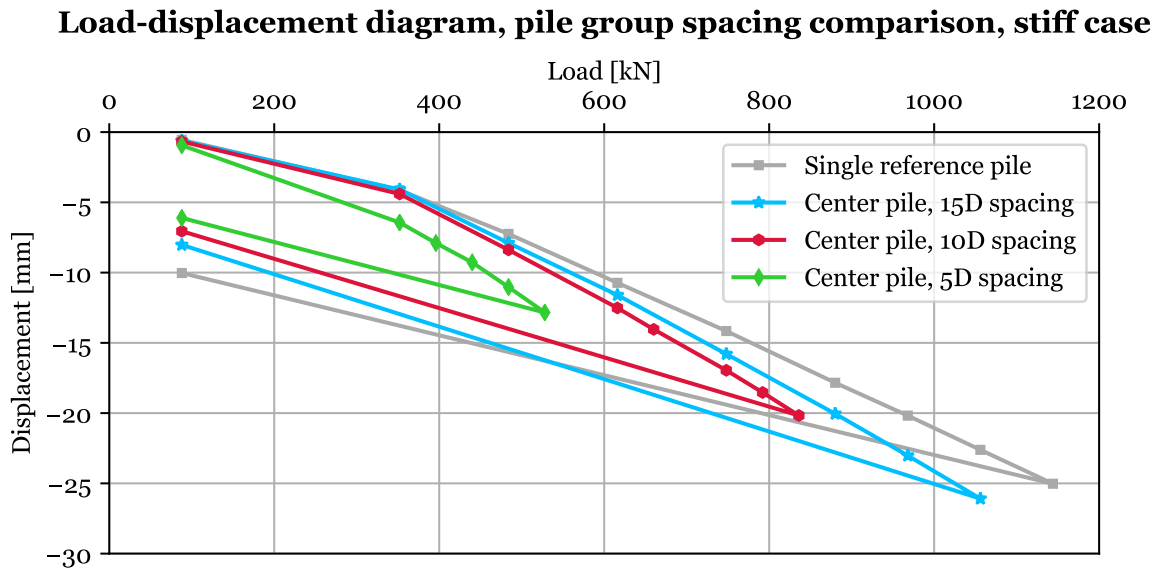
Figure B.24: The load-displacement behaviour of the three different pile group spacings compared for the stiff case.

The capacity reductions calculated for the stiff case models are the same as for the standard case models. The secant stiffness at 70% of the ultimate load level of the 5D spaced pile group compared to the 15D spaced pile group is reduced with 4%. The secant stiffness reduction of the 10D spaced pile group compared to the 15D spaced pile group is again insignificant.

In figures B.25 to B.28 the load displacement behaviour of each stiff case is plotted with the standard case. A comparison between the displacement difference for each model of both cases is presented in the main report, see subsection 4.3.2 figure 4.26.
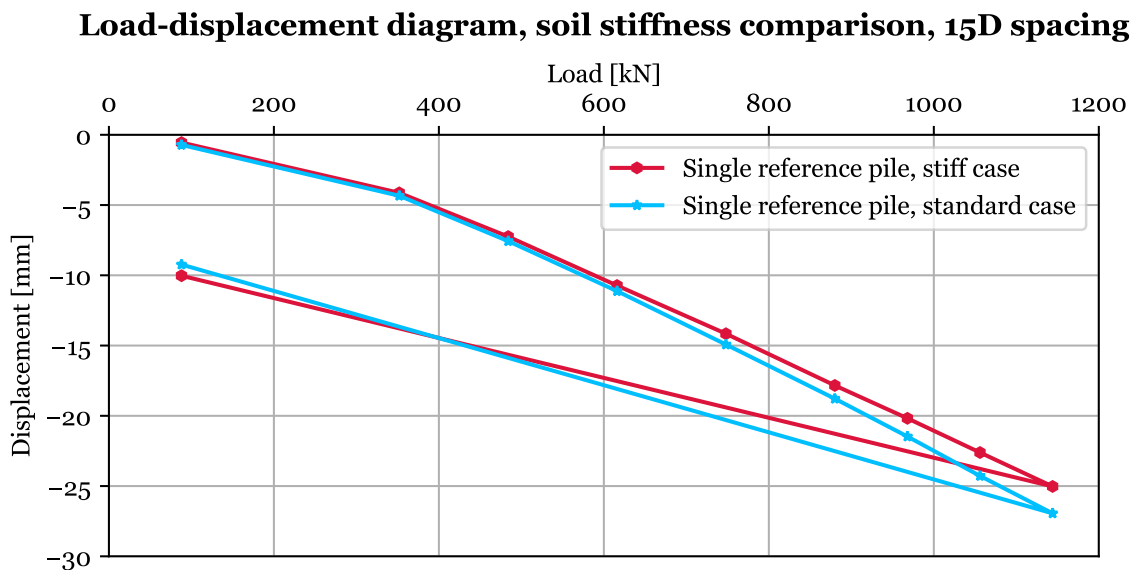
Figure B.25: The load-displacement behaviour of the standard and stiff case compared for the single reference piles.

Load-displacement diagram, soil stiffness comparison, 5D spacing
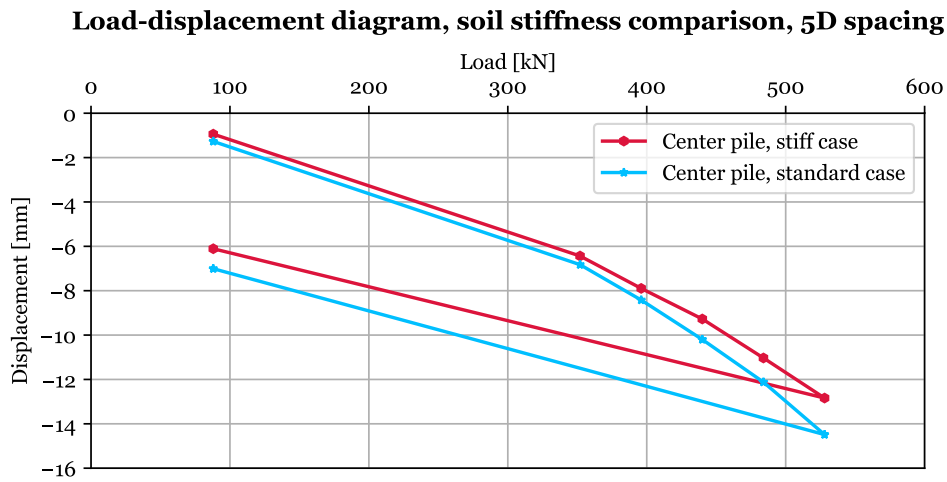
Figure B.26: The load-displacement behaviour of the standard and stiff case compared for the 5D pile group.

Load-displacement diagram, soil stiffness comparison, 10D spacing
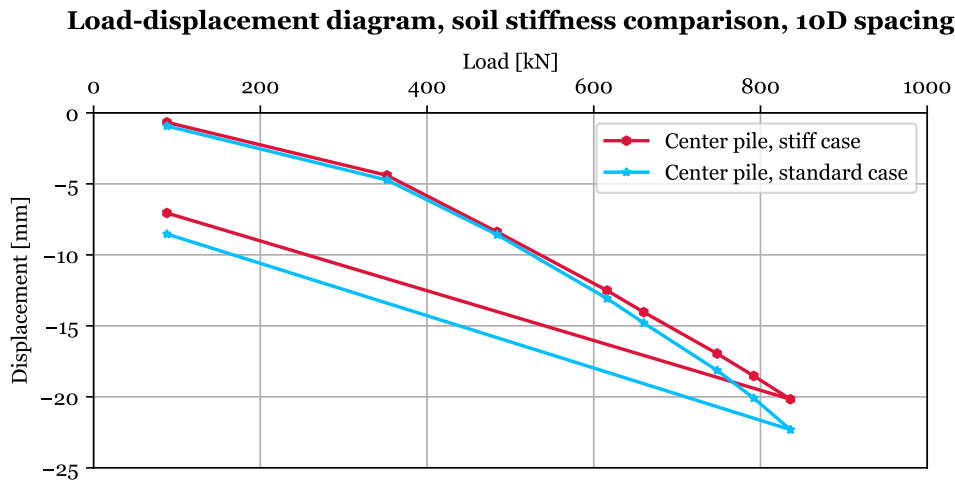
Figure B.27: The load-displacement behaviour of the standard and stiff case compared for the 10D pile group.

Load-displacement diagram, soil stiffness comparison, 15D spacing
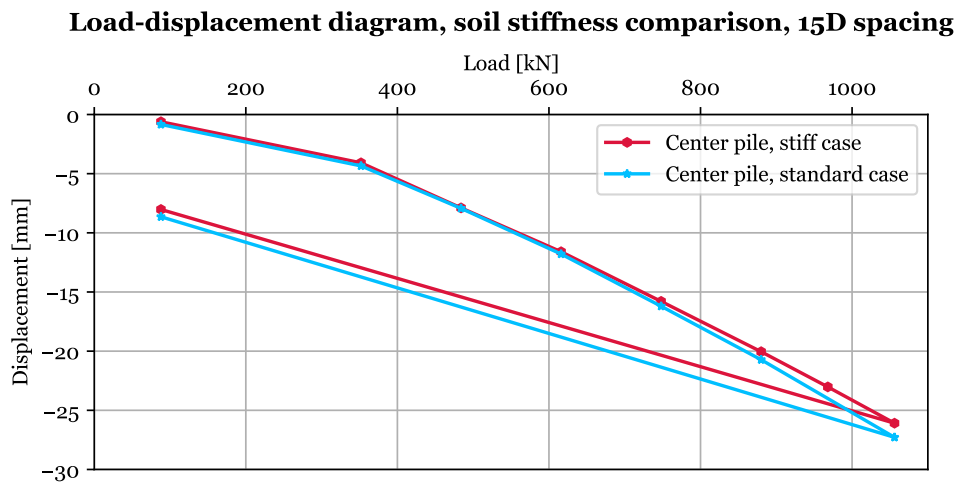
Figure B.28: The load-displacement behaviour of the standard and stiff case compared for the 15D pile group.

B.7. CUR 236 calculations

The CUR 236 calculations for the three different spacing cases are presented in this section. These calculations were done to compare the capacities of a single pile in a group according to the Plaxis 3D model with the current standards.

B.7.1. Representative CPT

Below the representative CPT profile is shown, this profile is used for the $q_{c;z;a}$ input in the CUR 236 calculations. The $q_{c;z;a}$ value is the lowest cone resistance value found per layer of 1.0 meter. The representative CPT profile shows the q_c-distribution over the depth at the site of the reference case in Amsterdam after excavation to -11.0 m NAP. The ultimate limit value used for the $q_{c;z;a}$ input value is 20 MPa. The red lines in the profile give the $q_{c;z;a}$ value for each layer where the micropiles are installed with pressure grouting.
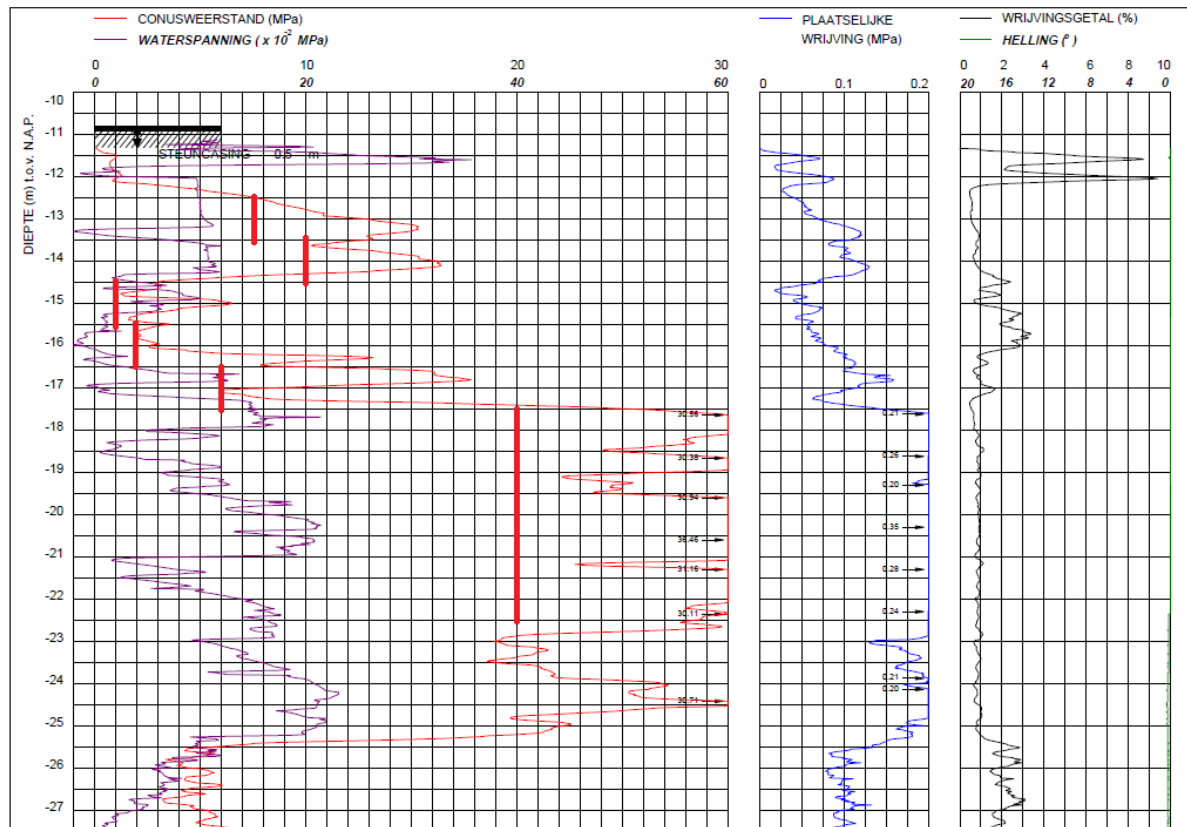
Figure B.29: The representative CPT profile at the case site of Amsterdam, the limiting values per meter soil are marked as red, straight lines.

B.7.2. Calculation sheets

Case Amsterdam

Input

ctc	1 m		2 m	3 m
D	0.2 m		0.2 m	0.2 m
A	0.96 m2		3.96 m2	8.96 m2

$f_{1;i}$	1.0 -		gamma_sat	19 kN/m3
$O_{p;1}$	0.628 m		gamma_water	10 kN/m3
alpha_t	0.0225 -		gamma_m;g	1.1 -
gamma_s;t	1.35 -		xie (4)	0.92 -
gamma_m;var;qc	1.0 -			

1m spacing case						$F_{r;tens;d}$		**153** kN	
Depth	d_i	$q_{c;z;a}$	$q_{c;d;i}$	γ'_d	M_i	$\sigma'_{v;d;j;0}$	$f_{2;i}$	$T_{d;i}$	SUM $T_{d;i}$
-12.5	1	0	0.00	7.3	0.0	0.0		0	0
-13.5	1	7.5	6.04	7.3	88.9	90.9	0.635	56.4	56.4
-14.5	1	10	8.05	7.3	118.6	98.2	0.304	36.0	92.4
-15.5	1	1	0.81	7.3	11.9	105.5	0.340	4.0	96.5
-16.5	1	2	1.61	7.3	23.7	112.7	0.324	7.7	104.2
-17.5	1	6	4.83	7.3	71.1	120.0	0.203	14.4	118.6
-18.5	1	20	16.10	7.3	237.1	127.3	0.051	12.0	130.6
-19.5	1	20	16.10	7.3	237.1	134.5	0.032	7.5	138.0
-20.5	1	20	16.10	7.3	237.1	141.8	0.031	7.3	145.3
-21.5	1	20	16.10	7.3	237.1	149.1	0.031	7.3	152.6
-22.5	1	20	16.10	7.3	237.1	156.4	0.031	7.3	159.8

2m spacing case						$F_{r;tens;d}$		**614** kN	
Depth	d_i	$q_{c;z;a}$	$q_{c;d;i}$	γ'_d	M_i	$\sigma'_{v;d;j;0}$	$f_{2;i}$	$T_{d;i}$	SUM $T_{d;i}$
-12.5	1	0	0.00	7.3	0.0	0.0		0	0
-13.5	1	7.5	6.04	7.3	21.6	90.9	0.892	19.2	19.2
-14.5	1	10	8.05	7.3	28.7	98.2	0.770	22.1	41.4
-15.5	1	1	0.81	7.3	2.9	105.5	0.775	2.2	43.6
-16.5	1	2	1.61	7.3	5.7	112.7	0.766	4.4	48.0
-17.5	1	6	4.83	7.3	17.2	120.0	0.715	12.3	60.4
-18.5	1	20	16.10	7.3	57.5	127.3	0.547	31.4	91.8
-19.5	1	20	16.10	7.3	57.5	134.5	0.408	23.4	115.2
-20.5	1	20	16.10	7.3	57.5	141.8	0.299	17.2	132.4
-21.5	1	20	16.10	7.3	57.5	149.1	0.222	12.8	145.2
-22.5	1	20	16.10	7.3	57.5	156.4	0.174	10.0	155.2

3m spacing case						$F_{r;tens;d}$		**1017** kN	
Depth	d_i	$q_{c;z;a}$	$q_{c;d;i}$	γ'_d	M_i	$\sigma'_{v;d;j;0}$	$f_{2;i}$	$T_{d;i}$	SUM $T_{d;i}$
-12.5	1	0	0.00	7.3	0.0	0.0		0	0
-13.5	1	7.5	6.04	7.3	9.5	90.9	0.951	9.1	9.1
-14.5	1	10	8.05	7.3	12.7	98.2	0.894	11.4	20.4
-15.5	1	1	0.81	7.3	1.3	105.5	0.896	1.1	21.6
-16.5	1	2	1.61	7.3	2.5	112.7	0.892	2.3	23.8
-17.5	1	6	4.83	7.3	7.6	120.0	0.868	6.6	30.4
-18.5	1	20	16.10	7.3	25.4	127.3	0.784	19.9	50.4
-19.5	1	20	16.10	7.3	25.4	134.5	0.711	18.1	68.4
-20.5	1	20	16.10	7.3	25.4	141.8	0.646	16.4	84.8
-21.5	1	20	16.10	7.3	25.4	149.1	0.589	15.0	99.8
-22.5	1	20	16.10	7.3	25.4	156.4	0.539	13.7	113.5

Case Amsterdam

input

phi	34 -			
Lower angle 1 [deg]	45 -	Lower angle 1 [rad]	0.8 -	
Lower angle 2 [deg]	22.7 -	Lower angle 2 [rad]	0.4 -	
Cone height 1	0.9 m	1.9 m		2.9 m
Cone height 2	2.2 m	4.5 m		6.9 m
gamma_sat	19 kN/m3	D	0.2 m	
gamma_water	10 kN/m3	A_pile	0.031 m2	
gamma_m;g	1.1 -	L	11.5 m	
ctc	1.0 m	2.0 m		3.0 m

1m spacing case	V_cone	V_cylinder	gamma'_d	F_r;tens;max;d	
Scenario 1	1.05	33.30	7.3	247	kN
Scenario 2	2.50	29.36	7.3	229	kN

2m spacing case	V_cone	V_cylinder	gamma'_d	F_r;tens;max;d	
Scenario 1	8.38	120.64	7.3	936	kN
Scenario 2	20.06	87.34	7.3	778	kN

3m spacing case	V_cone	V_cylinder	gamma'_d	F_r;tens;max;d	
Scenario 1	28.27	243.16	7.3	1971	kN
Scenario 2	67.70	128.82	7.3	1427	kN
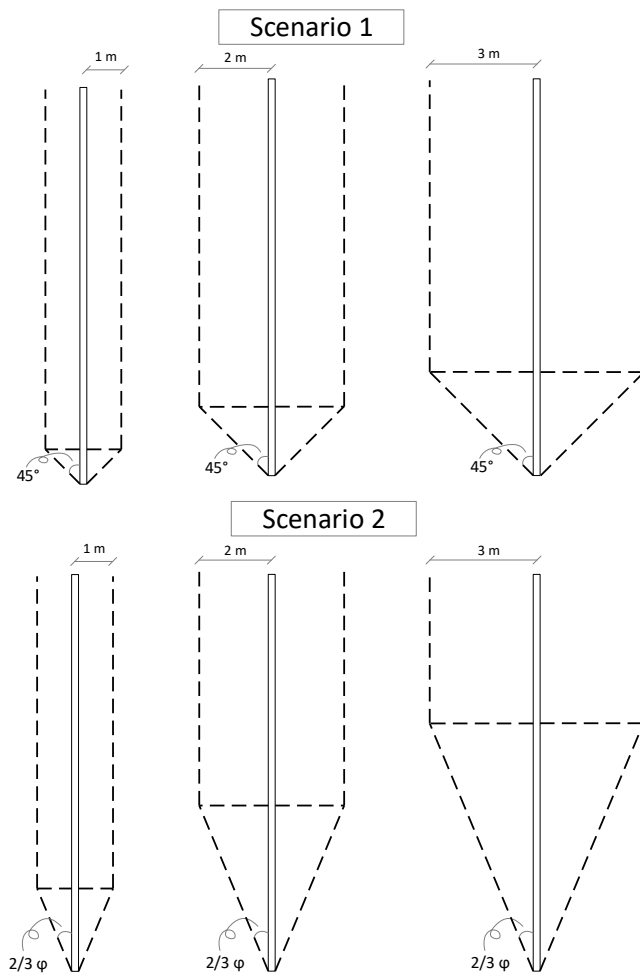
B.8. Micropile acceptance tests, field data

At the reference project in Amsterdam several acceptance tests were performed on the approximately 12 meter long production micropiles. The maximum test load was 880 kN which was reached after several unloading and reloading stages. The performance data of the micropiles shows a high level of scatter. It is unknown what the precise cause of the scatter is. The scatter in the acceptance tests is most likely due to the effects of the installation process. The high sensitivity of micropile performance in general is a well-known phenomenon and is the main reason for mandatory acceptance and suitability tests in construction projects.

In figures B.30 and B.31 the load-displacement behaviour of two sets of acceptance tests are presented. The scatter and some measurement errors are clearly visible in the data. In set 5 the capacity of the micropiles differs strongly, the variation in stiffness of the micropiles over the different loading stages is noted in set 6.

This data is not used for comparison with the pile group models and the reference single pile results. For all numerical models optimal soil conditions and positive installation effects are assumed as a starting point of the modelling approach. The variation visible in the field data is therefore not visible in the results of the numerical models.
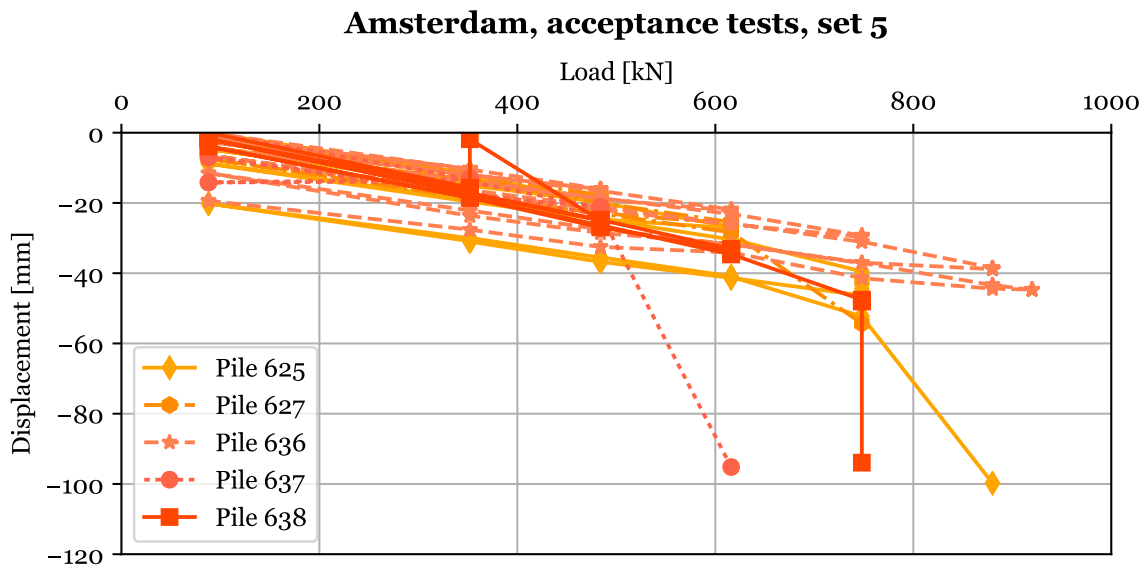
Figure B.30: The load-displacement diagram for series number 5 of acceptance tests performed in the reference project in Amsterdam.
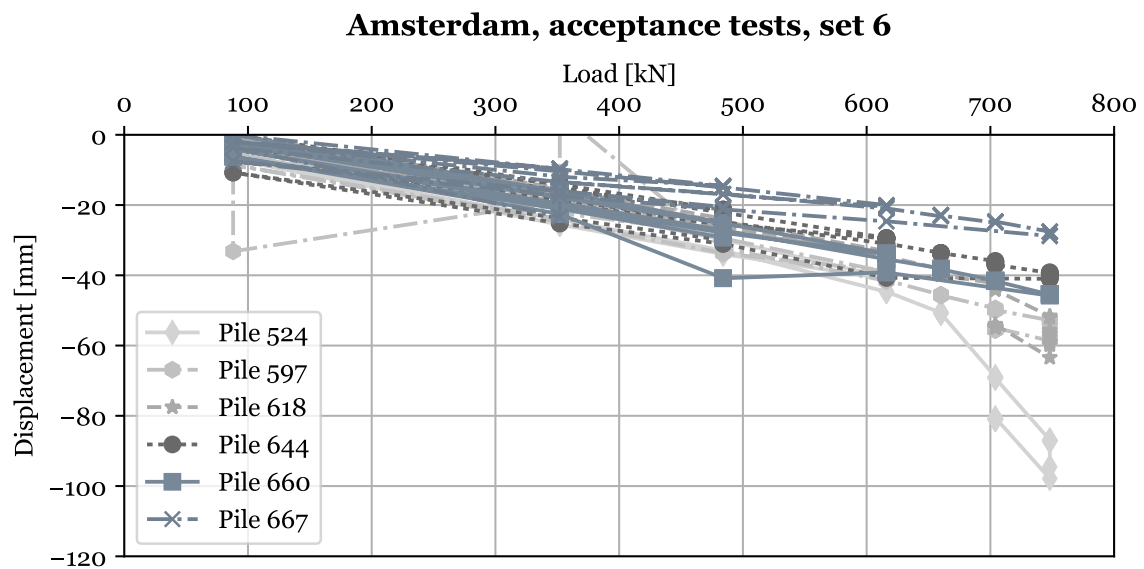
Figure B.31: The load-displacement diagram for series number 6 of acceptance tests performed in the reference project in Amsterdam.